2014

Evaluation of Functional Near Infrared Spectroscopy (fNIRS) for Assessment of the Visual and Motor Cortices in Adults

Brenna Giacherio
Wright State University

Evaluation of Functional Near Infrared Spectroscopy (fNIRS) for Assessment of the Visual and Motor Cortices in Adults

A thesis submitted in partial fulfillment
of the requirements for the degree of
Master of Science in Engineering

by

Brenna M. Giacherio
B.S., Hope College, 2006
M.A., Western Michigan University, 2010

2014
Wright State University

Wright State University
GRADUATE SCHOOL

June 3, 2014

I HEREBY RECOMMEND THAT THE THESIS PREPARED UNDER MY SUPERVISION BY Brenna M. Giacherio ENTITLED Evaluation of Functional Near Infrared Spectroscopy (fNIRS) for Assessment of the Visual and Motor Cortices in Adults BE ACCEPTED IN PARTIAL FULFILLMENT OF THE REQUIREMENTS FOR THE DEGREE OF Master of Science in Engineering.

Nasser H. Kashou, Ph.D.
Thesis Director

Thomas N. Hangartner, Ph.D., FAAPM
Chair, Department of Biomedical, Industrial
and Human Factors Engineering

Committee on
Final Examination

Frank W. Ciarallo, Ph.D.

Thomas N. Hangartner, Ph.D., FAAPM

Ping He, Ph.D.

Nasser H. Kashou, Ph.D.

Robert E. W. Fyffe, Ph.D.
Vice President for Research and
Dean of the Graduate School

ABSTRACT

Giacherio, Brenna. M.S.Egr., Department of Biomedical, Industrial, and Human Factors Engineering, Wright State University, 2014. *Evaluation of Functional Near Infrared Spectroscopy (fNIRS) for Assessment of the Visual and Motor Cortices in Adults.*

Introduction: Functional near-infrared spectroscopy (fNIRS) is a relatively young technique in the field of medical imaging. As such, it has yet to be widely implemented for clinical use, despite its promising advantages. However, unlike fMRI–its much bulkier and costly counterpart–fNIRS has yet to be proven as a standalone imaging tool within a clinical setting, particularly that of ophthalmology or physical therapy.

Methods: Ten healthy young adults (23.8 ± 4.8 years) participated in the study. Activation of the visual cortex was achieved utilizing various reversing checkerboard stimuli across three data collection sessions for each participant. Further, activation of the motor cortex was achieved using simple grasping and finger tapping tasks. Data was processed with MATLAB scripts and statistical analysis was performed using JMP.

Results: Quantitatively, statistically significant differences in the level of activation were elicited by some stimuli, but not others. No differences were discovered between the levels of activation for the two motor tasks. However, as expected, differences were observed between the hair types of participants for both visual and motor activation. Additionally, one of the three data collection sessions for each participant tended to give statistically different results than the other two. Qualitatively, the number of stimulus events and data channels which showed activation were inconsistent.

Conclusions: It has been shown, both previously (by others) and within this study, that fNIRS is indeed feasible for investigating the visual and motor cortices. However, a reliable level of robustness and sensitivity is required for clinical implementation. This research shows that fNIRS can in fact achieve an appropriate level of sensitivity for visual studies, but it still lacks an appropriate level of robustness in terms of repeatability and corporal differences for assessment of visual or motor dysfunction.

Contents

List of Figures

List of Tables

Acknowledgment

Introduction

The overall purpose of this thesis is to determine if functional near infrared spectroscopy (fNIRS) can be utilized as a standalone alternative to fMRI in its current state of development. Originally, the focus rested solely upon the visual cortex. After obtaining promising results from a simple validation method with the motor cortex, however, the focus was expanded to include that region. Suggestions for improvements are given that could lead to the use of this technology within, for example, an ophthalmology or physical therapy clinic. The specific aims of this project are to examine the sensitivity and the robustness (repeatability) of fNIRS measurements with a primary focus on the visual and motor cortices.

1.1 What is NIRS?

NIRS, or near-infrared spectroscopy, is a relatively new and non-invasive imaging modality. As its name suggests, NIRS is based in the infrared portion of the electromagnetic spectrum that lies nearest the visible range. The term spectroscopy refers to the fact that multiple wavelengths are used to determine composition. NIRS operates using a combination of sources that emit light between approximately 650-950 nm and photon detectors that measure light intensity at a given distance from the source. Changes in the concentration of the oxygen-transport molecule, hemoglobin, can be determined for biological tissues between each near-infrared (NIR) source and detector. These changes in concentra-

tion are related to the amount of activation, or use, within a given region-of-interest (ROI), which can allow NIRS to be used for monitoring levels of function or dysfunction. When a stimulus is used to trigger activation in a region of the brain, this modality is known as functional NIRS (fNIRS). Within this particular range of wavelengths, the amount of light that biological tissue absorbs is quite low. On the other hand, the same biological tissue will highly scatter these low-energy photons. Thus, unlike photons at the other end of the electromagnetic spectrum, such as x-rays, near infrared photons are not directly transmitted through tissue (Section 2.1.1).

1.2 History of NIRS

Sir William Herschel first discovered the existence of near infrared light in the year 1800. More than a century and a half–nearly two–passed before Jöbsis demonstrated in 1977 that it is possible to detect oxygenation changes in the adult brain via NIRS [1]. Twelve years later, the first commercial, single-channel (i.e., one source and one detector) NIRS instrument was produced by Hamamatsu Photonics. Then, in 1991 and 1992, the first fNIRS studies were performed, about which six scholarly articles were published in 1993. The following year, Hitachi introduced the first ten-channel NIRS instrument. Simultaneous fMRI and fNIRS studies began in 1996 while the initial 3D imaging with NIRS surfaced five years later. This past year, 2013, marked the twentieth anniversary of fNIRS study publications. In their 2012 review article, Ferrari and Quaresima [2] include a table of the main topics that have been addressed since the first fNIRS publications as well as a detailed history of this modality. Table 1.1 provides a short, nonexhaustive summary of studies which illustrates the various applications of NIRS.

Obrig states in his 2013 review article that in order for NIRS to be a promising tool for neurological fields, there needs to be "proof that beyond feasibility there is an indication for its routine use" [3]. In terms of assessing visual dysfunction, this indication exists for

Table 1.1: Nonexhaustive summary of various conditions studied using NIRS, listed alphabetically by topic.

Topic of Investigation	Brain/Body Region	Stimulus	Age	Study
Acupuncture	motor complex prefrontal cortex	acupuncture manipulation	adults	Hori et al. 2010
Alzheimer's	prefrontal cortex parietal lobe	calculation task	adults	Hock et al. 1996
Alzheimer's	parietal lobe	orientation task	adult patients & controls	Zeller et al. 2010
Bipolar Disorder	frontal lobe temporal lobe	finger tapping verbal fluency	adults	Kameyama et al. 2006
Deep Vein Thrombosis	leg	simulated thrombus	phantom	Hemelt et al. 1997
Depression	forehead	mirror drawing task	adults	Okada et al. 1996
Depression	prefrontal cortex	working memory task	adults	Pu et al. 2011
Depression	prefrontal cortex	verbal fluency	adult males	Sawa et al. 2013
Language	temporal cortex	speech & visual stimuli	infants	Bortfeld et al. 2009
Language	forehead	reading aloud	adults	Fallgatter et al. 1998
Language	prefrontal cortex	oral language tasks	young & old adults	Sakatani et al. 1999
Migraine	forehead	breath holding	adult patients & controls	Akin et al. 2005
MRI & NIRS	sensorimotor cortex	finger opposition	healthy adults	Kleinschmidt et al. 1996
Muscle Ischemia	forearm	tourniquet	adults	Hampson and Piantadosi 1988
Patent Ductus Arteriosus	brain, lung, kidney, deltoid	screening & post treatment	underweight infants	Underwood et al. 2007
Peripheral Vascular Disease	soleus muscle	plantar flexions	older adults	McCully et al. 1997
Schizophrenia	frontal lobe	verbal fluency working memory task	adults	Watanabe and Kato 2004
Sleep	visual cortex	REM sleep visual stimulation (awake)	adults	Igawa et al. 2001
Sleep	forehead	rest, hypoxia & sleep	adults with obstructive sleep apnea	Olopade et al. 2007
Stroke	motor cortex	hand movement task	adult patients & controls	Kato et al. 2002
Stroke	motor cortex	hand-grasping	adult patients	Nakamura et al. 2010

applications within an ophthalmology clinic. NIRS could be used in-house for prescreening and diagnosis. In terms of assessing motor dysfunction, there is potential for using NIRS to monitor and assist rehabilitation in a physical therapy clinic. What is more, its portability allows the system to be moved between patient examination rooms; an additional, dedicated space is not necessarily required as it is for other modalities with much larger equipment such as MRI. This allows increased privacy and convenience for the patient as well as the medical staff. Time-to-diagnosis can be saved when such equipment is housed within the clinic; there would be a decreased need to send patients elsewhere for diagnosis tools, which often involve a waiting list and increased cost.

1.3 Pros and Cons of NIRS

One of the primary advantages to using fNIRS is its incredibly low cost to both purchase and operate when compared to other imaging modalities–MRI in particular. MRI requires a large space and limits the patient to a supine (horizontal) posture with little to no range of motion. On the other hand, not only are fNIRS systems small and portable, but the patient (or research subject) is not limited to one single posture. Another advantage of fNIRS is that no ear protection is required (unlike with MRI) since the systems produce little to no sound. Other limiting factors for MRI, such as issues with patient claustrophobia and ferrous metallic implants, are also not an issue for fNIRS. This enables fNIRS to be utilized for bedside monitoring or in a smaller-scale clinical setting across a wider range of patients. Some systems, such as the NIRSport from NIRx Medical Technologies or the WOT from Hitachi, are now actually wearable and battery-operated to provide even greater portability than traditional NIRS devices. One drawback to this extra portability is that fNIRS measurements are sensitive to motion–although not nearly as much so as MRI–and care must be taken either during data collection to minimize motion or during analysis to account for it. Due to the nature of fNIRS–namely, the relatively sparse optode

arrangements and the scattering of NIR light in biological tissue–this modality provides low spatial resolution. Consequently, it is also quite sensitive to the placement of NIR sources and detectors. High scattering in biological tissue also limits the depth from which usable signals can be obtained. In addition to the scattering that occurs, signal intensity can be further reduced by hair and hair follicles; the darker and denser the hair, the more light that is absorbed. To improve signals received by the detectors, the use of gel can keep hair aside and improve optode contact with the skin, but this can get a bit messy and increase the setup time.

Despite the low spatial resolution and sensitivity to motion, there are still a few more advantages to fNIRS. First, it is noninvasive, nonionizing, and noncarcinogenic. No needles or contrast agents are necessary. The optodes are placed against the skin and secured in some manner–generally with elastic, Velcro, and/or some type of retaining cap. Also, the systems are fairly easy to operate. This, combined with the minimal risk procedures, allows for quick training of staff. NIRS is sensitive to both the oxygenated and deoxygenated forms of hemoglobin, whereas fMRI is primarily sensitive to the deoxygenated form. Measuring the two quantities in tandem gives information about blood oxygenation levels in the ROI. Last, and by no means least, NIRS gives excellent temporal resolution. This is owed mainly to a combination of fairly small ROIs and high sampling frequencies.

As with all imaging modalities, fNIRS has its share of strengths and weaknesses. Its strengths and advantages over other modalities are a great driving force to overcome its disadvantages. Yet, despite more than twenty years of research, much work still needs to be done as we strive toward clinical standards for both collecting and analyzing fNIRS data. This project strives to work toward optimizing data collection protocols, particularly for the notoriously challenging visual cortex. Reliability is also addressed for imaging the visual and motor cortices. By first assessing the current reliability of fNIRS measurements for healthy individuals, the feasibility of using fNIRS for clinical patients can be postulated. After all, if a certain level of reliability cannot be achieved using healthy participants, then

using fNIRS to assess dysfunction is questionable at best.

This study takes a small but important step toward the development of a standalone system for diagnosing visual disorders or monitoring rehabilitation. In doing so, several questions have been posed: How sensitive and robust is fNIRS for detecting changes in hemoglobin (cortical activation) levels? Can it detect differences in those changes that are elicited from various levels of stimuli? Will the same measurements be obtained upon repetition? Finally, is it currently feasible for use in a clinical setting?

Background

This chapter provides a brief overview of the physics behind interactions between light and matter such as different types of biological tissue. It then progresses to relevant anatomy and physiology before concluding with a literature review.

2.1 Physics of Light

2.1.1 Interactions of Light with Matter

Reflection and Refraction

Upon entering biological tissue, photons of light will either continue on a relatively straight trajectory, be scattered by a molecule within the medium, or be absorbed by another. First, those following relatively straight trajectories may undergo reflection and refraction. As light passes through an interface of two materials with different indices of refraction (n), the path of the light will change directions somewhat (Fig. 2.1). Transmittance is a measure of how much light passes through the interface into the second medium. Reflectance is a measure of how much light gets reflected by the interface and remains in the initial medium. By conservation of energy, the combined intensity of light that is reflected and transmitted is equivalent to the initial intensity. The resulting angles (θ) of reflected and transmitted light are defined by the law of reflection (Eq. 2.1) and Snell's law (Eq. 2.2), respectively.

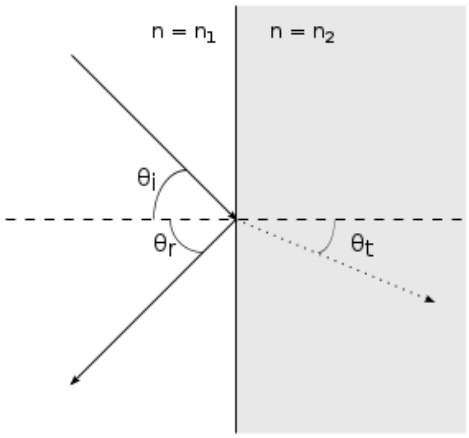

Figure 2.1: Illustration of light reflection and refraction. Light is incident from the upper left, strikes the interface between two media with different indices of refraction (n), and is reflected (solid line) or refracted (dotted line).

$$\theta_i = \theta_r \tag{2.1}$$

$$\frac{sin\theta_i}{sin\theta_t} = \frac{n_2}{n_1} \tag{2.2}$$

In these equations, the subscripts i, r, and t represent the incident, reflected, and transmitted light, respectively. The subscripts on the index of refraction correspond to the first and second media. The index of refraction is near 1.4 for most biological head tissues [25]. As such, this type of interaction does not have as large of an effect as it would, for example, between an interface with tissue and air. Unlike absorption and scattering interactions, reflection and refraction are not dependent upon the wavelength of the incident light.

Scattering

A scattering interaction occurs when light strikes a particle and changes direction. Numerous factors, such as wavelength and particle size, contribute to the prevalence of scattering. There are two general types of scattering: elastic and inelastic. With elastic scattering, no energy is lost; the light simply changes direction. With inelastic scattering, some energy is

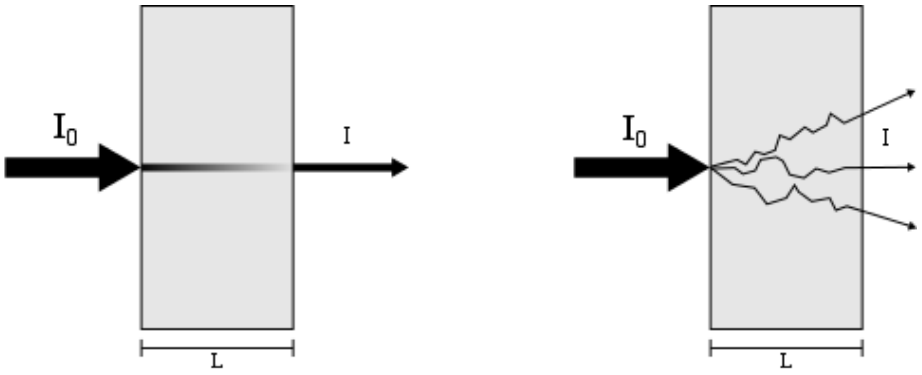

Figure 2.2: Illustration of two different modes of transmission through a medium. Simple absorption through a nonscattering medium is represented on the left and attenuation through a scattering medium is represented on the right.

lost from the incident light during the interaction, which would mean altered frequency and wavelength. The scattering considered here is the former. When light changes direction, the probability of reaching a given detector on the other side of the tissue is reduced. This phenomenon is called attenuation; the intensity of light measured by the detector (I) is less than the original intensity (I_0) of light incident on the tissue (Fig. 2.2). For scattering, this attenuation relationship is defined by the equation

$$I = I_0 e^{-\mu_s L}, \tag{2.3}$$

where μ_s is the wavelength-dependent scattering coefficient (with units of length^{-1}) of the medium and L is its thickness.

There are three classifications for scattering directions: isotropic, forward, and backward. Isotropic refers to the case when all scattering directions have equal probability. Forward and backward scattering are then, by definition, anisotropic. Scattering angles of less than 90° are considered forward scattering and angles greater than 90° are considered backward, as shown in Figure 2.3. Biological tissue is a strongly forward scattering medium [26].

For the adult head, due to scattering, only about one in 10^9 photons that enter the tissue

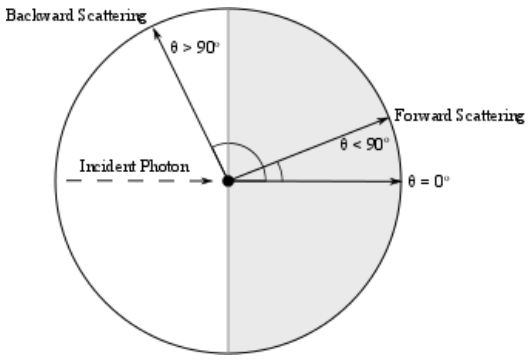

Figure 2.3: Representation of forward and backward scattering. The photon incident from the left strikes the center particle and is scattered in some direction. Forward scattering angles are depicted by the shaded region.

will actually reach the position of a detector located on the surface a few centimeters away from the source [27]. Absorption reduces the signal even more.

Absorption

Like scattering, absorption interactions also depend upon the wavelength of light and the molecular properties of the tissue. Particular atoms or molecules will absorb the energy of light at certain wavelengths. For example, beyond IR wavelengths of approximately 1300 nm, water is the primary absorber. For normal tissue, it will absorb all photons of light within just a few millimeters [1]. Within the NIR window, however, molecules such as water and lipids are minimal absorbers compared to the iron-containing hemoglobin present within the blood. Unfortunately, melanin–the dark pigment found in hair, skin, and eyes–is also incredibly absorbing in this region of wavelengths. Figure 2.4 illustrates these absorption properties.

The proportion of light that is received by a detector after passing through an absorbing medium is defined similarly to that of a scattering medium:

$$I = I_0 e^{-\mu_a L}. \tag{2.4}$$

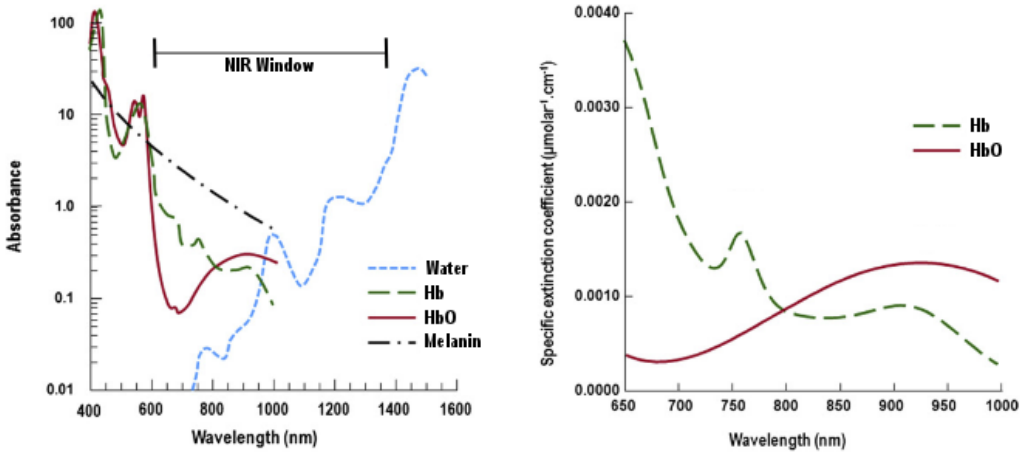

Figure 2.4: Light absorption due to common components of biological tissue. Note that within the so-called NIR window (left), water and melanin are both strong absorbers. The differences between HbO and Hb at wavelengths generally used in fNIRS can be observed in the graph on the right, which is essentially a magnified version of the graph on the left (but with different units). Units on the right-hand vertical axis give the extinction coefficient, ϵ, that is used in Equation 2.7. The crossover between the HbO and Hb curves is known as the isosbestic point. This figure was adapted from [28].

In this case, the scattering coefficient has been replaced by the wavelength-dependent absorption coefficient (again with units of length^{-1}) of the tissue. The absorbance equation (2.4) can be rewritten by taking the natural logarithm and then inverting terms.

$$ln(I) = ln(I_0) \cdot -\mu_a L \tag{2.5}$$

$$A = ln\frac{I_0}{I} = \mu_a L \tag{2.6}$$

The variable A is known as absorbance.

2.1.2 Direct Transmission

The Beer-Lambert law (BLL) expresses a linear relationship between absorbance and the concentration of a given absorber. By defining the absorption coefficient as the product of

absorber concentration $[C]$ and extinction coefficient ϵ, Equation 2.6 becomes

$$A = \epsilon[C]L. \tag{2.7}$$

Note that the extinction coefficient is wavelength-dependent like μ_a and that absorbance is typically represented in optical density units (OD). In order to determine concentrations of two absorbers, a minimum of two wavelengths of light must be used. This results in (at least) two equations with two unknowns. Common choices of wavelength include one above and one below the isosbestic point (Fig. 2.4) near 800 nm.

This relationship holds for light that is essentially traveling a straight path through a medium, such as the light transmitted in Figure 2.2. A particular application is a finger pulse oximeter, as one might find on a hospital patient, to measure oxygen saturation in the blood. A NIR source is placed on top of the finger–on or near the fingernail–and a detector on the underside of the finger so that light travels perpendicularly through the tissue to the other side of the finger. However, to perform the same measurement on a thicker part of the body–the head, for instance–a different configuration is required. If a detector was placed on the opposite side of the head as a source, the detector would not register a signal other than noise. Due to the highly scattering biological tissue, the NIR light emitted by the source would be attenuated by the tissue before reaching the detector. Instead, a detector can be placed on the scalp just a few centimeters away from the source. Doing so, however, means that light received by the detector will follow a curved rather than an essentially straight path and the total distance traveled will be significantly greater than the linear distance between source and detector (Fig. 2.5). This gives rise to the need for a correction factor to actually make measurements in this way.

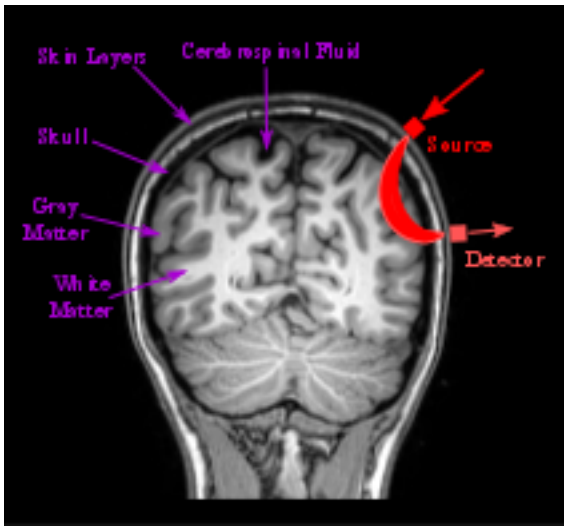

Figure 2.5: T1-weighted MRI image illustrating various layers that NIR light must pass through during fNIRS. Using sources and detectors just a few centimeters apart on the head means that the light which reaches the detectors has followed a curved rather than a straight path. The banana-shaped path shown is an approximation of the most likely path that any photon of light may traverse in order to reach the given detector.

2.1.3 Modified Transmission

The distance correction for the curved path is known as the differential pathlength factor (DPF) and, like other parameters in the Beer-Lambert equation, is dependent upon wavelength. The DPF has been studied or tabulated by numerous research groups for different tissue types and wavelengths. Applying this correction term to Equation 2.7 gives rise to the modified Beer-Lambert law (MBLL),

$$A = OD = \epsilon[C]LB, \tag{2.8}$$

in which *B* represents the DPF.

A change in the concentration of an absorber will cause a corresponding change in the light intensity (OD) detected. Incorporating the fact that several parameters are wavelength-dependent, Equation 2.8 becomes

$$\Delta OD^{\lambda} = \epsilon^{\lambda} \Delta C L B^{\lambda} \tag{2.9}$$

in which λ indicates a specific wavelength. The two absorbers, or chromophores, of interest in fNIRS are oxygenated (HbO) and deoxygenated (Hb) hemoglobin. A given system must then use at least two NIR wavelengths, as previously stated, in order to determine the concentration change for each. Equation 2.9 can be expanded for this application, as shown below.

$$\Delta OD^{\lambda_1} = (\epsilon_{HbO}^{\lambda_1} \Delta HbO + \epsilon_{Hb}^{\lambda_1} \Delta Hb) L B^{\lambda_1} \tag{2.10}$$

$$\Delta OD^{\lambda_2} = (\epsilon_{HbO}^{\lambda_2} \Delta HbO + \epsilon_{Hb}^{\lambda_2} \Delta Hb) L B^{\lambda_2} \tag{2.11}$$

Equations 2.10 and 2.11 can then be solved for the changes in HbO and Hb concentrations:

$$\Delta HbO = \frac{\epsilon_{Hb}^{\lambda_1} \Delta OD^{\lambda_2} / B^{\lambda_2} - \epsilon_{Hb}^{\lambda_2} \Delta OD^{\lambda_1} / B^{\lambda_1}}{(\epsilon_{HbO}^{\lambda_2} \epsilon_{Hb}^{\lambda_1} - \epsilon_{HbO}^{\lambda_1} \epsilon_{Hb}^{\lambda_2}) L} \tag{2.12}$$

$$\Delta Hb = \frac{\epsilon_{HbO}^{\lambda_1} \Delta OD^{\lambda_2} / B^{\lambda_2} - \epsilon_{HbO}^{\lambda_2} \Delta OD^{\lambda_1} / B^{\lambda_1}}{(\epsilon_{HbO}^{\lambda_1} \epsilon_{Hb}^{\lambda_2} - \epsilon_{HbO}^{\lambda_2} \epsilon_{Hb}^{\lambda_1}) L} \tag{2.13}$$

Choosing a wavelength above the isosbestic point will yield a measurement that is more sensitive to HbO. Similarly, a wavelength below the isosbestic point will yield a measurement that is more sensitive to Hb. This simple model for calculating concentration changes carries the assumption that these changes are uniformly distributed over the volume being examined, which is not necessarily the case [29]. However, it is the traditional and widely-used method and does provide a decent approximation for determining changes in the chromophore concentration.

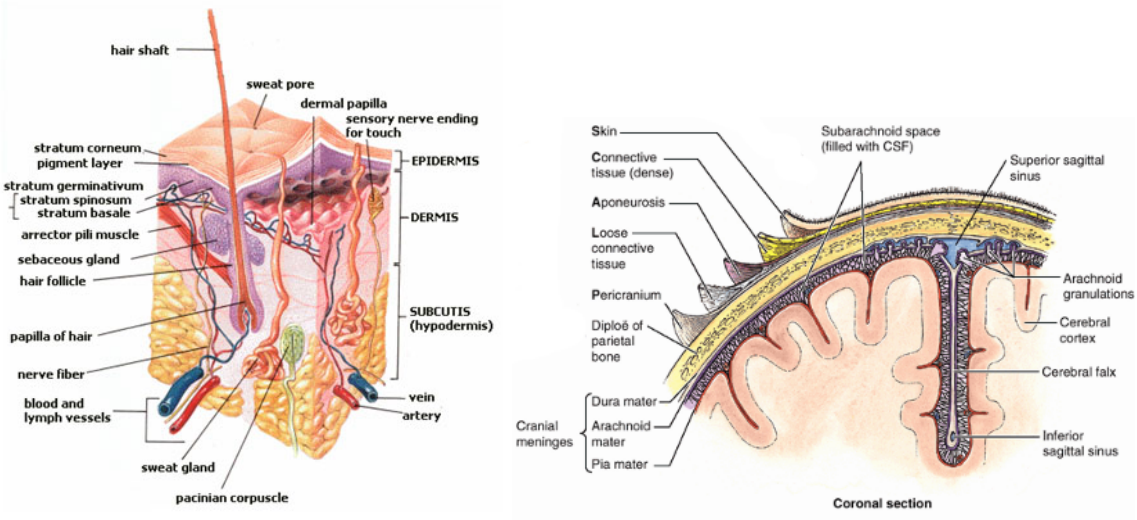

Figure 2.6: Detailed model of scalp structure (left) and tissue layers of the adult human head from the scalp down to the white matter of the brain's cerebrum (right). Despite different composition, the scalp and skull are often considered to be a single layer due to their similar absorption and scattering properties. Adapted from [30] and [31], respectively.

2.2 Propagation Through Biological Tissue

2.2.1 Tissue Layers of the Human Head

In order to measure hemoglobin concentration changes within the brain, near-infrared light must pass through several other layers of biological tissue both before and after reaching the brain itself. These additional layers include hair, skin, bone, and cerebrospinal fluid (CSF). Hair, first of all, is a strong absorber of near infrared light. The darker and coarser the hair, the stronger the absorbance. For this reason, hair should be pushed out of the way to allow direct contact between optodes and the skin, especially since the hair follicles embedded within the skin also absorb light. Thus, ideal candidates for fNIRS have fine, light-colored hair or are balding.

Next, skin is the largest organ of the body and forms a protective surface layer. It is within the central layer (dermis) of the skin that hair follicles originate. The dermis also contains nerves, sweat glands, and blood vessels. Epidermis, the outer layer, does not

contain these structures. Instead, it is composed primarily of dead skin cells and contains the light-absorbing pigment melanin. Below the dermis lies the fatty and vascular interior (subcutaneous) layer known as the hypodermis. For modeling purposes, and in representing absorption and scattering coefficients, the skin is generally considered a single layer of tissue with an approximate thickness of 2-3 mm [32, 33, 34].

Due to the presence of hair follicles and melanin within the skin layers, light is readily absorbed here compared to other tissues. As with hair, the amount of absorption by the skin itself is dependent upon the pigmentation. Individuals with darker skin naturally have more melanin present that those with paler skin. As such, NIRS signals will be reduced further for those with dark skin than it will be for those with pale skin. In fact, the absorption coefficient for those with dark skin was found to be more than seven times that for those with pale skin at 663 nm [35]. Despite this, however, light attenuation in skin is still dominated by scattering.

Another tissue layer of the head is bone. The adult human skull is composed of eight smooth, flat bones. Flat bones have a layer of spongy bone sandwiched between two layers of compact bone. Compact bone provides strength for protection while the spongy bone contains red marrow for blood cell production and is usually mixed with fat (fatty marrow). Spongy bone also contains an open network of bone strands called trabeculae that offers additional structural support. Despite the vasculature of bone, it does not have a significant effect upon absorption properties [36]. The absorption and scattering properties of the skull are actually comparable to the scalp (Table 2.1): highly scattering with a relatively low rate of absorption in the range of wavelengths for NIRS. As expected for biological tissue, the skull is extremely forward scattering [37]. Due to their similar absorption and scattering properties, models may consider the scalp and skull to be a single layer [38]. The thickness of the adult skull tends to fall within the range of 4-12 mm, depending upon the individual and the region of the head. Theoretical models tend to give a value between 7 and 10 mm [33, 34, 38].

Beneath the inner surface of the skull is the CSF-filled cranial cavity. Membranes, nerves, and blood vessels attach to this inner surface. Together with the CSF, these structures cushion and stabilize the soft tissue of the brain. CSF itself is a clear fluid that provides nutrients to the brain and is essentially nonscattering in terms of NIR photons. However, the membranes (meninges) which contain CSF tend to be fibrous and house a network of subcranial blood vessels. In other words, this layer is not completely nonscattering, although the membranes are very thin. Light can travel rather easily through this layer in a path perpendicular to the skull, but it will be absorbed by the network of blood vessels if it travels parallel to the skull [39]. Theoretical studies either simply consider this layer to be nonscattering or attempt to account for its effects [33, 34, 38]. Overall, however, this CSF-containing meningeal layer is seen to have relatively little effect upon light propagation [39].

Finally, gray matter composes the outermost layer of the brain that is imaged with NIRS. It is that layer on which functional studies focus. Theoretical models tend to represent the thickness of gray matter as around 4 to 7.5 mm [33, 34, 38]. Of course, the specific thickness depends upon the exact location on the head (Fig. 2.8). Interior to the gray matter layer is a region of white matter. Depending upon the experimental configuration, NIR light may not reach this depth. It can be observed from the coefficients in Table 2.1 that white matter is a significantly greater scattering medium than gray matter in the adult brain. However, gray matter is a great absorber. The higher scattering coefficient of white matter is due to the myelin sheaths on the prevalent neuronal axons, which have a high index of refraction [40].

2.2.2 NIR Light Penetration

In general, the greater the separation between sources and detectors, the deeper the measured light penetrates into the head. A common rule of thumb is that the measured light pen-

Table 2.1: Summary of measured absorption and scattering coefficients in the NIR region for tissues of the adult head.

Tissue Layer	μ_a (mm^{-1})	μ_s' (mm^{-1})	λ (nm)	Source
epidermis & dermis (pale)	0.024-0.042	2.19-3.27	663	[35]
epidermis & dermis (dark)	0.088-0.394	1.17-5.25	663	[35]
hypodermis	0.008-0.018	0.92-1.6	663	[35]
skull	0.04-0.05	1.3-2.7	650-950	[37]
gray matter	0.032-0.038	2-2.64	650-900	[41, 42]
white matter	0.0032-0.01	7.78-9.26	650-900	[41, 42]

etrates to an overall depth which is half that of the source-detector separation. Of course, the deeper the light penetrates, the greater the quantity scattered, or attenuated. This means that light intensity received by the detectors decreases with increasing distance. When the intensity falls below a certain threshold during instrument calibration, software can increase the gain settings–the amount which a signal is amplified–for a particular channel (source-detector combination). After a certain point, regardless of the gain, signals can no longer be distinguished from noise. Thus, there is a limit to the depth of the brain in which meaningful measurements can be obtained using NIR light.

Theoretically, meaningful signals can be obtained from an adult brain depth of 2 cm using a wavelength of 849 nm [43]. Realistically, current systems do not yet have low enough noise floors to allow this type of sensitivity. As technology improves, though, the sensitivity will eventually increase. A concurrent study is investigating the depth to which the system used for this project–and by this research group–provides worthwhile signals for the adult human head.

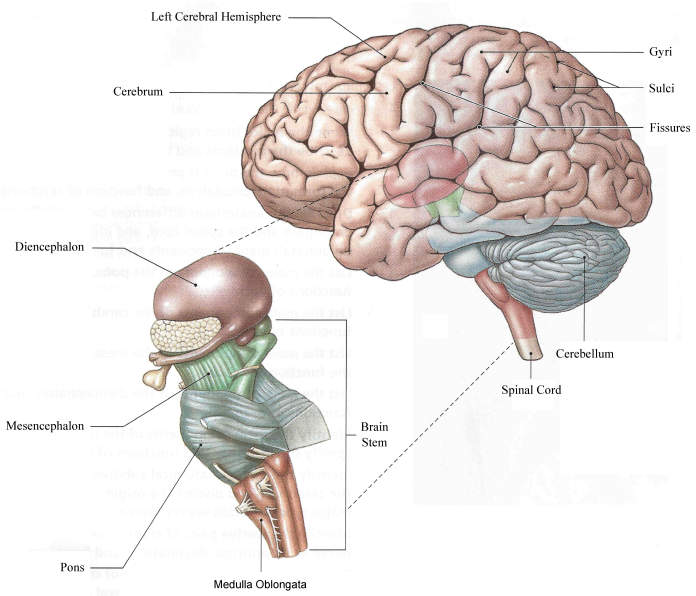

Figure 2.7: Major functional regions of the adult human brain. The upper brain stem is surrounded by the cerebrum and cerebellum. As such, the brain stem is also shown separately for detail. General structures of the cerebrum are also highlighted. Adapted from [44].

2.3 Anatomy and Physiology

2.3.1 Regions of the Adult Brain

By birth, the human brain is fully divided into its different functional regions: medulla oblongata, pons, cerebellum, mesencephalon, diencephalon, and cerebrum (Fig. 2.7). The medulla oblongata, pons, and mesencephalon are collectively known as the brain stem. These structures process and relay information to and from the cerebrum and cerebellum. The cerebellum deals primarily with involuntary control of body movements such as those needed for balance, whereas the diencephalon essentially provides a link between the brain stem and the cerebrum. The diencephalon is composed of structures called the hypothalamus, epithalamus, and thalamus. The thalamus relays sensory information, except for that of smell, to appropriate regions of the cerebrum, which is superiorly-located to the brain stem, diencephalon, and cerebellum.

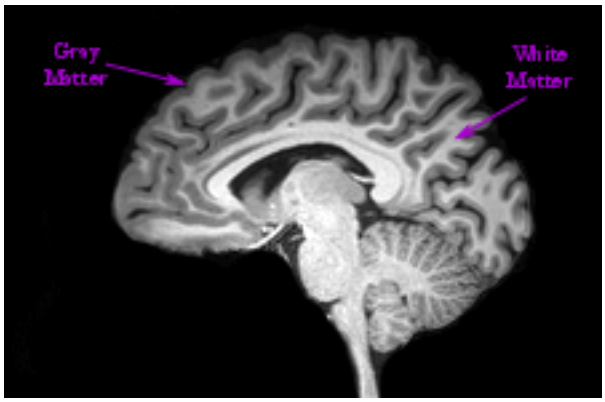

Figure 2.8: Sagittal view of the brain from a T1-weighted MRI. The gray matter of the cerebral cortex appears gray in this type of image whereas the underlying fat-like white matter appears bright white due to the abundance of myelin sheaths that surround nerve pathways.

The cerebrum is not only the largest region of the human brain, but is also the center for both conscious thoughts and higher-level functions. These higher-level functions take place in the gray matter which forms the outer layer of the cerebrum: the cerebral cortex. The cerebral cortex, in turn, is divided into several regions known as lobes that are named for the nearest bones of the skull. These lobes are the frontal, parietal, temporal, and occipital. Each lobe contains functional areas that receive and process specific types of information. For example, the primary motor cortex is an area housed within the frontal lobe and it directs voluntary muscle movements. Beneath the highly-folded gray matter of the cortex lies the white matter of the cerebrum. This white matter is composed of various types of fiber tracts which link one part of the brain to another, such as cortex to cortex or cortex to brain stem. Figure 2.8 is an MRI image that illustrates the cerebral layers.

2.3.2 The Visual Pathway

The visual pathway begins, naturally, with the eye. Basically, light enters the eye through the pupil, is focused by the lens, and falls on the posterior portion of the retina–the inner-

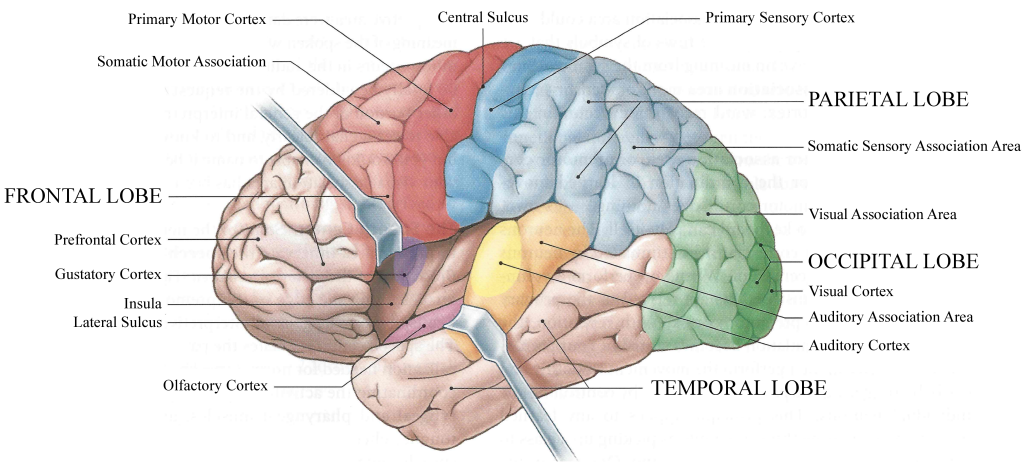

Figure 2.9: Major cortical regions of the adult human brain. The lobes of the cerebral cortex are highlighted along with the major cortical regions such as the centrally-located primary motor cortex and the posteriorly-located visual cortex (right). Adapted from [44].

most layer of the eye. Photoreceptors called rods and cones collect the photons of light that have reached this point. This information is then passed–via ganglion cells–to the optic nerve, which originates from the rear of the eye. The two optic nerves, one from each eye, cross at what is called the optic chiasm, which is located within the brain's diencephalon and is just superior to the pituitary gland. After passing the optic chiasm, the nerves become termed optic tracts. Each optic tract terminates in a posterior structure of the thalamus called the lateral geniculate nucleus (LGN). From here, the visual information is passed to both conscious and subconscious processing centers in the brain. The conscious center that receives visual information is known as the primary visual cortex (V1), which is housed in the occipital lobe at the posterior of the brain (Fig. 2.9). The visual cortex is split into left and right portions by the longitudinal fissure which separates the two hemispheres (left and right) of the brain.

Only about half of the total visual information is received by each hemisphere of the visual cortex. When the optic nerves meet at the optic chiasm, information from the right side of the left eye–which corresponds to the left field of vision–crosses over to follow the

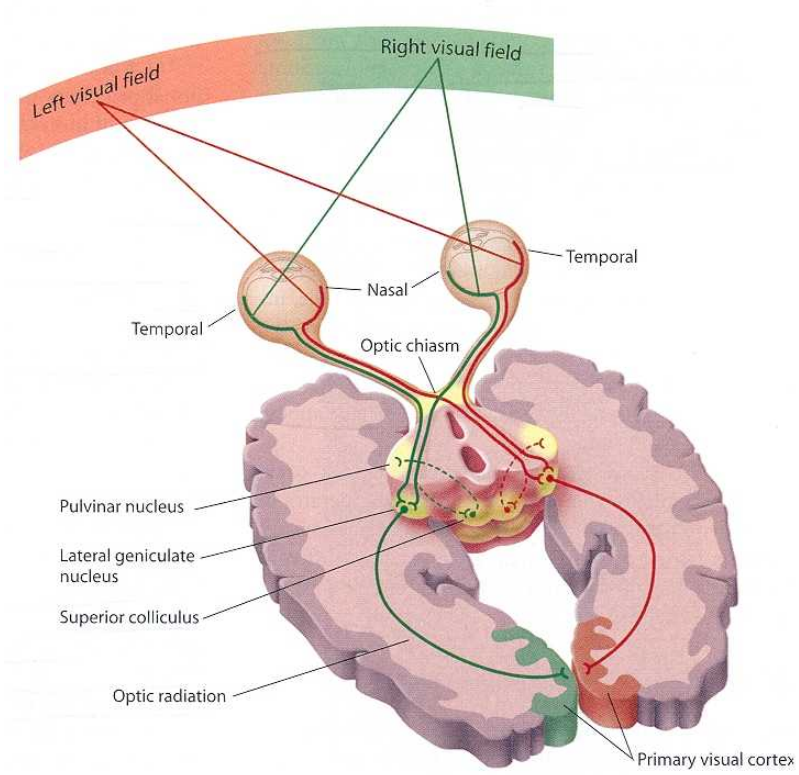

Figure 2.10: Illustration of left and right visual fields as well as the visual pathway through an axial slice of the brain. Crossovers occur both within the eye (light) and at the optic chiasm (visual information). Note that only one optical radiation is shown between the LGN and the visual cortex for each hemisphere and that the longitudinal fissure falls between the left and right halves of the visual cortex. Image obtained from [45].

optic tract in the right hemisphere. The same crossover phenomenon occurs for the right field of vision of the right eye. Thus, information from the left visual field is received by the visual cortex in the right hemisphere and information from the right visual field is received by the visual cortex in the left hemisphere.

Information from the visual periphery is received in the deepest portions of the visual cortex whereas information from the center of the visual field is received in the surface regions of the visual cortex. Since NIRS does not penetrate deep into the cortical tissue, most activation will be seen when the central field of view is stimulated. Hence, understanding the visual pathway and analyzing the fNIRS results of stimulation could allow clinicians to

prescreen or even diagnose visual dysfunction.

2.3.3 The Motor Pathway

Voluntary motor function of peripheral skeletal muscles, such as those of the hands, falls under the body's somatic nervous system (SNS). The motor pathway begins with neurons in the primary motor cortex (Fig. 2.9), which are known as pyramidal cells due to their shape. Neurons in the primary motor cortex control the most complex bodily movements. Increasingly complex movements become possible as a human's brain develops from infancy. To control movement of the limbs, the pyramidal cells directly synapse with lower motor neurons in the spinal cord. These, in turn, synapse directly with a motor unit within skeletal muscle. If neurons in the primary motor cortex activate lower motor neurons, then any connected skeletal muscles will contract. Pyramidal cells also have the ability to inhibit lower motor neurons to prevent muscle innervation. Damage to lower motor neurons destroys control over any associated skeletal muscle units.

The specific skeletal muscles that are activated depend upon the location of activated pyramidal cells within the primary motor cortex. In general, the skeletal muscles on one side of the body are controlled by the motor cortex in the opposite (contralateral) hemisphere of the brain. A map was created mainly by neurosurgeon Wilder Penfield in order to illustrate which regions of the cortex correspond to voluntary control of certain parts of the body. This map is termed the motor homunculus. The number of neurons in the cortex that are dedicated to a given peripheral region in correlated with the amount of fine motor control possible. Thus, the region of the cortex dedicated to hand movement is quite large.

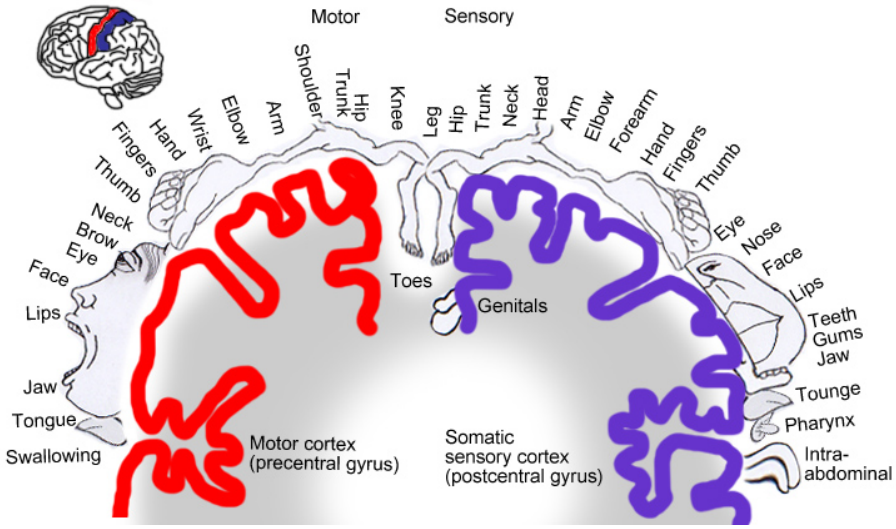

Figure 2.11: A representation of the motor homunculus (left) and the sensory homunculus (right). This is essentially a map of the cortical regions (for a single hemisphere) which control voluntary motions of and receive sensory information from the body. The larger a body part is depicted, the more fine motor control or sensory ability is available. Image obtained from [46].

2.4 Hemodynamics and Activation

2.4.1 Hemoglobin

Blood is composed of several types of formed elements that are suspended within a solution called plasma which is 92% water. These formed elements include red blood cells (RBCs), white blood cells (WBCs), and platelets. A whole blood sample of the average adult male is composed of approximately 54% plasma, 45% RBCs, and 1% WBCs and platelets by volume. A measure called hematocrit gives the percentage of formed elements within a sample of whole blood. Typical hematocrit values for adults range from 42 for women to 46 for men. With a proportion of 99.9%, RBCs are by far the most abundant formed element. [44]

RBCs are biconcave, lack a nucleus, and function as oxygen carriers to peripheral tissues. Essential to this role is the molecule hemoglobin which accounts for the vast majority of proteins within RBCs. In fact, there are approximately 280 million hemoglobin

molecules per RBC [44]. Each hemoglobin molecule is composed of four globular protein subunits and each subunit contains a heme molecule. Hemes possess an ion of iron to which both oxygen and carbon dioxide can bind. Nearly all oxygen in the blood stream is transported this way. When oxygen is bound to the hemes, the molecule is oxygenated and becomes known as oxyhemoglobin. Logically, then, a deoxygenated molecule in which oxygen is not bound to the hemes is known as deoxyhemoglobin.

2.4.2 What is Hemodynamic Response?

An increase in neuronal activity, which is generally prompted by a stimulus of some sort, results in an increase of metabolized oxygen as well as a corresponding increase in cerebral blood flow (CBF). The body tends to overcompensate, however, which means that the increase in CBF is greater than the increase in the amount of oxygen that is required for the activity. The metabolism of oxygen uses HbO, thereby increasing the proportion of Hb within the stimulated region. The large increase in CBF, however, actually increases the proportion of HbO and usually decreases that of Hb. Thus, overall, the stimulus induces an increase in HbO and a decrease in Hb. The total quantity of hemoglobin (tHb)–equivalent to the sum of HbO and Hb–increases. These changes in concentration due to the stimulus comprise what is called the hemodynamic response. A typical hemodynamic response curve can be seen in Figure 2.12. An additional point to note is that the direction of change in HbO, whether increasing or decreasing, is the same as that of the change in regional CBF. However, changes in Hb do not necessarily follow that trend. As such, HbO is more sensitive to changes in brain activation than Hb [47].

For approximately seven to ten seconds after the onset of a stimulus, the concentration of HbO increases significantly to reach a plateau [48, 49, 50, 51]. It takes the same or similar amount of time for Hb to decrease. Once the stimulus ends, approximately ten to twelve seconds are needed for HbO and Hb to return to normal levels [48, 51, 52]. The time to reach an HbO maximum varies with the stimulus protocol used. For a 30-second

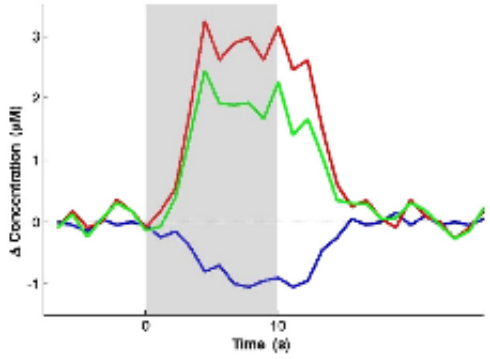

Figure 2.12: This figure illustrates a typical hemodynamic response from a theoretical perspective [2]. HbO and Hb concentrations are represented by the upper (red) and lower (blue) curves, respectively, while tHb concentration is represented by the central (green) curves. The shaded region represents the duration of a stimulus.

on and 30-second off protocol, for example, stability is reached by twenty seconds with a maximum occurring at approximately 26 seconds [49, 51]. For a 10-second on and 20-second off protocol, a maximum occurs one to two seconds after the stimulus ends [48] before values begin returning to baseline.

2.4.3 Effect of Age upon Response

More than a few studies have focused on identifying age-related differences in hemodynamic response patterns. For example, in 1995, Hock et al. [53] showed that a calculation task elicited a reduced mean activation level (change in HbO) in older adults (52 ± 10 years) as compared to younger adults (28 ± 4 years). Then, Sakatani and colleagues studied the effect of age upon oxygenation changes (hemodynamic response) between young (28.8 ± 4.4 years) and older (50.7 ± 8.0 years) adults in their 1999 paper [14]. This data from six different language-related tasks was analyzed qualitatively for patterns. It was determined that different patterns were dominant for younger versus older adults as a result of verbal fluency and reading tasks. For younger adults, the characteristic increase in HbO and slight decrease in Hb was evident. For older adults, on the other hand, a decrease in

HbO was present for the majority of subjects along with little to no decrease in Hb. This HbO decrease was most prevalent while reading. Further, in a 2003 study, Schroeter et al. [54] used a Stroop task to compare the hemodynamic response between young adults (23.9 ± 3.1 years) and seniors (65.1 ± 3.1 years). A Stroop task involves identifying the text color of various words, which is more cognitively challenging than just reading the words themselves [55]. It was found that, in general, the mean hemodynamic response was greater in younger adults. That is, the level of hemodynamic response in adults tends to decrease with age.

2.4.4 Response within Different Cortical Regions

An hemodynamic response, which is marked by an increase in HbO, within a given region of the brain does not always possess the same timing [2]. There are actually regions of the brain in which the responses of HbO and Hb begin at the same time and others in which one appears slightly delayed. For example, Steinbrink [56] and others [57, 58] have noted that the Hb response began about 1.7-2 seconds after that of HbO within the motor cortex, but that the timing of HbO and Hb responses is equivalent within the visual cortex–there is no delay. Table 2.2 includes a brief summary of some fNIRS studies that have been done along with the resulting hemodynamic response.

As it was mentioned, the timing of the responses has been shown to be the same for both HbO and Hb in the visual cortex. The hemodynamic response in this region also exhibits the typical pattern: a marked increase in HbO and a less pronounced decrease in Hb. Greatest levels of activation, and therefore increase in HbO, have been observed from optodes that overlie the primary visual cortex [58, 59, 60]. The amount of activation measured tends to decrease with radial distance from this location. Using the International 10-20 System for electrode placement [61], which is depicted in Figure 2.13, Wijeakumar and coworkers showed that the largest changes in hemoglobin concentration occurred at O1, O2, and 5% above each [51]. They also demonstrated that the greatest and longest

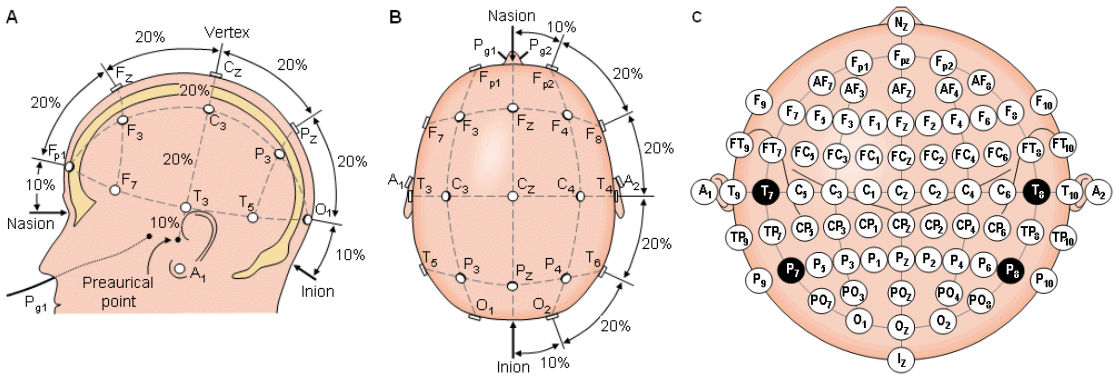

Figure 2.13: Diagram of the International 10-20 System for EEG electrode placement from sagittal (A) and axial (B) views. This EEG placement system has been extended to use in the field of fNIRS. Commercially-available optode retaining caps utilize this system for NIRS optode placement and many groups report results using the positions defined by this system. As an example, seventy-five specific locations are represented from an axial perspective (C). The letters indicate the general region of the head, such as *O* for occipital, and the subscripts indicate distance from the midline (z) with odd numbers for the left hemisphere and even numbers for the right. Specific distances between points vary slightly from person to person due to the fact that this system is based upon percentages. See Appendix A for examples of optode arrangements using the 10-20 system. Image obtained from [63].

activations were stimulated using pattern-reversing checkerboards (as opposed to static checkerboards or a simple pattern onset/offset). The current ISCEV standard for clinical visual evoked potentials [62] suggests a pattern reversal rate of 1.0 Hz, which corresponds to two reversals per second, in order to obtain a reliable EEG signal. However, studies have shown that higher reversal rates produce a greater response.

Numerous studies use sweep visual evoked potential (sVEP) to measure contrast sensitivity and visual acuity at reversal rates of 6 Hz, many of which are mentioned in a review article by Almoqbel, Leat, and Irving [64]. Some have studied a range of frequencies up to 12 Hz. Heine and Meigen [65] found that the greatest magnitudes and significance could be obtained by using pattern-reversal checkerboards at rates between 4 and 8 Hz for VEP. Another previous study [66] suggested that, for larger checker sizes, a higher temporal frequency would produce a better response. Thus, since the checker sizes used in this project

are considered large by ISCEV standards [62]–i.e., spanning at least one degree of arc–and it has been demonstrated that good fNIRS results are attainable [50, 51], a temporal frequency of 7.5 Hz was chosen for a pattern-reversal checkerboard stimulus (Section 4.1).

2.4.5 NIRS and the Adult Visual Cortex

An early fNIRS study by Villringer and colleagues [77] compared the effects of visual and cognitive stimuli on their respective processing areas in the brain. They found that the signal-to-noise ratio (SNR) was worse for visual data obtained at the posterior of the head than for cognitive data obtained at the forehead. This feature was attributed to a greater skull thickness and the presence of hair in that region of the head. Many others have noted the same trend. Some specifically state that only those with light-colored or no hair were used due to the low signal intensity from those with dark hair [49, 51]. More often, however, hair color is not reported, although studies have noted subject exclusion due to low signal intensity [52]. This, then, begs the question: how many studies have obtained usable signals across all hair types? And if subjects were excluded from analysis, why–specifically–were they excluded? Was hair color the culprit?

Like Villringer [77], other studies compared different functional areas of the brain. Wolf et al. [58] compared motor and visual regions. In the process, they discovered evidence to indicate that the amount of oxygen consumed by the visual cortex during activation noticeably increases. The amount consumed by the motor cortex, however, barely changes. As such, a larger-amplitude HbO signal would be seen in the motor cortex than in the visual. And, thus, another challenge was presented for fNIRS and the visual cortex.

A popular modality comparison is fNIRS and EEG (electroencephalogram). For measurements on the visual cortex, the electrical activity measurements are referred to as visually evoked potentials (VEPs). Wijeakumar et al. [50] performed one such fNIRS and VEP correlation study using stereoscopic (having the illusion of 3-D) stimuli. Oxygenated

Table 2.2: Nonexhaustive summary of studies and results for hemodynamic response in the brain using NIRS, listed alphabetically by first author. A * indicates the number for each wavelength and ** indicates an exception for the oldest subject (problem solving) or dominant hemisphere (emotional stress).

Study	Sources/Detectors	Wavelength (nm)	Stimulus	Age	Region	Response
Akin et al. 2005	4/10	735, 850	holding breath	adults	frontal	↑HbO, ↓Hb
Colier et al. 2001	2/2	775, 848, 901	reversing checker	adults	occipital	↑HbO, smaller ↓Hb
Hock et al. 1995	1/1	775, 825, 850, 904	calculations aloud	adults	left frontal	typical ↑HbO, ↓Hb
Hoshi and Tamura 1993	1/1	780, 805, 830	problem solving	adults	frontal	↑HbO, ↓Hb**
			emotional stress			↑HbO, ↓Hb**
Hoshi and Tamura 1993	5/5	780, 805, 830	problem solving	adults	frontal, temporal	↑HbO, ↓Hb(f); ↑HbO, ↑Hb(t)
			classical music		temporal, occipital	↑HbO, ↑Hb(t); ↓Hb(o)
			flashing light		occipital	↑HbO, ↑Hb; ↓HbO(sleep)
Jasdzewski et al. 2003	2/4	682, 830	open/close hand	adults	sensorimotor	↑HbO, ↓Hb(lag)
Karen et al. 2008	4/4	730, 830	flashing LEDs	neonates	occipital	↑HbO, smaller ↓Hb
Kato et al. 1993	1/1	780, 808, 828	flashing LED	adults	occipital	↑HbO, ↓Hb
		850, 870, 904				
Kleinschmidt et al. 1996	2/2	775, 825, 850, 904	finger opposition	adults	motor cortex	general ↑HbO, ↓Hb
McIntosh et al. 2010	4/1	690, 830	reversing checker	adults	occipital	↑HbO, smaller ↓Hb
Obrig et al. 2000	1/1	700-1000	reversing checker	adults	visual cortex	↑HbO, smaller ↓Hb
Olopade et al. 2007	8*/2	690, 830	sleep	adults	frontal	↓HbO, smaller ↓Hb
Rovati et al. 2007	1/1	670-980	reversing checker	adults	occipital	↑HbO, smaller ↓Hb
Sassaroli et al. 2005	16*/4	690, 830	finger tapping	adults	motor cortex	↑HbO, smaller ↓Hb
Schroeter et al. 2003	2/2	775, 825, 850, 904	color-word Stroop	adults	frontal, parietal	↑HbO, smaller ↓Hb
					motor cortex	
					visual cortex	
Shimada 2012	8/8	780, 805, 830	eye contact	adults	temporal	↓HbO
Taga et al. 2007	2/8	780, 830	speech sounds	infants	temporal	↑HbO, smaller ↓Hb
Toronov et al. 2007	16/4	690, 830	reversing checker	adults	visual cortex	↑HbO, smaller ↓Hb
Villringer et al. 1993	1/1	775, 825, 850, 904	addition & subtraction	adults	left frontal	↑HbO, ↓Hb
			flash-light & picture		right occipital	
Wijeakumar et al. 2012	16/2	690, 830	checkerboard (3 types)	adults	occipital, parietal	↑HbO, ↓Hb
Wijeakumar et al. 2012	8/1	692, 834	checker, random dots	adults	occipital	↑HbO, ↓Hb
Wobst et al. 2001	1/1	720-920	reversing checker	adults	visual cortex	↑HbO, ↓Hb
Wolf et al. 2002	2/8	758, 830	palm squeezing	adults	motor cortex	↑HbO, ↓Hb(lag)
	2 crossed pairs	670, 830	checkerboard		visual cortex	

hemoglobin was found to be the most stable of the measured NIRS quantities. It was also found that oxygenated hemoglobin concentrations were correlated to VEP amplitude and that more prominent responses were seen in the left side of the visual cortex.

Investigations involving both fNIRS and fMRI are also quite prevalent, whether data is collected simultaneously or not. This has been done both as a comparison between the imaging modalities and as an anatomical check of the region being measured by fNIRS. One simultaneous visual fMRI and fNIRS study [76] noticed that, first, there is a more prominent response to stimuli on the left-hand side of the visual cortex and, second, higher stimulus frequencies produced responses over a greater cortical area. Additionally, it was noted that data from two subjects was excluded due to poor positioning of the optodes. This notation illustrates the fact that fNIRS measurements are, due to low spatial resolution and localized responses, sensitive to source and detector placement.

Another such comparison study [52] examined the effect of saccadic eye movements on blood flow in the visual cortex. They concluded that the rate of blood flow into the region is reduced to a greater extent than the rate of oxygen consumption, which results in hypooxygenation. Since NIRS provides more information on blood oxygenation levels than fMRI, this conclusion could not have been reached using fMRI alone. This particular fact bodes well for the future of fNIRS.

Another point that bodes well for the future is the predictability of a normal fNIRS response curve. In this case, such predictability would contribute to the prescreening or diagnostic power of fNIRS for assessing the presence of visual dysfunction. Wobst and colleagues [78] were able to successfully predict visual fNIRS responses using an impulse response function convolved with a rectangular window that represented stimulus duration and adding a delay of a few seconds. This was accomplished using four different stimulus lengths ranging from short (three seconds) to long (twenty-four seconds). This showed both significance for a wide range of visual studies and that responses from long stimuli can be predicted from short ones. Another fact the authors noted was that low frequency

oscillations (LFO) were present in the signals for subjects with small responses to the stimuli–responses that already have relatively low SNR.

Obrig et al. [71] studied the LFO commonly present in fNIRS data and found that they had approximately the same magnitude as responses from visual stimuli. Further, the oscillations managed to survive a grand average of responses across all subjects under normal conditions, but was attenuated during periods of high carbon dioxide within the blood (hypercapnia). Because inducing hypercapnia is not necessarily advisable for actual patients, another method of approach may be required for extension to the ophthalmology clinic for patients with low-magnitude signals.

Twelve years later, a 2012 study by Wijeakumar and colleagues [51] compared three different modes of visual checkerboard stimulus presentations as well as fifteen different measurement locations. The authors subsequently focused their investigation on the stimulus protocol and the five measurement locations which produced the greatest-magnitude responses. It was found that the best signals were produced using a pattern-reversal checkerboard stimulus and at locations presumed to lie directly over the primary visual cortex. Additionally, their results further supported Toronov et al. [76] in that a more prominent response was seen on the left-hand side than on the right.

In 2010, McIntosh et al. [49] used what is termed a frequency-domain multidistance (FDMD) method to estimate absolute–rather than relative–changes in blood oxygenation. They showed that absolute quantification of HbO and Hb is indeed possible with the right devices and signal processing. It was also concluded that not only does hair color affect signal quality, but that, logically, hair density does as well. In other words, the darker and denser a person's hair, the lower the quality of received signals.

2.4.6 NIRS and the Adult Motor Cortex

The visual cortex is notoriously more difficult to study using NIRS due primarily to the increased skull thickness and quantity of hair, which noticeably decreases SNR. In order to

serve as a basis for comparison, an additional functional imaging protocol was employed for another region of the brain. For simplicity on the part of both participants and experimenters, as well as the favorable results obtained from a preliminary trial, the motor cortex was chosen. Studies involving both the motor and visual cortices are not uncommon [57, 58] and studies focusing on the motor cortex are quite prevalent. Subudhi et al. [79], for example, compared oxygenation changes in three cortical regions–prefrontal, premotor, and motor–during maximal exercise. Ikegami and Taga [80] observed that the amount of cortical activation was positively correlated with the level of kinetic movement. The also discovered a decrease in the sensorimotor cortex activation (ΔHbO) as subjects learned the multi-joint upper limb motor task, which was attributed to changes in motor commands. Hatakenaka et al. [81] found that activation shifted posteriorly (from the presupplementary motor area to the supplementary motor area) with task repetition. These claims were further supported by the findings of Morihiro and colleagues [82]. They noted a decreasing tendency in the magnitude of HbO changes within the primary motor cortex, which suggested that the specific active areas of the brain change over the course of learning a motor task.

As with the visual cortex, many many motor cortex studies have also compared multiple modalities. Rather than utilizing fMRI as a tool to locate or confirm regions of high activation on individual subjects for fNIRS studies, one group actually used transcranial magnetic stimulation (TMS). During a hand grasping task, Akiyama et al. [83]utilized TMS to determine the specific area which had the highest activity prior to application of NIRS sources and detectors. Also, once again, the use of fMRI in combination with fNIRS is quite common. In 2006, Huppert et al. [84] utilized NIRS simultaneously with each of two separate fMRI protocols: arterial spin labeling (ASL) and blood oxygen level dependent (BOLD). High correlation was found between NIRS HbO and tHb measures and the CBF measured via ASL fMRI. Similarly, high correlation was found between NIRS Hb response and the BOLD fMRI signal.

Gagnon and colleagues [85] investigated cortical versus superficial oxygenation changes elucidated from a finger tapping task during simultaneous fNIRS and BOLD fMRI. In addition, yet another group looked at cortical activation during apple peeling using fNIRS and fMRI. Real apple peeling was performed while fNIRS measurements were recorded; mock apple peeling was performed during concurrent fNIRS and fMRI recording. It was found that while the motor cortex showed activation in both cases, the prefrontal cortex only showed activation during the real case. This illustrates that fNIRS alone–as an alternative to fMRI–is promising for the study of cortical activation during everyday tasks.

A popular topic for imaging research is stroke rehabilitation and the neurological changes that occur during the process. Strokes occur when the blood supply is blocked to any given region of the brain. If the blockage lasts more than a few minutes, cells begin to die. Most often, blockages are located in the middle cerebral artery, which can lead to loss of sensation and control over the opposite (contralateral) side of the body [44]. At least some loss of motor function in the upper limbs results from approximately eighty percent of strokes [86].

Kato and colleagues [23] compared fNIRS and fMRI for detection and monitoring of cortical motor organization following hemiparetic (one-sided weakness) stroke. They found that movement of the affected hand displayed significant motor cortex activation in both hemispheres rather than just the contralateral hemisphere. In terms of stroke rehabilitation, however, fMRI is limited to rather simple motions of the upper limbs while lying down.

Larger body motions are not feasible using fMRI due to posture and excessive signal noise, but are for fNIRS. As an example, Miyai and colleagues [87] studied hemiparetic gait of poststroke patients using a treadmill before and after two months of rehabilitation. Improvement in hemispheric asymmetry was correlated with improved gait, which confirmed that changes in cortical activation do occur during recovery.

Many suggestions have been made for using fNIRS in stroke rehabilitation. One idea

is to monitor the status of neural activity and observe the effect of various treatments on that activity [88]. This would allow rehabilitation that is specifically tailored to each patient. In a similar vein, it has been suggested to simply either employ real-time imaging during therapy or immediately before and after [89]. In fact, Mihara et al. [90] found greater cortical activation and functional gain in the hands for poststroke patients that were provided direct feedback of their fNIRS signals.

Another promising possibility is the use of NIRS for a brain-computer interface (BCI). A group from the National University of Ireland Maynooth proposed that cortical activation during imagined movement (motor imagery) can be utilized in an optical BCI, which can then be used to control a robotic splint or a virtual environment to give the patient positive feedback [91, 86]. Sagara, Kido, and Ozawa [92], based upon the methods of Haida et al. [93] actually developed a portable NIRS-based BCI to control television programming or propel a toy robot. More recently, a group combined fNIRS data with other physiological signals–heart and respiration rate, blood pressure, and skin conductance–as a step toward developing a real-time BCI for controlling a virtual reality robot.

Instrumentation

This chapter presents an overview of NIRS devices. Specific hardware and software systems that were utilized over the duration of this project are then introduced.

3.1 Hardware

3.1.1 Basics of NIRS Devices

In its simplest form, a device used for fNIRS requires a NIR-emitting light source and a detector to measure light intensity. Collectively, these sources and detectors are referred to as optodes. Options for the choice of NIR sources include lasers, laser diodes, light-emitting diodes (LEDs), and incandescent bulbs [39]. At typical fNIRS optode separation distances, the intensity of light that penetrates the head and actually reaches the detector is very small–on the order of only 10 pW [29]. With this minute intensity, high-sensitivity detectors are necessary. Thus, options available for the choice of detectors include light-sensitive diodes, photomultiplier tubes (PMTs), and CCD cameras [29, 39].

3.1.2 Types of NIRS Devices

Several types of systems are currently available for fNIRS measurements: frequency domain (FD), time domain (TD), and continuous-wave (CW). Theoretical light penetration

depths and sensitivity profiles are extremely similar for a CW system, a 200 MHz modulated FD system, and a 500 ps pulsed TD system [29]. However, FD and TD systems can typically penetrate deeper into the brain than CW systems. In addition, it is feasible with both FD and TD systems to differentiate between the brain and extra-cerebral tissue in superficial regions [2].

FD systems operate by emitting light continuously from a source. That light varies as a sinusoid in intensity with frequencies on the order of megahertz. Detectors measure both the reduction in intensity and the phase shift of the light after it passes through tissue [29]. Combining this information allows a direct measure of absorption and scattering coefficients by assuming that HbO and Hb are the only absorbers that contribute significantly, which eliminates the necessity to define a pathlength for the light [94]. The two main advantages of FD systems are high temporal resolution and absolute quantification of HbO and Hb concentrations. Disadvantages include a relatively large amount of noise within scattering measurements [29] as well as greater complexity and, therefore, cost than some other NIRS systems.

Unlike FD systems, TD systems emit light in short, picosecond-order bursts–or impulses–rather than continuously. These short impulses are broadened to a few nanoseconds, as well as reduced in amplitude, upon transversing biological tissue and the resultant signal is known as either the temporal point spread function (TPSF) or the distribution time-of-flight (DTOF). The broadening of the initial impulse is a consequence of the highly scattering biological tissue; not every photon will follow the same path between source and detector. By determining the photon's time of flight, pathlength can be directly calculated using the speed of light. Like FD systems, TD systems are also able to determine absorption and scattering coefficients. However, TD systems have an even greater overall cost than FD systems. They also require relatively long acquisition times to obtain a reasonable SNR and possess somewhat large dimensions with the need for physical stabilization [29]. An advantage of TD systems over others, though, is the potential for greater spatial resolution

as Torricelli and colleagues demonstrated with zero-separation measurements [95].

Similar to FD systems, the light sources of CW systems emit light continuously, as their name implies. Depending upon the specific hardware, the emitted light intensity either has a constant amplitude or varies sinusoidally with frequencies at or below tens of kilohertz [29]. Combining the detected signal intensities with estimates of the pathlength allows for calculation–via the MBLL–of relative hemoglobin concentration changes. Primary advantages of CW systems over others include their simplicity, smaller size, and low cost. And of the three types of systems, CW provide the best SNR at sampling frequencies above 1 Hz [29] as well as the potential for the highest sampling rate [2]. However, they also have several disadvantages. First, CW systems cannot determine absolute quantities of HbO and Hb. Previously tabulated values of or models for the DPF must be used to estimate concentration changes. This DPF approximation introduces an additional measure of uncertainty; DPF varies between tissues, people, and even age [29]. Further, measurements are more sensitive to superficial regions due to the nature of the path of light as it traverses the tissue [96]. Last, any change in optode position or amount of pressure against the scalp could significantly alter detected intensities.

3.1.3 Experimental NIRS Hardware

The compact, CW NIRScout neuroimaging system from NIRx Medical Technologies is commercially available in a range of configurations–up to sixteen sources and twenty-four detectors–and can also be used in tandem with another system. The fNIRS Laboratory at Wright State University houses a NIRScout system with eight sources and twelve detectors and connects to the data acquisition computer via a USB 2.0 cable. This allows a total of 96 possible measurement channels for data collection. Each LED illumination source emits NIR light at two fixed wavelengths: 760 and 850 nm. LEDs generally offer more temporal stability than lasers [97] and the power of each LED source is near 5 mW per wavelength.

Figure 3.1: Face of the tabletop NIRScout NIRS imaging system. The dimensions of this main unit are 26 x 17 x 33 cm (WxHxL). Ports on the front, from left to right, include twelve detectors, USB output to a data acquisition computer, parallel input from a stimulus computer, and eight NIR sources.

Utilizing all eight sources during data collection provides a sampling frequency of 6.25 Hz when the sources are lit sequentially (standard mode). An increase in sampling frequency can be obtained in one of two ways with NIRScout. First, the bilateral mode can be activated. This mode causes two sources to emit light simultaneously. However, this should only be used when sources are sufficiently far apart so that no single detector is receiving light from both sources (i.e., when imaging different functional regions of the adult brain). For this particular system, the separation required would be at least 5-7 cm. The other way to increase the sampling frequency is to reduce the number of sources used during data collection. Employing only half of the eight NIRScout sources, for example, results in a sampling frequency of 10.42 Hz–an increase of more than 4 Hz.

The detectors of the NIRScout system are silicon photodiodes, which are sensitive to intensities of less than 1 pW. Silicon detectors possess high SNR and sensitivity at NIR wavelengths and provide quick signal acquisition [98]. Detectors are connected to the main unit by optical fibers. Optical fibers consist of a core for transmitting light and a covering to both keep internal light from escaping and external light from entering. Light transmission down the length of the cables is governed by Snell's law (Eq. 2.2) in which the refractive index of the core is greater than that of the protective covering. If light has

an angle of incidence (θ_i) greater than a critical value, then it will not pass through the interface between the core and covering. Rather, it will undergo total internal reflection and continue on its path down the fiber.

Total internal reflection occurs when the transmitted angle is at least 90°. The corresponding incident angle can then be calculated from Snell's law.

$$sin\theta_i = \frac{n_2}{n_1} sin(90^\circ) = \frac{n_2}{n_1} \tag{3.1}$$

$$\theta_i = \theta_c = arcsin\frac{n_2}{n_1} \tag{3.2}$$

Therefore, incident angles greater than θ_c, the critical angle, will be totally and internally reflected.

3.1.4 Physiological Monitoring System

The BioRadio system (Great Lakes NeuroTechnologies) for measuring additional physiological parameters during fNIRS data collection consisted of a set of electrocardiography (ECG) leads, a respiration belt with leads, and a finger pulse oximeter. All may be connected to a small, portable hub that transmits data wirelessly, via radio frequencies (RF), to a nearby data acquisition computer. First, the set of ECG leads involve a positive, negative, and ground which snap onto electrodes that are placed on the skin: one on the sternum and one on each clavicle. ECG measures the heart's electrical activity, thereby providing information on heart rate and heart rate variability. Next, the respiration belt is an elastic band containing very thin, coiled wires and which fastens–with Velcro–around the rib cage. Two leads, or interface cables, attach to snaps on the belt in order to provide a measure of respiratory effort (plethysmography) by monitoring the expansion and contraction of the chest. Specifically, these elastic bands are referred to as respiratory inductance plethysmography (RIP) belts. Together with the interface cables, they measure changes in the small mag-

netic field in the coils of the RIP belt [99]. This then shows the respiration rate over time. Finally, a simple pulse oximeter (Section 2.1.2) clips onto a finger to monitor peripheral oxygen saturation and pulse.

The wireless hub of the BioRadio unit is powered by a pair of AA batteries that offer approximately ten to twelve hours of operation. The device itself takes the data received from the attached leads, then amplifies and digitizes it before transmitting it over RF to the USB receiver that is attached to the data acquisition computer [99]. Available digital sampling rates range from 128 to 960 Hz. A few specialized preprogrammed channels, such as the one for pulse oximetry, sample data at only one-tenth the rate of the others. A single BioRadio unit is capable of monitoring up to a total of eleven physiological sensors at once. And, although not utilized in this specific application, it can measure a subject's movement and changes in orientation when worn on the body.

3.2 Software

3.2.1 NIRS System

NIRStar (v. 12.4), the data acquisition software packaged with NIRScout, streams hemoglobin data for general real-time visualization. Running calibration in NIRStar prior to data collection automatically adjusts the gain settings for each source-detector combination. This means that channels with raw signals below a threshold of 0.1 V receive an increase in gain, or signal amplification factor. Gain settings are the same for both wavelengths of emitted light. Therefore, only signals from one wavelength need to fall within the optimal range (0.1 - 1.0 V) during calibration. Following calibration and subsequent data recording, the data acquisition software saves the raw data in a format which is compatible with NIRx's proprietary analysis software as well as other open-source programs for data analysis.

With NIRStar, the user is able to define a channel layout by entering source-detector

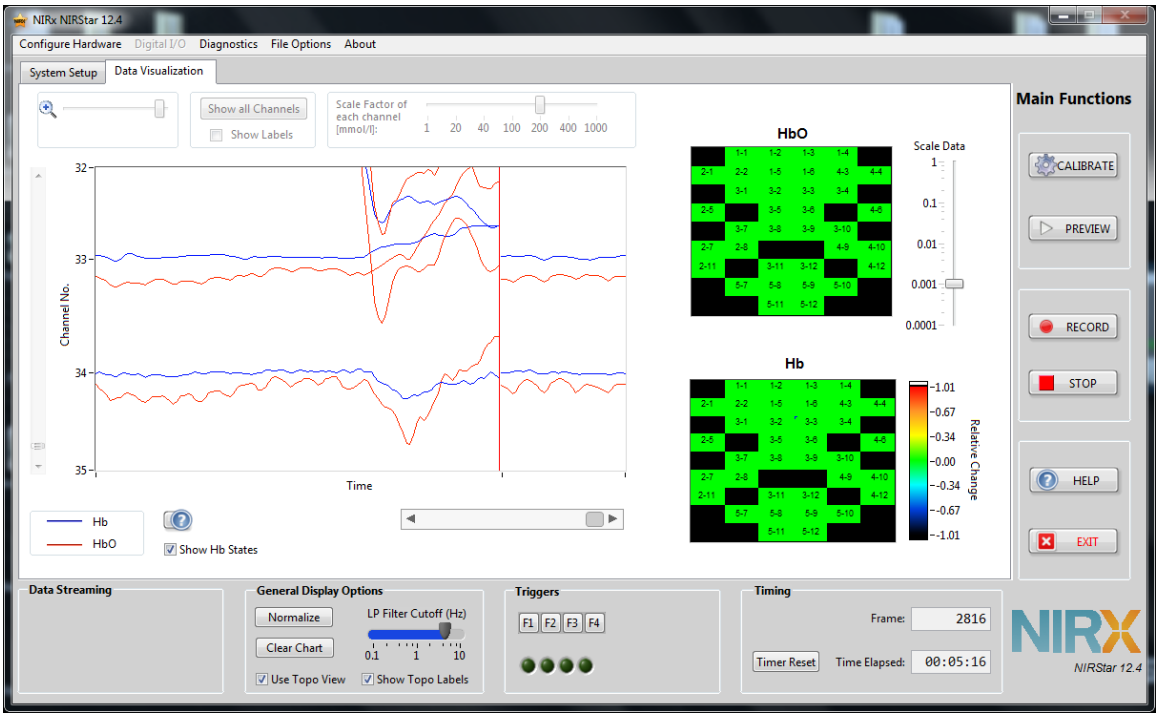

Figure 3.2: Screenshot of the NIRStar data acquisition software for the NIRScout system. The large box on the left shows streaming data by channel number. To the right of this are two boxes that illustrate relative changes in the data in terms of a user-defined geometric layout. This image was captured immediately following the completion of a data collection trial and shows not only a visible heart rate in the signals, but motion artifacts just prior to the trial's conclusion. These motion artifacts are the large jumps seen in both the HbO and Hb just to the left of the solid vertical line, which marks the passage of time.

combinations into a grid, which is then used to display both gain settings and real-time data (Fig. 3.2). This user-defined layout also defines the numerical order of the channels for display and saving. NIRStar also accepts up to four different markers, or triggers, to denote events during data collection. Triggers can either be entered manually or routed to the device from an outside source.

3.2.2 Physiological System

The BioCapture (Great Lakes NeuroTechnologies) software package enables configuration of the BioRadio hardware as well as data management. Data collected by BioRadio can be displayed, recorded, and exported into ASCII format with this software. It also holds

the capability to include manually-entered event markers with recorded data. Analysis of physiological data is an additional option with BioCapture, but such analysis is beyond the scope of this particular project.

A program called AutoHotkey was used in tandem with the BioCapture data acquisition software. AutoHotkey is an open-source utility, developed by Chris Mallet and others, that can be used to automate tasks and create macros within a Windows environment. In this case, it was programmed to automatically send keystrokes (event markers) to BioCapture upon an initial button press that was synchronized with the beginning of a fNIRS data collection trial. The timing scheme of the stimulus protocol was preprogrammed into an AutoHotkey script.

3.2.3 Data Processing and Analysis

The proprietary data analysis software package for use with NIRScout systems is called NAVI–Near Infrared Analysis, Visualization, and Imaging. NAVI utilizes the MATLAB (The MathWorks, Inc.) environment and runs on a Windows platform. This software package allows processing of raw data and visualization of signals by individual channels as well as topographically. Additionally, preliminary analysis, such as general linear model (GLM) and principal component analysis (PCA), can be viewed. For example, running the GLM utility will produce a plot of t-values for each channel and chromophore. Export is available for processed hemoglobin data–HbO, Hb, HbT, and SatO2–to be used in other software packages, particularly for more complete statistical analysis. Overall, NAVI is a powerful platform for data processing and viewing. However, it still has a few weaknesses. Model regions available for defining optode layouts are limited. If a layout is not able to be specifically defined, a dummy layout can be implemented or the user can request that NIRx Medical Technologies create a customized model. Further, despite the necessity to define and load a finite element model (FEM) with the appropriate optode configuration, this geometry is only used for topography and display purposes and not in calculating

hemoglobin concentrations. Rather, the software uses a default source-detector separation of 1 cm and a DPF of 1 for all channels. Incorporation of user-defined separations has been under development and will be included in future releases [100]. This software package was mainly used to visualize the data following preliminary collection sessions.

Another software package, Homer2 [27, 101], is a program that is free to the public and the development of which is supported by the National Institutes of Health. It is a graphical interface program that runs within MATLAB and allows its user to process, analyze, and interpret NIRS data from nearly any commercial system. It not only runs on Windows, but is also able to operate on a Macintosh platform. All that is necessary is a conversion script to transcribe the data from a certain NIRS system's format into a Homer2-compatible format, which is in the form of a *.nirs* file. Unlike NAVI, Homer2 allows the user to define the separation distance for each source-detector combination and calculates the MBLL accordingly. It also allows the user to define a separate DPF for each NIR wavelength. Additionally, the data processing stream can not only be chosen and adapted by the user, but can be exported for use outside of Homer2.

There are three levels of data processing and analysis within the Homer2 program: scan, session, and group. The scan level handles individual experimental files and provides the widest functionality. Session level can handle joint processing of all files from one data collection session on one experimental subject. Similarly, joint processing can also be accomplished at a group level with data across several sessions or subjects. Motion correction and filtering is performed at the scan level with numerous options including PCA, bandpass and wavelet filtering, and short-separation regression (SSR). The program also allows many options when visualizing the data. In the case of this project, Homer2 was used primarily for its easily-adaptable processing power and for a brief initial look at the collected data. Analysis beyond that of the Homer2 processing stream was performed using additional MATLAB scripts, which were written by the author, as well as JMP by SAS Institute, Inc.

3.2.4 Stimulus

Presentation (Neurobehavioral Systems, Inc.) was used to create and display the stimulus protocols detailed within the experimental methods of Section 4.1. Doing so was facilitated by a combination of their online support and their built-in functions for making checkerboards and gratings. Additionally, this software permitted coupling to NIRStar data acquisition in order to synchronize stimulus onset and offset times, which was done by sending event markers in the form of short pulses through a parallel port to the NIRScout hardware and onward to the data acquisition computer.

Experimental Methods

This chapter provides details on the methodology used during experimental procedures for imaging the visual and motor cortices over the entire course of the project. It includes not only the final protocol, but the evolution of methods and the reasoning behind choices and changes that have not already been described.

4.1 Visual Stimulation

The visual stimulus was created with Presentation and displayed on a 60 x 33.75 cm LCD monitor with a 60 Hz refresh rate. Each stimulus protocol utilized a combination of black-and-white (100% contrast) checkerboards to stimulate the visual cortex and a black screen to provide a rest period, or baseline. Checkerboards underwent pattern-reversal at a rate of 7.5 Hz. Both the stimulus and baseline contained a gray cross at the center of the screen, which acted as a fixation point for the participant. Every stimulus protocol began with a full minute of baseline and then cycled between checkerboards and baseline (Fig. 4.1). There were eight 30-second cycles–10 seconds of checkerboard and 20 seconds of baseline–following the initial rest period so that each stimulus protocol lasted a total of five minutes.

Each of the five stimulus protocols utilized a single spatial frequency (checker size) in order to test the sensitivity of fNIRS for the visual cortex. The checker sizes ranged

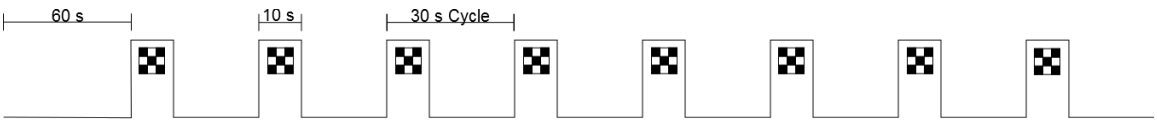

Figure 4.1: Graphical illustration of each stimulus protocol.

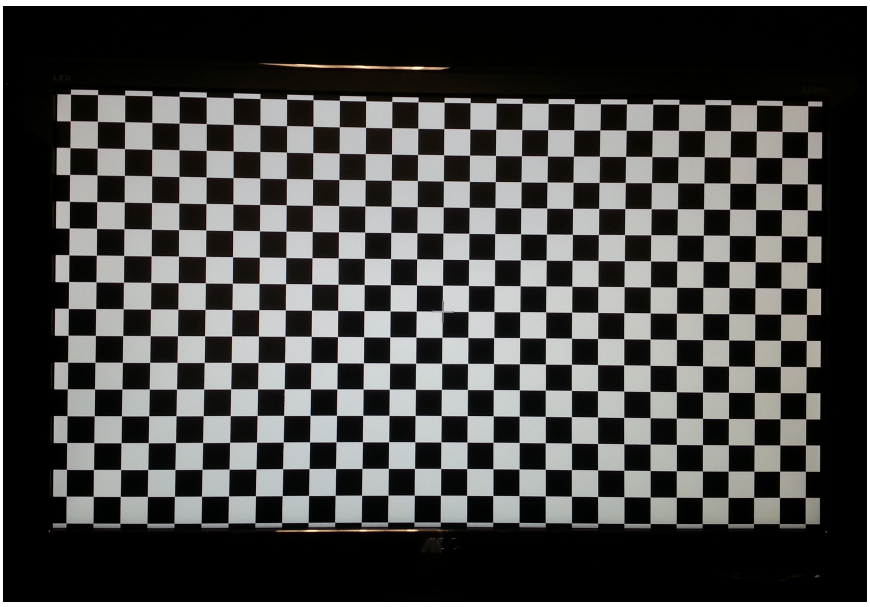

Figure 4.2: Still photograph of a checkerboard stimulus used during the visual cortex protocol. The one shown here uses the small–2 x 2 cm–checker size, which subtends the entire screen. A small, gray fixation cross is located at the center of the screen, although it is difficult to discern in the relatively small photo, and the monitor is surrounded by black cloth.

from small to large squares. An example of a single checker size is shown in Figure 4.2. One experimental run included all five spatial frequencies for a total of 25 minutes of data collection. Each subject participated in one randomized experimental run on each of three separate days to give a total of fifteen trials and 120 stimulus events per subject.

4.2 Subject Participation

A total of ten healthy adult participants were recruited from the population of Wright State University. Consent forms were obtained from all subjects prior to their participation in the study. The protocol was approved by the Institutional Review Board at Wright State

Table 4.1: Summary of study participants by gender and age. All were right-handed.

	Participants	Mean Age (years)	Median Age (years)
Female	5	23.1 ± 3.6	22.4
Male	5	24.4 ± 6.1	23.5
Total	10	23.8 ± 4.8	22.6

University and considered to be no more than minimum risk to the participants. Specific procedures and reasoning were explained to each participant and they were given an opportunity to ask questions before beginning official participation. Participants were assigned a number based on the order in which they participated in the study. In other words, Subject 1 corresponds to the very first individual on which data was collected and Subject 10 corresponds to the last.

Elements of the BioRadio system were first attached to the participant and the hub was either placed on the table or kept in his or her lap, depending upon the participant's preference. Prior to fNIRS data collection, the circumference of each participant's head was measured in order to determine the appropriate size of optode retaining cap (52, 54, 56, or 58 cm). The cap was subsequently fitted onto the subject's head and a snug fit ensured before proceeding. Usually, this required using a cap at least one size smaller than the participant's head circumference. Each participant was then asked to sit fairly still in the dark while electrode gel was applied and the optodes (five sources and twelve detectors) were placed in the optode retaining cap, as shown in Figure 4.3. Care was taken to ensure that the optodes sat flush with, and perpendicularly to, the scalp. Once acceptable, a thick fleece cap was placed over the head and optode retaining cap. Calibration was then performed to obtain gain settings. Any gain settings that were too high to achieve a reliable fNIRS signal prompted further adjustment of the optodes.

Following initial setup and optimization, the participant was asked to place his or her

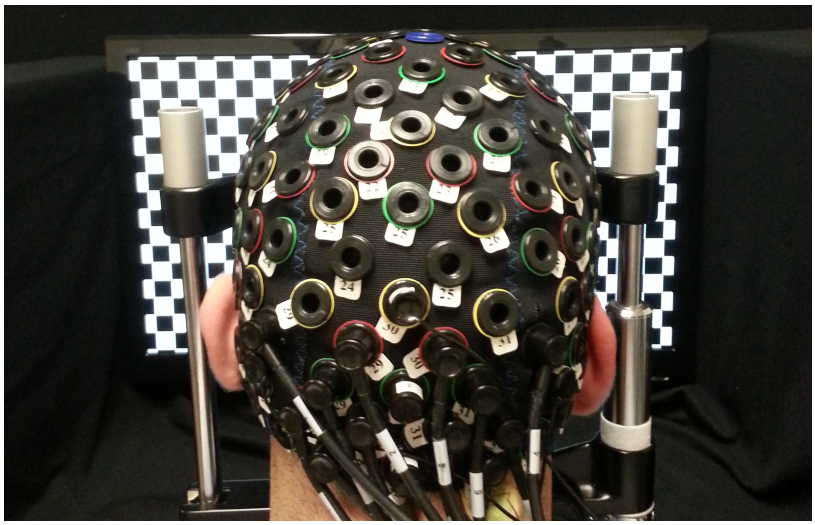

Figure 4.3: Example of the experimental setup for the visual cortex protocol (including the optode configuration), as viewed from directly behind the participant. The participant's head is supported by a chin rest, which is a fixed distance away from the stimulus display screen on which a checkerboard pattern can be observed. Five sources and twelve detectors were utilized to provide a sampling frequency of 8.929 Hz. The specific layout can be seen in Figure A.4 of Appendix A.

head upon a chin rest located at a fixed distance in front of the visual stimulus display. Then the participant was asked to focus on a cross at the center of the screen during data collection while remaining silent and as still as possible. Comments were accepted after each trial.

For the final experimental configuration in which the ten participants were used, the stimulus display was located approximately 55 cm from the subjects' eyes when their heads were supported by the chin rest. At this distance, the display subtended a visual area of 47.5° by 31.5° and, to the nearest integer, each checker subtended an area of 1°, 2°, 5°, 9°, or 18° square depending upon the trial. A schematic of equipment setup for data collection is given in Figure 4.4.

This study immediately succeeded each experimental run for the visual cortex with one for the motor cortex. That way, each participant needed to only attend a total of three data collection sessions. Additionally, placing the motor stimulation after the visual stimu-

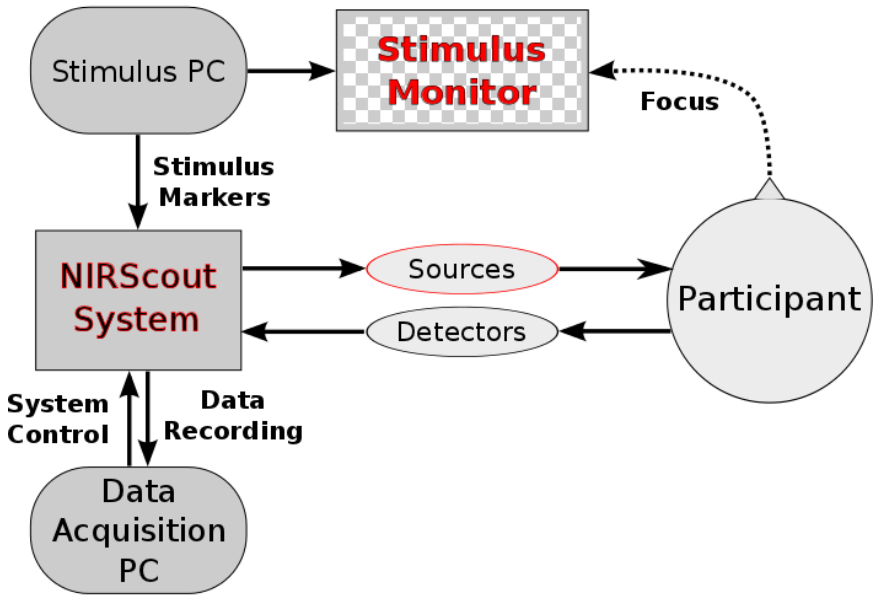

Figure 4.4: Flow chart of experimental equipment setup. Stimulus markers sent from the stimulus PC to the NIRScout system occur at the beginning of every baseline segment as well as the beginning of each visual (checkerboards) or motor (tapping/grasping) stimulus. These markers are included in recording of detector data by the data acquisition PC–the computer which also controls the NIRScout system.

lation kept the participant more alert when sitting in a dark and quiet room for an extended period of time. The participant was actually required to perform simple hand movements in this instance rather than simply focusing on a computer screen.

4.3 Motor Stimulation

Stimulation of the motor cortex was achieved via two types of hand movements: sequential finger opposition and whole-hand grasping. For each, the participant was asked to be as consistent as possible during the task while keeping the rest of their body as still as possible. Since it has been previously demonstrated that no significant differences in oxygenation changes occur for frequencies between 1 and 4.5 Hz [102], the frequency of grasping or tapping was not explicitly regulated; participants used a speed with which they felt comfortable. Prompts were given to each participant via the same method as the visual

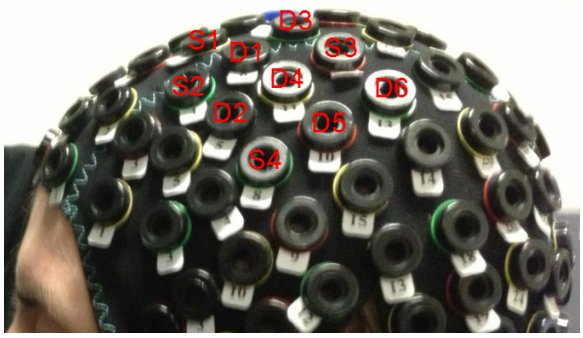

Figure 4.5: Layout of sources (*S*) and detectors (*D*) for trials involving finger opposition and grasping tasks. The layout is mirrored for the right hemisphere to give a total of eight sources and twelve detectors.

stimulus protocol (Section 4.1). However, rather than pattern-reversal checkerboards, the word "Tap" was displayed in the center of the screen. The participant was instructed to perform the appropriate task during this period of time. Three trials were conducted for each type of hand motion: both hands, right-only, and left-only. Prior to each trial, the participant was told which hand movement task to perform and on which hand(s). For movements requiring the use of both hands, the pulse oximeter was temporarily removed. Otherwise, it was kept on the index finger of the motionless hand. Similar to the case of the visual protocol, one complete experimental run consisted of a randomized set of all six hand-motion combinations. One run was performed on each of three separate days in order to give a total of eighteen trials and 144 stimulus events per subject.

Originally, the motor cortex protocol possessed the same timing as the 20-second on and 20-second off visual protocol (Section 4.4.2). However, after timing tests were completed for the visual protocol (Section 4.4.5), the timing of the motor protocol was adjusted for consistency (Fig. 4.1). Thus, the methods for the motor and visual protocols were kept nearly identical. Refer to Figure 4.5 for the 36-channel motor cortex optode configuration and Section 4.2 for additional details on setup and subject participation.

4.4 Evolution of Experimental Procedures

The specific experimental setup and procedures have evolved over the course of this research project. As the project progressed, new discoveries were made that would optimize the data collection process and enable greater consistency. In the beginning stages of the project, there were some difficulties in optode application, hardware settings, and, by extension, obtaining observable hemodynamic responses. One incarnation of the project was specifically dedicated to testing various optode arrangements and timing of the stimulus protocol. The different incarnations are detailed in the following subsections and were stepping stones to reach the final stage of the project, which was detailed in the previous sections of the chapter.

4.4.1 First Incarnation

A single visual trial in the first incarnation consisted of an alternating minute of baseline with twenty seconds of reversing checkerboards to give five total stimulations. Each individual trial lasted seven minutes and forty seconds. The checkerboards reversed at a frequency of 7.5 Hz with 100% contrast. Five different checker sizes were used and each trial utilized one of these sizes. The order of the stimulus sizes was randomized and the participant was unaware of that order. A full run of the five sizes was performed on each of three days for a total of fifteen trials and 75 stimulus events.

The participant sat with his head resting on a chin rest at a fixed distance from the monitor in order to minimize motion and to keep a constant eye-to-screen distance. The stimuli were presented on a laptop with a screen that subtended a visual area of approximately 30° x 23° when the participant's eyes were 53.5 cm away. Checker sizes were–to the nearest integer–1°, 2°, 3°, 6°, and 12° at this eye-to-screen distance. The baseline was a gray screen. However, the gray screen was found to strain the eyes, especially when staring at the monitor for such long intervals in a darkened room.

Setup in this incarnation was kept as simple as possible in an attempt to minimize duration and maximize participant comfort. Optodes were preloaded into the cap prior to the participant's arrival according to the layout shown in Figure A.1. The cap was centered and secured on the participant's head prior to the start of data collection. No gel was used. However, a fleece cover was placed over the participant's head to shield the optodes from ambient light from the monitors. A BioRadio system was borrowed from colleagues to monitor physiological factors–respiration, heart rate, and pulse oxygenation–for incorporation into analysis at a later time.

Overall, setup took approximately 20-30 minutes with 40 minutes of data collection each day. Visual motion after-effects were noted by the participant during some of the trials. These occurred when the stimulus switched from checkerboards to baseline and were greatest in length for the smaller checker sizes. Effects were negligible for larger sizes. The participant also noted that the gray screen used as a baseline was actually hard on his eyes. In addition, the length of time spent focusing on the monitor in a darkened room not only caused him to feel sleepy, but also dried out his eyes. Dry eyes tend to cause excessive blinking, which could potentially confound the study.

4.4.2 Second Incarnation

For the next experiment, the visual stimulus was reprogrammed so that the initial baseline for each trial still lasted a full minute, but each baseline thereafter was only twenty seconds–the same time span as the flashing checkerboards. This thus reduced the overall duration of data collection from 7 minutes and 40 seconds to 4 minutes and 20 seconds per trial. Further, the baseline was changed from a gray screen to a black screen so that it was easier on the participant's eyes and reduced the chance that it would cause activation in the visual cortex.

A new, slightly larger screen was also employed during this round of data collection. At an eye-to-screen distance of 52.5 cm, the screen subtended a visual area of approxi-

mately 36° x 30° with checker sizes of 1°, 2°, 4°, 9°, and 16°. Additionally, a smaller optode cap–a 2 cm difference in circumference–was used on the participant for better contact between the optodes and the scalp. Electrode gel was applied after placing the cap on the participant's head and before placing the optodes in the cap's receptacles. This allowed hair to be moved aside as well as reduced any air interface between the optodes and skin. No BioRadio system was employed.

The stimulus utilizing small (2°) checkers produced two different temporal frequencies during the data collection. This was most likely due to the age–and, therefore, lack of processing power–of the computer used for presenting the visual stimulus. In order to send the timing triggers from Presentation to NIRStar, a parallel port is required. Since newer computers, such as the ones then available to the research group, no longer tend to come with parallel ports, an older computer was necessary. However, after this frequency issue, a search began for a more powerful computer with a parallel port.

A mirroring effect–in which signals are mirror images of each other and completely uncorrelated with stimuli–as well as high voltage values were seen in many of the channels upon preliminary analysis (Fig. 4.6). This indicates detector saturation. When this occurs, NIRStar should automatically reduce the gain settings. However, this did not happen. It was later discovered that the hardware settings for the NIRScout system were somehow incorrect, which was deemed the cause of the mirroring effect in this instance. A single visual trial was then performed to ensure that the issue had been resolved.

4.4.3 Third Incarnation

The same procedures as the latter incarnation were used for this single visual trial with the medium (4°) checkerboard size. Data was processed immediately afterward and it was found that the mirroring issue had indeed been resolved. A simple finger-tapping trial was subsequently performed as an additional validation method. This served as an extra check

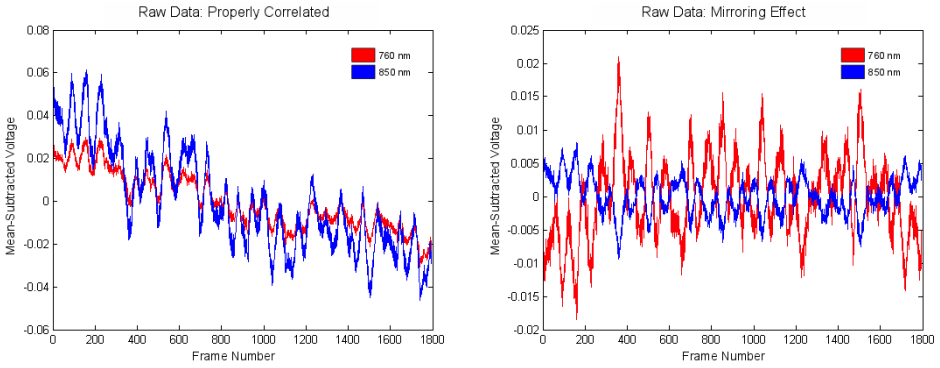

Figure 4.6: Sample raw data from the second experimental incarnation. A normal data channel is pictured on the left and a so-called mirrored channel on the right. Normally, the raw data exhibits a positive correlation between the two NIR wavelengths. If, for example, the hardware settings are incorrect and the mean voltage is too large, then a strong negative correlation can result. This gives rise to the mirroring effect, which survives processing. In these graphs, the specific correlations are r = 0.97519 and r = -0.99852, respectively.

to ensure that the NIRScout system (and software) was working correctly, even if optimal signals were not obtained from the visual cortex. As with the visual stimulus protocol, the motor cortex protocol cycled between twenty seconds of stimulus and twenty seconds of baseline for five complete cycles. The optode configuration was also kept simple for this brief trial with two sources and four detectors (eight channels) oriented over the motor cortex of the left hemisphere (Fig. A.2). Tapping was performed with the right hand. Audio cues prompted the participant to begin and cease tapping. Event markers were manually entered through the data acquisition computer.

4.4.4 Fourth Incarnation

A new physiological system (BioRadio) was purchased for the Wright State University fNIRS Laboratory in order to monitor and record respiration, heart rate, and peripheral oxygen saturation during data collection on the visual and motor cortices. The additional physiological data will be incorporated into future analysis of the fNIRS data.

For this experimental incarnation, the old laptop was replaced with a desktop PC that has a parallel port. This desktop has a better processor than the laptop and, therefore,

would not produce the same frequency inconsistencies. It also provided better support for a monitor upgrade. Both the new monitor and chin rest were fixed to a table and the surrounding area was lined with black cloth. The black cloth allowed the participant to focus completely on the monitor without any distractions from the peripheral field of view. It also reduced ambient light from the data acquisition monitors which could reflect off the light-colored table and walls and enter the participant's eyes. This setup produced an approximate 55 cm eye-to-screen distance with a corresponding visual area of 47.5° x 31.5°. Checker sizes were 1°, 2°, 5°, 9°, and 18°, to the next integer.

For analysis purposes, the number of channels included in data collection was expanded to include several with slightly longer source-detector distances without changing the actual optode configuration. The expanded visual cortex layout included 35 channels with an average source-detector separation of about 2.9 cm. A dark adaptation period was also added to the experimental setup procedures. The participant's eyes were closed and covered with heavy cloth while the experimenter set up the BioRadio system and optode cap, which generally took at least 20 minutes. Visual stimulus protocols remained otherwise unchanged for this incarnation.

The simple motor protocol used in the previous incarnation, however, was greatly expanded (mostly as a consequence of the favorable results obtained during the third incarnation). First, the optode layout was adapted to include both hemispheres and employ all eight sources and detectors (Fig. A.3). Then, the number or trials was increased to six for each of three data collection sessions. Like the checkerboard sizes, motor tasks were randomized. Each trial used one of the six possible combinations between task type and hand(s) used: whole-hand grasping, sequential finger opposition, left hand, right hand, and both hands. The timing of stimulus and rest periods remained the same, but verbal cues were replaced by on-screen prompts.

4.4.5 Fifth Incarnation

Preliminary results from the previous incarnation prompted reevaluation once again. Since acceptable results were obtained for the motor cortex during the fourth incarnation, this fifth incarnation focused on optimization of the visual cortex portion of the study. As such, no data was collected for the motor cortex during this time. First, smaller optode retaining caps were ordered to ensure a snug fit over the occipital region, especially on more petite individuals. A fixation cross was added to the visual stimulus protocol to further aid the participant's ability to focus. Additional data processing and analysis software was investigated and the possibility of writing such a program from scratch was also explored.

When hemodynamic responses could not be obtained on a different member of the research group during simple trials, the hardware and data acquisition software received much attention. After running a few diagnostic tests, it was determined that both pulse and motion could be seen in real-time with the data acquisition software. Channels in which pulse could be observed, then, were deemed capable of measuring hemodynamic responses during data collection.

Following the hardware validation, new optode layouts were designed and tested for the visual cortex. The objective was to determine an optimal layout that was more localized to that region without necessarily utilizing every available source and detector. Five different layouts were tested using the twenty-second on/off medium (5°) checkerboard stimulus on a single subject (refer to Figs. A.4-A.8 in Appendix A). The one with the greatest number of usable channels and least number showing detector saturation due to high gain was chosen. Further, in order to test SSR with Homer2, the optode retaining caps were modified to include two short-distance channels. Although a separation of 0.8 cm is recommended for this procedure [103], the NIRScout optodes do not physically allow separations less than about 1.3 cm. Additionally, the first two rows of optode holders were removed from the caps to decrease unnecessary pressure against the forehead and, hence, increase comfort of the participant.

Table 4.2: Summary containing the number of trials and participants used in each experimental incarnation, which are detailed in Sections 4.1 to 4.4. Some participants were used for optimization in multiple incarnations of the experiment; Subjects 4-10 only participated in the final incarnation.

Incarnation	Number of Participants	Subject Number(s)	Cortical Region	Total Number of Trials
1	1	1	Visual	15
2	1	1	Visual	15
3	1	1	Visual	1
			Motor	1
4	2	1,2	Visual	5 per subject
			Motor	5 per subject
5a	1	3	Visual	5
5b	1	3	Visual	3
5c	1	3	Visual	2
Final	10	1-10	Visual	15 per subject
			Motor	15 per subject

Using the updated layout for the visual cortex, stimulus timing tests were then performed for additional protocol optimization. Three trials were run, again with the medium checkerboards, each using a randomized order of stimulus durations. Six different durations were used–1, 5, 10, 15, 20, and 30 seconds–with the usual twenty-second baselines between and minute baseline initially. It appeared that a decent response could be seen with as little as a ten-second stimulus. Timing optimization was then carried one step further in order to test the length of the inter-stimulus baseline. One trial was run using a ten-second on and ten-second off pattern and another using a ten-second on and twenty-second off pattern. Each protocol was designed to last five minutes. This means that, following the initial minute of baseline, twelve cycles of ten-second on/ten-second off or eight cycles of ten-second on/twenty-second off were included in a trial. It was deemed that the ten-second inter-stimulus baseline did not allow enough time for hemoglobin concentrations to return to pre-stimulus levels. Hence, the inter-stimulus baseline was kept at twenty seconds.

4.5 Further Reasoning

According to ISCEV standards for clinical VEP, the visual display should provide a field of view (FOV) that is at least 15° along the narrowest dimension. All incarnations met this criterion. In particular, the 55 cm eye-to-screen distance–which falls within the 50-150 cm recommended by ISCEV–used in the final incarnation allowed more than double the minimum FOV. This point fits their additional suggestion that investigations using multiple channels (a single channel is standard) for the study of visual pathway dysfunction should use a 30° FOV. Since the ISCEV defines small checkers as subtending 0.25°$\pm$ 20% arc in a given FOV and large checkers as 1°$\pm$ 20%, all checkers used throughout this project are considered large (or beyond) by their standards. From a review of literature, large checker sizes combined with high pattern-reversal rates (i.e., 4-8 Hz rather than the 1 Hz for ISCEV) will produce a good level of activation. The fixation cross implemented at the center of the visual stimulus display is positioned so that it is at the corner of four checker squares, which again agrees with ISCEV standards.

Consistency is of utmost importance for a validation project such as this; as many parameters as possible should be carefully controlled. Both the chin rest and the stimulus display were fixed to the table on which they sat. The height of the adjustable chin rest was also fixed to prevent movement of any kind. Only the chair used by the participants was left adjustable for their comfort. Keeping the former parameters constant provided consistent eye-to-screen distances and ensured the participant's eyes were centered with respect to the visual stimulus display.

One important limitation of using any type of visual protocol is the experimenter's lack of control over the subject's attention to presented stimuli [104]. Waning focus, or wandering eyes, could decrease the level of hemodynamic response produced in the visual cortex and in the visual association area which surrounds it. It is primarily for this reason that data collection for this project occurs in a quiet, darkened room and that black fabric lines the periphery of the screen on which the visual stimulus is presented. This is also the

reason for the gray fixation cross that was present for the duration of both the checkerboards and black baseline screen.

A process known as bleaching is responsible for the visual after-effects sometimes reported by subjects upon switching from the checkerboards to the black screen. Especially with the longer stimulus durations and smaller checker sizes while sitting in a dark room, the cells in the retina can get saturated. It is this saturation that may leave a lingering visual impression on the retina. Normally, this only lasts a few seconds at most, but contributed to the decision to shorten the duration of the checkerboard stimuli while keeping the longer baseline duration. The ten-second checkerboard duration does not result in much bleaching and the twenty-second baseline allows ample time for levels to return to normal, regardless of bleaching. Additionally, NIRS signals are known to fluctuate during states of stimulation as well as rest [105, 106]. A full minute of initial baseline was chosen for this reason in order to obtain a good estimate of variance as well as to determine prestimulus levels to see if hemoglobin levels were actually returning to normal.

Dark-adaptation is the process by which visual pigments in the retina recover from photobleaching due to activities in the light. Sitting in the dark, or with one's eyes closed, for 20-30 minutes allows a person to attain a dark-adapted state, during which the retina is highly sensitive. This means that the visual cortex should receive a greater amount of visual data, which would in turn result in greater cortical activation and, therefore, blood flow.

Either a fleece cap to cover the optodes or a tightly tied bandanna with a piece of fleece material draped over the participant's head was used for two reasons. First, it provided extra pressure to hold the optodes in contact with the scalp. Second, it was deemed important to protect the detectors from any ambient light [107] in the room–namely, the computer monitors used for data acquisition and stimulus presentation.

Methods of Analysis

As with any type of measurements, some level of uncertainty, or error, will be present. This is especially true of biological signals–in this case, hemoglobin levels measured with fNIRS. There, of course, is natural variability occurring within the dynamic human body. Blood especially is in constant motion. It is this variability that tends to prompt the use of a long initial rest period in fNIRS measurements. The initial rest period gives a baseline for comparison and provides an estimate of variability.

Estimating hemoglobin concentrations from the change in light intensity (Section 2.1.3) at two or more wavelengths carries an error which stems from the change in absorption coefficients. The measured absorption coefficient can be written as

$$\mu_a^\lambda = \epsilon_{HbO}^\lambda \Delta HbO + \epsilon_{Hb}^\lambda \Delta Hb \tag{5.1}$$

or

$$\mu_a = \epsilon \mathbf{C} \tag{5.2}$$

in matrix form. This can of course be rewritten in order to solve for the concentration changes in HbO and Hb:

$$\mathbf{C} = (\epsilon^T \epsilon)^{-1} \epsilon^T \mu_a. \tag{5.3}$$

The change in absorption coefficients for each wavelength is stored in the vector μ_a, extinction coefficients of HbO and Hb (again for each wavelength) are stored in the matrix ϵ, and

calculated concentration changes are stored in the vector **C**. Where random error present in μ_a is denoted by $\boldsymbol{\sigma_\mu}$, the error $\boldsymbol{\sigma_c}$ in concentration changes is then propagated as [108]

$$\boldsymbol{\sigma_c}^2 = (\epsilon^T\epsilon)^{-1}\epsilon^T\boldsymbol{\sigma_\mu}((\epsilon^T\epsilon)^{-1}\epsilon^T\boldsymbol{\sigma_\mu})^T. \tag{5.4}$$

5.1 Data Filtering

Physiological noise in fNIRS signals can be caused by factors such as heart rate, respiration rate, and bodily motion. Heart and respiration rates are usually eliminated using a simple bandpass filter since their frequencies are generally much higher than the typical hemodynamic response. Bodily motion, on the other hand, can be more difficult to filter out of the signal. While subject motion was kept to a minimum in this study, participants may have moved or shifted in their chairs during data collection. As a precaution, filtering was performed to reduce or remove any large data variations caused by motion. Motion artifacts tend to appear as sudden large spikes within the usually slow hemodynamic signal changes.

There are several potential techniques available for the reduction of physiological noise in fNIRS signals. The choice of technique generally depends upon the situation such as the type of instrumentation being utilized as well as the type of task being investigated. As such, there is not yet a "golden standard" for physiological noise reduction at this point in the evolution of fNIRS.

One reduction technique utilizes assumptions of independence or orthogonality to differentiate between physiological noise and actual functional brain signals. Another technique involves taking physiological measurements simultaneously with fNIRS. This procedure, however, requires additional equipment such as respiratory belts, pulse oximeters, and ECG electrodes. It also operates on the assumption that these peripheral measurements are at least similar to their counterparts in the brain–an assumption which is currently under

investigation [by collaborators]. Yet a third technique is SSR. SSR requires using a set of very short source-detector separations that will only image the superficial regions (scalp and skull) in addition to the normal source-detector separation lengths which image the brain. By averaging the signals from the channels with short separations, the superficial signals can then be removed from longer-distance channels by a linear regression model. The challenge here is that many optode caps do not have the necessary receptacles for these shorter-distance measurements on the adult head and not all optode designs allow it. A fourth technique employs adaptive filtering, of which there are numerous types.

Despite the many available options for filtering signals, the one chosen in this fNIRS study was a wavelet filter. In the wavelet filtering method of Molavi and Dumont [109], motion artifacts are considered outliers. If they are deemed to have a probability less than α of being part of the true hemodynamic signal, then the filter is applied. Otherwise, the data is left as-is. No auxiliary signals are needed. Since this method takes the entire time series (data trial) into account and uses probability rather than a hard threshold, it adapts to the variability of each individual dataset. However, this also means that data processing must take place offline and that this particular method cannot be applied in real time.

Wavelet filtering has shown more stability and consistency than a Kalman filter or PCA, for example, and it does not require any strict assumptions or the inclusion of additional physiological measures. Further, wavelet filtering has proven to be effective in the reduction of low-frequency oscillations (Section 7.3.1) and motion artifacts that are often present in fNIRS signals [110]. The specific value of the tuning parameter ($\alpha = 0.10$), which is a probability threshold, was chosen based upon precedent [110, 111, 109]. In Homer2, the wavelet filtering function is based upon the 2012 manuscript by Molavi and Dumont [109] and requires MATLAB's wavelet toolbox. Following application of the wavelet filter to each dataset, a simple bandpass filter was also used. This allowed elimination of physiological noise such as heart rate as well as any very low frequency system drift without removing artifacts that may be related to hemodynamic response.

5.2 Data Processing

In order to view and process the data obtained using the NIRx hardware and software, the data files first needed to be converted into a Homer2-compatible format. A conversion script written in MATLAB used the raw data from each wavelength (.wl1 and .wl2 files) as well as the stimulus event markers (.evt file) which were saved at the conclusion of each trial. Additionally, the script read in the number of sources and detectors utilized plus the device's sampling frequency to create a time vector. Built into the script is a 3-D matrix to define coordinates (in mm) for each source and detector, which the user must define for each optode arrangement. Homer2 uses these coordinates for visual display and calculation of concentration changes via the MBLL. The conversion script can also be utilized to specify which of the total number of data collection channels will be imported into Homer2 for further processing and analysis. This script was adapted to be as automated as possible.

Next, a data processing stream was created using Homer2 and exported for use in an automated, stand-alone MATLAB script. The Homer2 functions operate by first converting raw intensities at each wavelength into optical density values. Following this conversion, filtering was performed–in this case both wavelet and bandpass. Wavelet filtering for motion and oscillation correction used the default interquartile range (IQR) of 1.5, which corresponds to the $\alpha = 0.10$ mentioned above. Standard bandpass filtering was performed using a highpass filter of 0.01 Hz and a lowpass filter of 0.5 Hz. The filtered signals were then used to calculate concentration changes in HbO and Hb via the MBLL as described in Section 2.1.3 with the DPF values described in the following section. Figure 5.1 illustrates the order of data processing. Once concentration changes were calculated, block averages could be found if desired. Since the processing stream was used as a stand-alone script, an automated data export was added. This extracted values such as the peak and baseline for each stimulus event in each defined data channel and saved them in a file–along with the entire time series, individual stimulus responses, and block-averaged data–that could

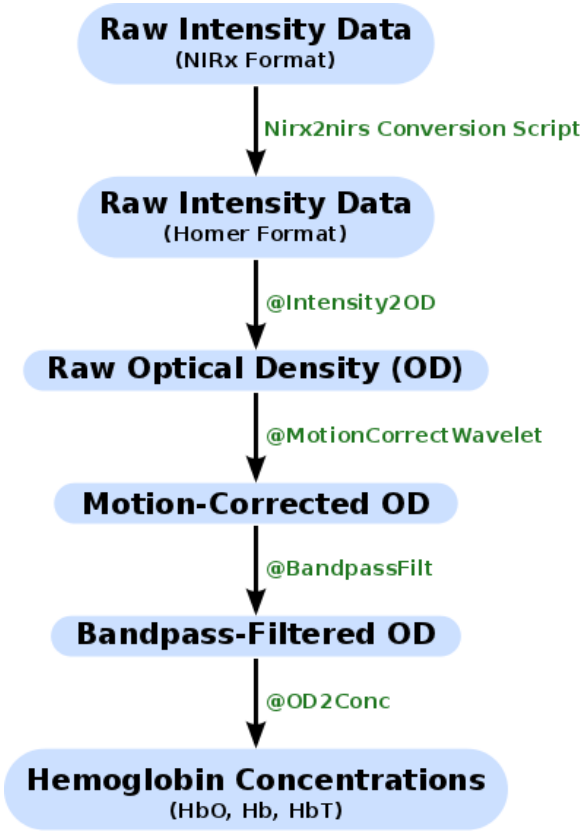

Figure 5.1: Flow chart illustrating the general data processing sequence. Raw data was first converted into a Homer2-specific format. The @ symbol indicates a built-in Homer function and was included in the succeeding stand-alone data processing script. (The format conversion and data processing were performed using two separate MATLAB scripts.)

be used later for statistical analysis.

5.3 Choice of DPF

The choice of DPF values is a topic of some disagreement. It is commonly known that the DPF is a function of wavelength; it also varies with cortical region and age. In other words, the DPF associated with a wavelength of 760 nm for the frontal cortex of a 55-year-old will not be the same as that of 850 nm for the occipital region of a 20-year-old, for example. Skin color does not appears to be a factor [112] in this case. Different NIRS data processing programs use different default values for the DPF. One references Essenpreis et al. [113] for its wavelength-dependent values–7.15 and 5.98 for wavelengths of 760 and 850, respectively. Another uses a default value of 6.0 regardless of the wavelength. This is due to findings that, for source-detector separations of more than 2.5 cm, the DPF remains essentially constant at that value [42, 114].

Most reported DPF data represents the frontal region, which could perhaps be due to lack of hair and an abundance of cognitive studies. A 1995 manuscript [112] presents equations for calculating the DPF in the frontal region based upon age (A) for four fixed nanometer wavelengths.

$$DPF_{690} = 5.38 + 0.049A^{0.877} \tag{5.5}$$

$$DPF_{744} = 5.11 + 0.106A^{0.723} \tag{5.6}$$

$$DPF_{807} = 4.99 + 0.067A^{0.814} \tag{5.7}$$

$$DPF_{832} = 4.67 + 0.062A^{0.819} \tag{5.8}$$

Using the mean age of participants in this current study and a cubic fit, the DPF values were interpolated for 760 and 850 nm and found to be 6.14 and 5.09, respectively. This can be used in conjunction with data from a multi-region study [115] to obtain approximations

for the motor and visual regions of the brain. In that study, it was found that values for the frontal and motor regions were essentially the same. Hence, 6.14 and 5.09 can also be used for determining hemoglobin concentration changes within the motor cortex.

Zhao et al. used three wavelengths in their study. Thus, a quadratic fit was used to once again interpolate values. Ratios were calculated to see how much the DPF increased between the frontal and occipital regions and then used to determine an approximation for determining hemoglobin concentration changes in the visual cortex. In this case, the values for a mean age of 23.8 years and wavelengths of 760 and 850 nm are 7.57 and 6.26, respectively.

5.4 Post-Processing

All processed data began with qualitative analysis to determine when and where hemodynamic responses could be observed. Once that was determined, statistical analysis could be performed for a quantitative perspective. The most consistently active channels were chosen for the quantitative analysis of data from each participant to keep the statistical power as large as possible. All quantitative analysis of the observed hemodynamic responses began with one-way ANOVA. Tukey's test was then administered in order to compare all possible differences between factor levels (stimulus types) and data collection blocks (sessions). Unlike a standard t-test, Tukey's corrects for an experiment-wide error rate in order to reduce type I error. In other words, it is more conservative. Since Tukey's test assumes a normal distribution, this was double-checked as well.

Tukey's test performs pairwise comparisons between groups of equal sample sizes. This, however, is not always the case since not every stimulus event may have elicited an observable response. JMP happens to use an adapted version of Tukey's test, known as the Tukey-Kramer HSD, which allows unequal sample sizes like those involved here. Matched pairs was used for any additional desired comparisons between hemispheres or a specific

pair of subjects.

Originally, two channels were chosen as the main focus for comparison: one on each side of the midline and that are presumed to directly overlie the primary visual cortex. Since the experiment utilized a symmetric test pattern and both of the subject's eyes were kept open, the signals received from both hemispheres should be similar–barring any visual dysfunction, of course. As such, the results from these two channels could be analyzed separately or they could be combined in order to give a greater quantity of data points for statistical analysis. It is more prudent, however, to analyze these separately since some studies have discovered more activation in the left hemisphere than the right. After qualitative analysis, however, it was realized that selecting these channels across all participants would result in very few statistics.

5.4.1 Hemodynamic Response

For statistical analysis, the change between each pre-stimulus baseline and peak response was compared. It has been shown that fNIRS signals take approximately ten to twelve seconds to return to normal levels after stimulation ceases. Hence, baseline was calculated as the average concentration values over the ten-second period before each stimulus onset, which also corresponded to the period of time ten to twenty seconds after the previous stimulus ended. As discussed in Section 2.4.2, literature indicates that HbO signals reach peak approximately seven to ten seconds after stimulus onset. Therefore, peak value was defined as the extremum reached between five and fifteen seconds after onset of the stimulus. Since each trial carried out during data collection presented eight stimulus events, there are eight data points for each factor level and for each randomized block (collection session). These extracted values can also be compared with those obtained from block-averaging the time series.

Comparison Between Stimuli: Sensitivity

To assess the sensitivity achievable by fNIRS of the visual cortex, the responses to the five different checker sizes were first analyzed for each session of each participant. The responses for each checker size were then pooled across the three data collection sessions for each participant. Finally, responses for each checker size were pooled across all sessions and participants to give a grand overall comparison.

Comparison Between Blocks: Robustness

To assess the robustness, or repeatability, achievable, the responses between each of a participant's data collection sessions were the main point of focus. The data was analyzed to see if statistical differences could be observed from a quantitative standpoint. Data was also compared qualitatively between the sessions for each participant. And, as with analysis of sensitivity, a grand overall comparison between sessions was performed.

Comparison Between Subjects

For a comparison between the responses of the ten participants, a combination of the above analysis methods was used. In other words, qualitative and quantitative results for the hemodynamic responses obtained from each participant were studied. Factors such as hair type, optode cap fit, and reported alertness levels were considered to help explain any differences seen between overall results of individual participants. Attention was also paid to measurements of sensitivity and robustness.

Table 5.1: Summary to help illustrate the methods of experimental analysis used on the data from each participant in this project. Tukey's test was employed following one-way ANOVA in order to determine if the observed mean response magnitudes differed across any factor levels or blocks.

Sensitivity: One-Way ANOVA

Region	Factor Level	Data Points / Session	Total Possible Data Points	Test
Motor	Tapping	8 HbO, 8 Hb	24 HbO, 24 Hb	Tukey
	Grasping	8 HbO, 8 Hb	24 HbO, 24 Hb	
Visual	XS checker	8 HbO, 8 Hb	24 HbO, 24 Hb	Tukey
	S checker	8 HbO, 8 Hb	24 HbO, 24 Hb	
	M checker	8 HbO, 8 Hb	24 HbO, 24 Hb	
	L checker	8 HbO, 8 Hb	24 HbO, 24 Hb	
	XL checker	8 HbO, 8 Hb	24 HbO, 24 Hb	

Robustness: One-Way ANOVA

Region	Data Block	Data Points / Factor Level	Total Possible Data Points	Test
Motor	Session 1	8 HbO, 8 Hb	16 HbO, 16 Hb	Tukey
	Session 2	8 HbO, 8 Hb	16 HbO, 16 Hb	
	Session 3	8 HbO, 8 Hb	16 HbO, 16 Hb	
Visual	Session 1	8 HbO, 8 Hb	40 HbO, 40 Hb	Tukey
	Session 2	8 HbO, 8 Hb	40 HbO, 40 Hb	
	Session 3	8 HbO, 8 Hb	40 HbO, 40 Hb	

Results

This chapter describes qualitative and quantitative results of the project. It begins with the single data trial from the third experimental incarnation (Section 4.4.3), details a concurrent motor cortex study, and proceeds to the original heart of this research: the visual cortex. Results which are not explicitly reported within this chapter may be found in Appendix B.

6.1 Preliminary Single Trial

In the third experimental incarnation, a single trial each for the visual cortex and the motor cortex were performed (on a single participant) using five repetitions of a twenty-second stimulus followed by a twenty-second rest period. Of the five stimulus events for the visual cortex, only two (40%) showed the typical increase in HbO–and corresponding lower-magnitude decrease in Hb–that is associated with cortical activation. Additionally, prominent oscillations, with amplitudes on the order of the observed response, were observed in the HbO signal for one of these two events. The other three (60%) events actually displayed a decrease in the amount of HbO at the onset of the visual stimulus with little to no change in the Hb level. There was no discernible pattern to the order of these stimulus-induced HbO increases and decreases.

For the simple eight-channel configuration (Fig. A.2) for the single motor cortex trial, a small increase in HbO and decrease in Hb was seen in several channels. However, one channel showed significantly more activation than the others. This channel was presumed

to lie directly over the portion of the primary motor cortex that is responsible for hand motion. Moving one optode receptacle location inferior to this, then, would have corresponded to the portion responsible for finger motion. For this most active channel, all five stimulus events displayed the typical hemodynamic response. The response induced by the first stimulus event was slightly less than half the magnitude of the other four. Quantitative analysis was not carried out on visual or motor data from the preliminary trial due to small sample sizes.

6.2 The Motor Cortex

Since trials on the visual cortex involve stimulation of the entire visual field with both eyes open, analysis of the motor cortex trials, for consistency, was limited to those involving both hands simultaneously performing a task. In other words, one trial of each whole-hand grasping and sequential finger opposition was included per session to give a total of six trials per subject (two trials for each of three sessions).

6.2.1 Hemodynamic Response

An example of elicited hemodynamic responses is shown in Figure 6.1. Representative responses, which were not necessarily of the same quality, for all other participants are given in Appendix B. As expected from motor trials performed during the fourth experimental incarnation (Section 4.4.4), the most active and consistent channels overall were centered around channels 3-6 and 7-12 (Fig. A.3). The largest number of events and channels in which a hemodynamic response was observed occurred for Subjects 1 and 2. Both Subject 6 and Subject 7 also had more than 40 events in which a response was observed. Subjects 5 and 8 had the fewest number of events showing activation. The fewest total active channels were seen with Subjects 8 and 10, which were followed closely by Subjects 4 and 5. For a

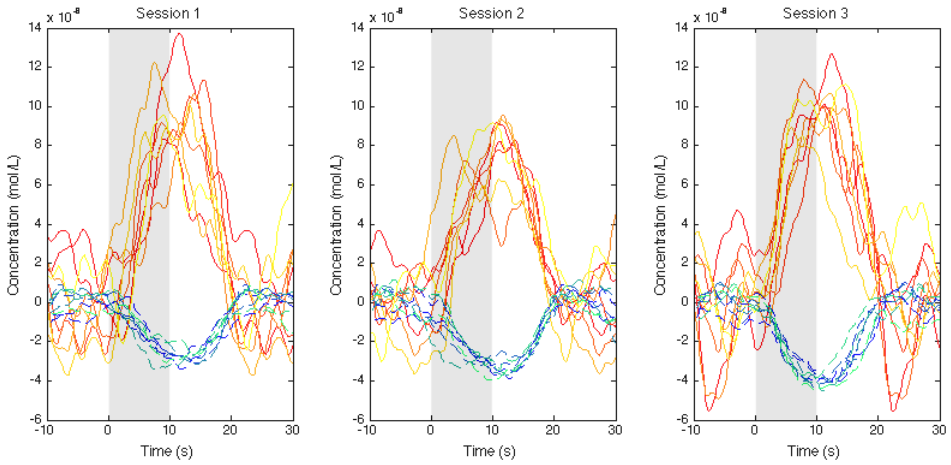

Figure 6.1: Hemodynamic responses for three trials of the finger opposition task–one from each data collection session–for Subject 1. All eight stimulus events from each trial are overlaid on a single graph for a representative channel. HbO curves range from red (first event) to yellow (eighth event) and Hb curves range from blue to green. The shaded region indicates the duration of the stimulus.

visual comparison, these data are summarized in Figure 6.2, in which they are also broken down by session.

Subject 1 For the first participant, a hemodynamic response was observed in all six trials and in an average of 20 (55.6%) of the 36 total channels per stimulus event. Some responses exhibited a double-peak phenomenon, which survived block averaging. Timing of the responses often varied from event to event. For some stimulus events, the HbO began to increase at the same time that Hb began to decrease. For others, Hb did not to decrease until 1-2 seconds after HbO began to increase. In addition, a brief prestimulus increase in HbO was often observed to begin 2-3 seconds prior to the start of the finger opposition or grasping task. Figure 6.1 illustrates the measured responses for the finger opposition task across three data collection sessions.

Subject 2 Like Subject 1, hemodynamic responses were observed in all six trials for this participant, but the average number of active channels was slightly lower at 18 (50%) out

of 36. However, trials involving the grasping task resulted in much noisier signals with concentration changes that were generally smaller in magnitude, although the differences did not reach significance. Refer to Figures B.1 and B.2 for a comparison of the tasks. In many cases, a small HbO increase was observed to begin 3-4 seconds prior to the beginning of the task. The Hb remained essentially constant during this time. This participant also presented a 1-2 second lag in the Hb response, which was most noticeable for the first trial of the finger opposition task. The double-peak phenomenon was also present in many of the responses. A larger peak was observed to reach a maximum between 5 and 8 seconds after beginning the task. The second and smaller peak was observed to reach a maximum 2-3 seconds after completing the task.

Subject 3 Qualitatively, the signals analyzed for this participant were very noisy with rather large oscillations present in the HbO signal. By comparison, the level of Hb barely changed. The period of these large oscillations was 10-12 seconds and their magnitude was so great that, in nearly all events, any possible hemodynamic response was obscured. In the responses that were actually distinguishable for this participant, a prestimulus increase in HbO appeared as its own small peak rather than a shoulder attached to the larger peak. The concentration of Hb remained constant during this prestimulus time period. An overall average of 14 channels (38.9%) showed activation for this participant.

Subject 4 For this participant, there were fewer channels which showed activation: an average of only 6 (16.7%) per event. Three or four channels presented as random noise in each session. In many of the remaining data channels, oscillations like those for Subject 3 obscured any hemodynamic response that may have been present. The most consistent channels were located within the inferior portion of the optode arrangement and were associated with sources 4 and 8.

Subject 5 Only one of the six trials for this participant showed an observable response for most events that was not obscured by noise or dominant large-magnitude oscillations. This trial involved the sequential finger opposition (tapping) task and a response was observed in an average of 19 channels (52.8%) per event. By comparison, the overall average of active channels for the six trials was only 7 (19.4%) of the 36 total channels per event. For the trial in which a response was observed for the majority of events, one large peak in the HbO reached its maximum between five and six seconds after beginning the finger tapping task for five of the eight events. A second peak reached maximum between two and five seconds after completing of the task. In three of the events, only the second peak was observed. In one, both peaks were present. Block averaging preserved both peaks as well as a prestimulus shoulder that was observed in three of the events.

Subject 6 Overall, the HbO and Hb signals obtained from this participant looked better than the previous three (i.e., Subjects 3-5) and the average number of active channels per event was 9 (25%). The grasping trials were very noisy from event to event, but block averaging resulted in a large peak that resembled a hemodynamic response. For the three trials which involved tapping, either a double peak was present, a single peak during the stimulus, or a single peak after. The double peak survived block averaging and a prestimulus increase in HbO was observed in two of the trials.

Subject 7 An average of 15 channels (41.7%) per event showed activation. Signals were dominated by oscillations, which survived block averaging, in two of the six trials. Both single and double peaks along with a prestimulus increase in HbO were seen in trials containing observable responses.

Subject 8 Dominant oscillations were once again present to obscure hemodynamic responses. These oscillations also survived block averaging. Several channels for each session contained random noise and others exhibited a mirroring phenomenon. The overall

average number of channels showing an observable hemodynamic response was 5 (13.9%) of 36 channels.

Subject 9 With an average of 9 (25%) per event, the number of active channels for this participant was slightly higher than Subject 8. Several channels showed random noise for each trial. Dominant oscillations for this subject displayed a period of approximately 8 seconds. Tapping trials displayed a response for most stimulus events. On the other hand, trials involving hand grasping proved to contain fewer observable hemodynamic responses. The double HbO peak was present in two trials with the main peak occurring at approximately 5 seconds after tapping began and the second peak 1-2 seconds after tapping ceased. One trial showed a prestimulus increase which began 2-3 seconds prior to tapping.

Subject 10 Similar to Subject 4, the most consistently active channels were located in the inferior region of the optode layout, but a couple channels within the expected ROI were also consistent. Despite the fact that the majority (60.4%) of the events showed activation, a response was only observed in an average of 4 channels (11.1%) per event. In most trials, there was a trend in which every other event contained observable responses.

6.2.2 Motor Stimuli Statistics

Subjects 1 & 2 Statistical results for the first two participants are summarized in Table 6.1. There was not evidence to indicate a significant difference (α = 0.05) between the level of hemodynamic responses for whole-hand grasping and sequential finger opposition (tapping) in either participant. However, there was a higher level ($p < 0.0001$) of activation in the left hemisphere of the motor cortex than in the right for both participants. Comparing the level of activation between the two participants showed that there was no significant difference between the magnitude of the HbO response. On the other hand, Subject 2

Table 6.1: Mean hemodynamic responses by motor task and data collection session for two subjects and including all events. Motor cortex data reported for the left hemisphere corresponds to channel 3-5 and that of the right hemisphere to channel 7-11 (Figs. 4.5 & A.3). All values are given in nmol/L. No significant difference was found between the HbO levels for these two participants, but the magnitude of Hb change was greater ($\alpha = 0.05$) for Subject 2 than for Subject 1. For both subjects, the magnitude of the response was greater for the channel overlying the left hemisphere. Note: The use of a * indicates a significant difference from both of the other sessions and a † indicates a significant difference only between those marked with the same symbol. In other words, the p-values for these particular statistics are less than 0.05.

		Left Hemisphere		Right Hemisphere	
		ΔHbO	ΔHb	ΔHbO	ΔHb
Subject 1	Session 1	94 ± 7	-27.6 ± 1.7	78 ± 8	-23.6 ± 1.8
	Session 2	$76 \pm 5^\dagger$	-31.8 ± 1.8	$50. \pm 5^*$	$-21.2 \pm 1.4^\dagger$
	Session 3	$106 \pm 6^\dagger$	$-40.3 \pm 1.2^*$	78 ± 7	$-28.0 \pm 1.2^\dagger$
	Tapping	98 ± 5	$-30.0 \pm 1.4^\dagger$	71 ± 6	-25.2 ± 1.2
	Grasping	86 ± 6	$-30.5 \pm 1.8^\dagger$	66 ± 7	-23.3 ± 1.5
Subject 2	Session 1	66 ± 4	-27 ± 2	59 ± 4	-24 ± 2
	Session 2	78 ± 8	-35 ± 3	44 ± 6	-16 ± 3
	Session 3	$129 \pm 11^*$	$-56 \pm 5^*$	$113 \pm 11^*$	$-49 \pm 5^*$
	Tapping	93 ± 6	-43 ± 2	79 ± 7	-35 ± 3
	Grasping	89 ± 11	-35 ± 5	$66 \pm 10.$	-25 ± 4

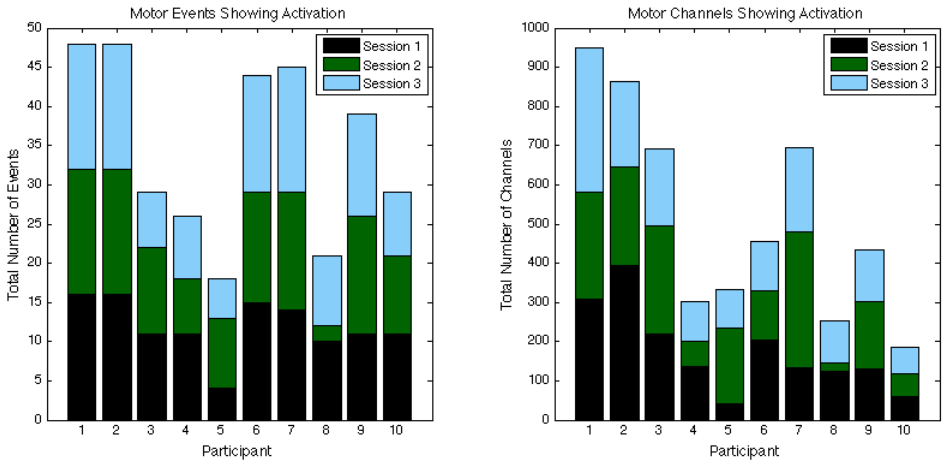

Figure 6.2: Summary of qualitative statistics for motor cortex trials. A total of 48 motor cortex stimulation events were analyzed for each of ten participants. Each event possessed a total of 36 possible data channels to give a total of 1726 channels for each participant that were analyzed for the presence of an observable hemodynamic response. The number of events (left) and channels (right) in which a response was observed are illustrated. Note that the highest number of each were obtained for the first two participants.

exhibited a greater magnitude Hb response than Subject 1 for $\alpha = 0.05$.

For Subject 1, there was evidence of a difference in the level of activation between the second and third data collection sessions. Other differences in the mean response did not reach significance ($\alpha = 0.05$). Residuals displayed no alarming patterns and showed no evidence to indicate a non-normal distribution.

For Subject 2, the third data collection session displayed responses that were greater in magnitude ($p < 0.0001$) than the first two. The third session also had the largest variability in the results and the first session provided the lowest variability. Similarly, the grasping task showed more variability than the tapping task. There was no evidence to suggest that the hemodynamic responses in the motor cortex were not normally distributed. The residuals for this participant displayed a slight funnel-shape for both the session and task comparisons.

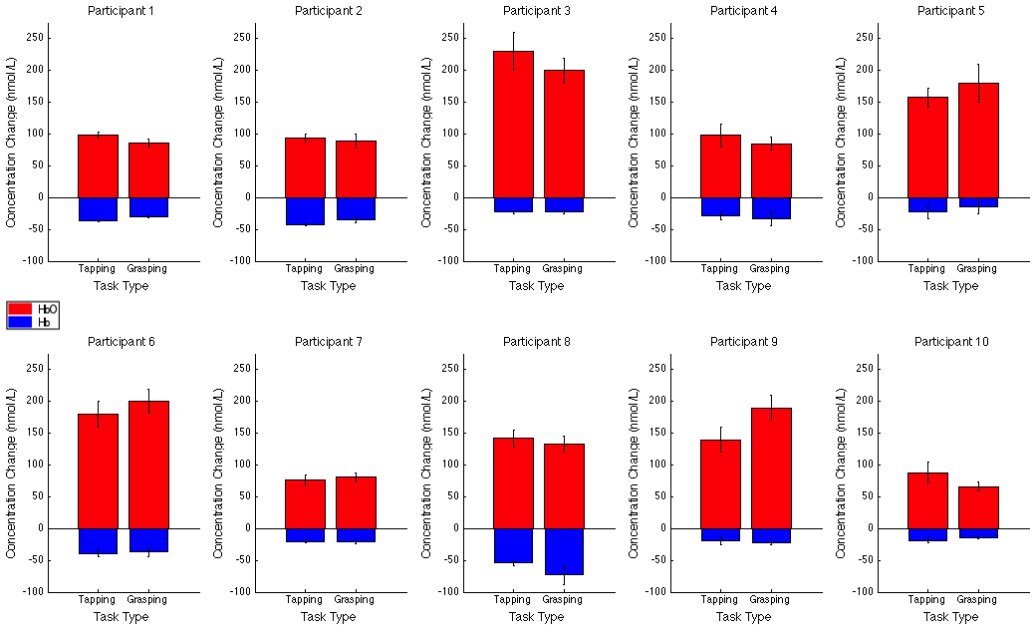

Figure 6.3: Summary of quantitative results obtained for task types using the most consistent motor cortex channel in each of the ten participants. Associated error bars for the HbO (red) and Hb (blue) responses are given in black. Differences in response magnitudes did not reach significance ($p < 0.05$) for any participant.

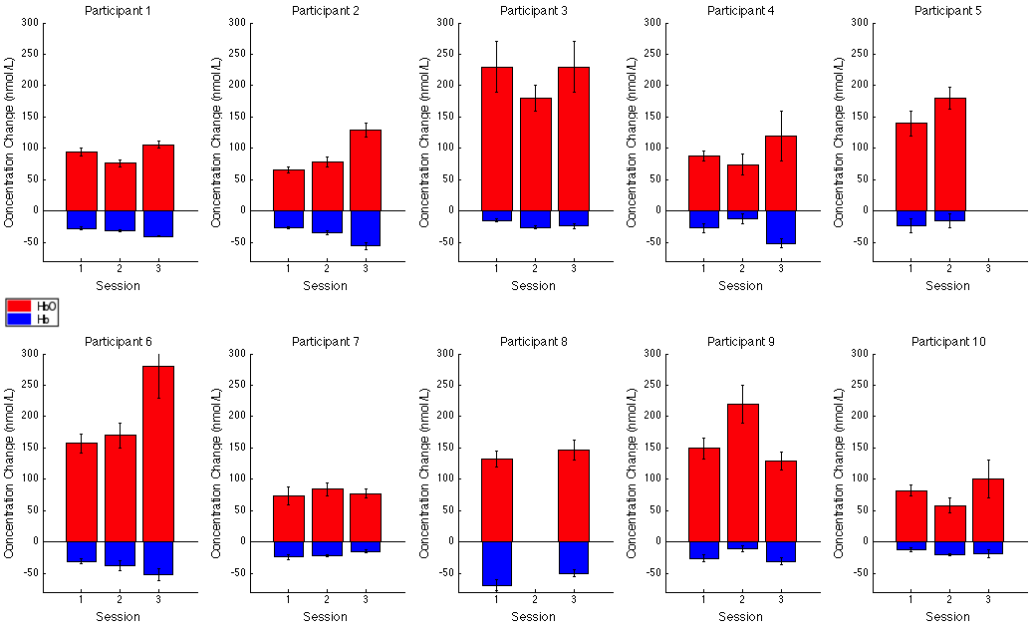

Figure 6.4: Summary of quantitative results obtained across the three data collection sessions for the most consistent motor cortex channel in each of the ten participants. Associated error bars for the HbO (red) and Hb (blue) responses are given in black. Differences in response magnitudes for both HbO and Hb only reached significance ($p < 0.05$) for two of the ten participants. Refer to Table B.1 for details.

6.3 The Visual Cortex

Most results of visual cortex trials did not produce reliable data. That is, no hemodynamic responses were observable for the majority of stimulus events. One participant, however, produced consistent results across both the motor and visual cortex trials. Hence, a greater focus was placed on this participant in the data reporting that follows.

6.3.1 Hemodynamic Response

It was seen that the vast majority of observable hemodynamic responses reached their extrema–maximum for HbO and minimum for Hb–between 10 and 15 seconds after stimulus onset. This is at or after the point in which the reversing checkerboards switched to a black screen. Overall, the magnitude of the change in concentration of Hb was approximately half, or less than, that of the HbO. An example of the elicited hemodynamic responses for one checker size and participant is shown in Figure 6.5. Similar to the motor cortex trials, representative responses for all other participants are given in Appendix B.2. A summary table detailing the mean responses and number of included events for each participant is also included in that section. Qualitatively, the results for Subject 2 far surpassed the rest, as shown in Figure 6.6 and by a simple visual comparison between Figures 6.5 and B.11-B.19. Poorest results were obtained from Subjects 1, 5, 8, and 9.

Subject 1 Data from this participant exhibited large oscillations even within the Hb signals. These oscillations displayed a period of approximately 12 seconds. In addition, they not only survived averaging across eight stimulus events, but their magnitude obscured many possible hemodynamic responses. In all, responses were observed in only an average of 2 (7.1%) of 28 channels and in 41 (34.2%) of 120 total events.

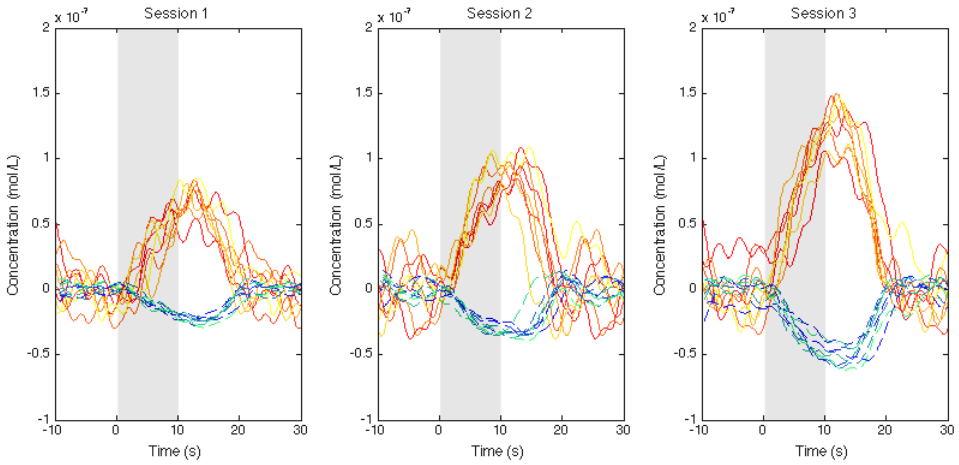

Figure 6.5: Hemodynamic responses for three trials using the extra-small checker size–one trial from each data collection session–for Subject 2. All eight stimulus events from each trial are overlaid on a single graph for a representative channel. HbO curves range from red (first event) to yellow (eighth event) and Hb curves range from blue to green. The shaded region indicates the duration of the stimulus and the third session was found to produce significantly different ($p < 0.05$) results than the other two for both HbO and Hb.

Subject 2 In general, more prominent responses were observed over the left hemisphere and channel 3-2 displayed responses of the highest magnitude. This channel was positioned slightly superior to the location of the left primary visual cortex (per the 10-20 system). Overall, the trial block averages across eight stimulus events appeared very smooth with an easily discernible hemodynamic response, even when one or two of those events did not exhibit a response. Of the 120 total events, a hemodynamic response was observed in 117 (97.5%) with an average of 10 channels (35.7%) per event. An example of the responses for one checker size across all three sessions is shown in Figure 6.6.

Subject 3 Data from this participant was, like Subject 1, dominated by large oscillations which obscured many potential hemodynamic responses. Responses were only observed for 48 (40%) events in an average of 3 (10.7%) channels.

Subject 4 In one trial using the smaller checker size, typical hemodynamic responses were observed in channels over the right hemisphere for seven of the eight stimulus events.

In a second trial using the medium checker size, responses were seen for all eight events. Only three to four events showed a response in two of the other trials. Others did not produce discernible responses. Overall, responses were observed in an average of 4 (14.3%) channels and 74 (61.7%) events. Even in channels which contained a discernible response, periodic (10-12 s) oscillations were present. The third session and the latter half of trials in the second session were the worst in terms of noise and periodic oscillations.

Subject 5 All trials were dominated by random noise or periodic oscillations, but responses were discernible in a few channels for 33 (27.5%) of the 120 events. One trial during the third data collection session was somehow not recorded and saved by the data acquisition software. If this trial was removed from the total number of events, then the percentage would increase to 29.5%. Only an average of 3 channels (10.7%) per event showed a discernible hemodynamic response.

Subject 6 Fifty-two (43.3%) events of the total 120 showed any signals which could be considered an observable response. The average number of active channels per event was 4 (14.3%) of 28.

Subject 7 Five trials contained oscillations with periods of approximately thirty seconds that were not correlated with the stimulation protocol. Seventy-two (60%) stimulus events exhibited anything that resembled a response with an average of 7 channels (25%) per event.

Subject 8 The first two sessions were primarily dominated by noise or periodic oscillations. The third session contained more trials with observable responses, which were predominantly over the right hemisphere. The most consistent was for the second trial in which responses were seen in six events. Overall, responses were observed in an average of 2 (7.1%) channels and 45 (37.5%) events.

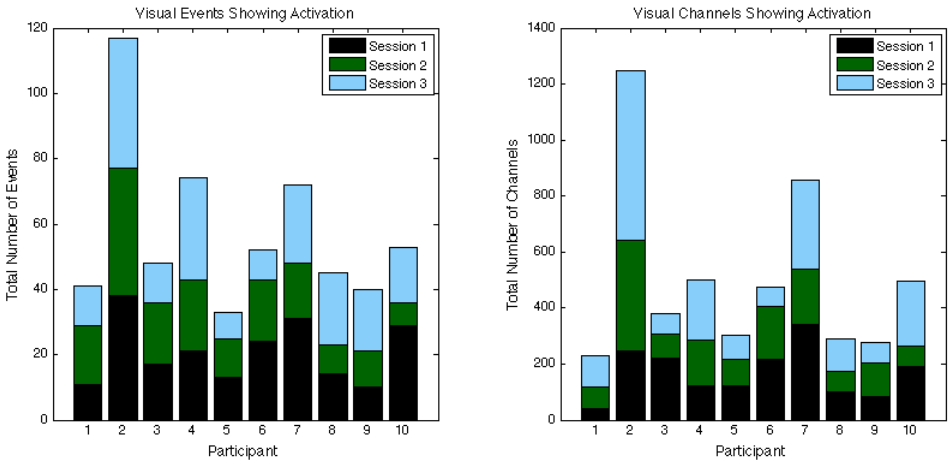

Figure 6.6: Summary of qualitative statistics for visual cortex trials. A total of 120 visual cortex stimulation events were analyzed for each of ten participants. Each event possessed a total of 28 possible data channels to give a total of 3360 channels for each participant that were analyzed for the presence of an observable hemodynamic response. The number of events (left) and channels (right) in which a response was observed are illustrated. Note that the highest number of each were obtained for participants 2, 4, 7, and 10.

Subject 9 Many trials were again dominated by noise and periodic oscillations. However, similar to Subjects 1 and 8, a total of 40 (33.3%) events showed observable responses in an average of 2 (7.1%) channels.

Subject 10 Fifty-three (44.2%) of the 120 events exhibited an observable hemodynamic response. The first and third sessions contained large oscillations with a period that ranged between 30 and 40 seconds. These oscillations were not correlated with the stimulus protocol. Additionally, one trial in the third session showed oscillations with even longer periods: approximately 60 seconds. An overall average of 4 (14.3%) channels were active for each event.

Table 6.2: Mean hemodynamic responses by visual stimulus and data collection session for Subject 2. Reported data corresponds to channel 3-5 which was over the left primary visual cortex (Figs. 4.3 & A.4). Quantitative statistics for the visual cortex Concentration changes are given in units of nmol/L and uncertainty is reported as standard error. Note: The use of a * indicates a significant difference from all the other sessions or checker sizes for a participant. A † or § indicates a significant difference only between those marked with the same. In other words, the p-values for these particular statistics are less than 0.05.

		Sample Size	ΔHbO	ΔHb
Subject 2	Session 1	38	53 ± 3	$-17.6 \pm 0.9^*$
	Session 2	39	64 ± 4	$-23.6 \pm 1.4^*$
	Session 3	40	$92 \pm 5^*$	$-36.4 \pm 1.9^*$
	XS	24	$102 \pm 6^*$	$-38 \pm 3^\dagger$
	S	24	$82 \pm 6^\dagger$	$-30.3 \pm 1.9^\S$
	M	23	62 ± 5	$-24 \pm 2^\dagger$
	L	22	$57 \pm 4^\dagger$	$-20.6 \pm 1.8^{\dagger,\S}$
	XL	24	$45 \pm 3^\dagger$	$-16.7 \pm 0.5^{\dagger,\S}$

6.3.2 Visual Stimuli Comparison: Sensitivity

For nine of the ten participants, no statistical differences were found in mean hemodynamic responses across factor levels (visual stimuli). From a qualitative comparison of responses across the visual stimuli, however, there did appear to be a somewhat decreasing trend in the magnitude of responses as the checker size increased for a few participants. All others showed little to no visible difference. Analysis of the residuals across the five stimulus checker sizes displayed no alarming pattern or enough evidence to suggest that the data are not normally distributed.

Subject 2 Across all three data collection sessions, the extra-small (1°) checker size produced the greatest magnitude responses in HbO and Hb for this participant: 102 ± 6 and -38 ± 3 nmol/L, respectively. The small (2°) checker size resulted in the second-highest magnitudes overall (82 ± 6 and -30.3 ± 1.9 nmol/L) and the extra-large (18°) size resulted in the lowest magnitude (45 ± 3 and -16.7 ± 0.5 nmol/L). There was not enough evidence found to indicate a difference ($\alpha = 0.05$) between the HbO responses for medium

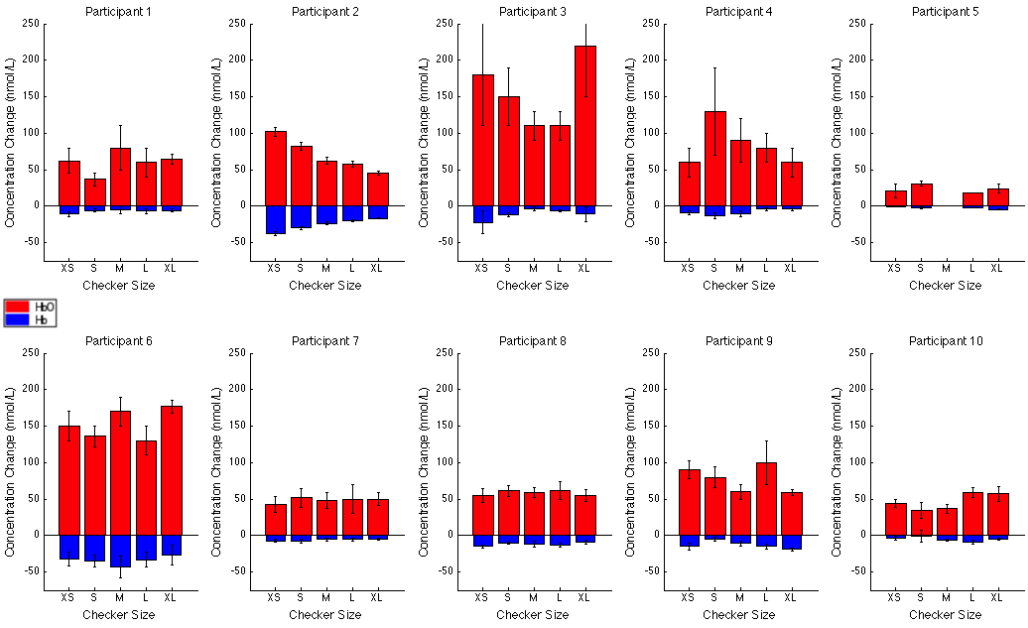

Figure 6.7: Summary of quantitative results obtained across checker sizes for the most consistent visual cortex channel in each of the ten participants. Associated error bars for the HbO (red) and Hb (blue) responses are given in black. Differences in response magnitudes only reached significance ($p < 0.05$) for the second participant. Refer to Table B.5 for details.

and extra-large checkers, large and extra-large checkers, or medium and large checkers. Further, for the Hb responses, there was also not evidence to suggest that extra-small and small checkers or small and medium checkers produced different results.

6.3.3 Visual Block Comparison: Robustness

Data from seven of ten subjects exhibited significant differences between at least two of the three data collection sessions for either HbO, Hb, or both. Subjects 1 and 3 produced differences in HbO response levels; Subjects 4, 5, and 6 produced differences in Hb response levels; and Subjects 2 and 8 produced differences for both hemoglobin response levels. Additionally, no responses were observed for the third session of Subject 5, which means that there are no quantitative statistics reported for those five trials. Analysis of the residuals across the data collection sessions displayed no alarming pattern or enough evidence to

suggest that the data are not normally distributed.

Subject 2 Average magnitudes of the hemodynamic responses, both HbO and Hb, were greater for the final data collection session than the first two ($p < 0.0001$). There was no significant difference ($\alpha = 0.05$) found between the first and second sessions. As with the motor cortex, the third session also contained the largest variability in the data. Again, the residuals across the sessions displayed no alarming pattern and there was no evidence to suggest that the data are not normally distributed. The third and final data collection session contained more average channels with an observable hemodynamic response within the eight-channel ROI. The first two sessions possessed a grand average of 3 and 4 channels, respectively, whereas the final session possessed a grand average of 6 channels per even that exhibited signals which were classified as a hemodynamic response. The two consistent channels across all the sessions were 3-2 and 3-5, which were positioned over the left primary visual cortex.

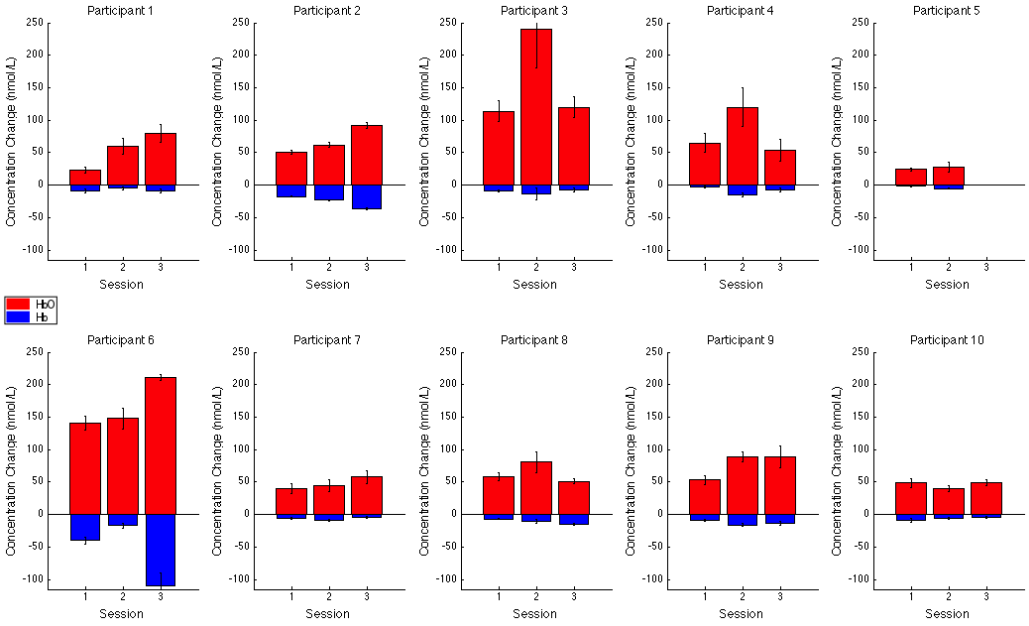

Figure 6.8: Summary of quantitative results obtained across data collection sessions for the most consistent visual cortex channel in each of the ten participants. Associated error bars for the HbO (red) and Hb (blue) responses are given in black. Differences in response magnitudes for both HbO and Hb only reached significance ($p < 0.05$) for two of the ten participants. Refer to Table B.5 for details.

Discussion

This chapter compares the results of the current project to previous studies. It strives to provide an explanation for any inconsistencies or differences observed within the data as well as postulate what can be done to resolve them. Particular attention is paid in terms of potential application to the clinical realm.

7.1 Cortical Hemodynamic Data

Results show that at the onset of stimulation, the level of HbO rises significantly and the level of Hb falls to a lesser degree. The overall increase in blood flow, tHb, can be caused by dilation of blood vessels or possibly opening additional vessels. This large increase in oxygenated blood flow supplied by the arteries causes a washout of Hb. It is for this reason that Hb is observed to decrease whether metabolic rate increases–as has been suggested for the visual cortex–or not.

To make a brief but slightly more in-depth overall analysis (as opposed to subject-by-subject), JMP's Fit Model option was used in two ways. First, the subject number was categorized as a blocking factor and set as a model effect along with session and checker size (visual) or task (motor). In a second model, hair color and thickness were set as the model effects. Results of the first of these two models are summarized in Tables B.2 and B.6. The first model confirms the results of the one-way ANOVAs; there was no overall significant difference in hemodynamic response levels between motor tasks or in ΔHbO

levels between checker sizes. For overall Hb response, however, a significant difference was found between the extra-small and the two largest checker sizes. The first model also confirms that significant differences in response levels occurred between data collection sessions. Discussion of results from the second model are given in the following sections.

7.1.1 Motor Cortex

In general, the data for hand-grasping was noisier than the finger-opposition data. Hand-grasping usually produces more bodily motion due to the fact that it is a more forceful movement. Finger-opposition, on the other hand, is a finer, more delicate movement. Additionally, it has been noted that these motor stimuli tend to slightly increase heart rate and, in turn, blood flow and oxygenation [78, 116]. This could contribute somewhat to the pronounced hemodynamic response that is observed for both types of motor stimuli over the visual stimuli–regardless of increased motion noise. Another contributor could be the difference in oxygen metabolism within the two regions, as described by Wolf and colleagues in their 2002 study on neonates [58] and in Section 2.4.5 of this thesis.

It is common in functional studies of the motor cortex, especially those with twenty-second stimuli, to see not one but two peaks in the HbO response curve [58, 117, 118, 119]. This phenomenon was indeed present in the results of six subjects for stimuli with only half that duration. However, it was observed that not all stimulus events exhibited a double peak in the HbO response; some only showed one. For the vast majority, the double peak survived block averaging even when not present for every event. Some studies have also discovered evidence that the HbO response can begin a couple seconds prior to the stimulus itself, which has been attributed to mental simulation in preparation for the movement task [58, 117]. This prestimulation increase in HbO is not present in every event or even every subject, but does survive block averaging for six of the ten participants. It tends to appear as a small shoulder of the large peak observed at the actual onset of the stimulus. Further, as previously mentioned in Section 2.4.4, the HbO response generally precedes that of Hb

Table 7.1: Summary of quantitative motor cortex data organized by hair type. Responses are given in units of nmol/L. Within each section and column–like the JMP connecting letters report–if factor levels are not connected by the same letter, then they are considered significantly different ($p < 0.05$). *Note: If a t-test is applied rather than Tukey's test, then medium hair also produces a response that is significantly different than coarse hair.

Hair Color	Subject(s)	ΔHbO	ΔHb
Blond/Light	2, 7, 10	$120. \pm 13^{a}$	-25 ± 4^{a}
Brown	1, 4, 5, 8, 9	129 ± 8^{a}	-28 ± 3^{a}
Black	3, 6	158 ± 15^{a}	-41 ± 5^{a}
Hair Thickness	**Subject(s)**	**ΔHbO**	**ΔHb**
Fine	2, 4, 7, 10	$100. \pm 12^{b}$	-34 ± 4^{ab}
Medium	1, 8, 9	$132 \pm 11^{ab*}$	-38 ± 3^{b}
Coarse	3, 5, 6	174 ± 13^{a}	-22 ± 4^{a}

by approximately two seconds for stimulation of the motor cortex. The results of this study support this finding.

For the motor cortex, there is evidence that hair thickness affects the hemodynamic response results. Subjects with coarse hair produced significantly different results than either those with fine hair (HbO) or with medium hair (Hb). A p-value of 0.2750 was not enough evidence to conclude that hair color alone was a factor. However, the participants in this project who had the darkest hair also had the coarsest. As such, there may be an underlying interaction between the two effects, but it cannot be investigated using the data from this series of experiments. Future studies could be specifically designed to investigate the possibility.

7.1.2 Visual Cortex

Time offset, or lag, is not common to visual hemodynamic response curves, unlike motor response. Jasdzewski et al. [57] posit that the absence of Hb lag in the visual cortex may be due to different transit times for the blood through capillaries. Another possible explanation they give is that the metabolic rate increases before blood flow does. These two reasons

could also of course go hand-in-hand. Additionally, it was observed in this study that there was a tendency for signals to be more delayed (both HbO and Hb) in lateral regions for visual trials. The visual association area is located lateral to the visual cortex and this delay, then, is consistent with activation of the association area following activation of the visual cortex.

It was also observed that an appropriate level of sensitivity is achievable for visual cortex studies, but is not yet reliable across the population. Data for only one in ten participants reached significance for the various spatial frequencies used in the study. Since the largest response was observed for the smallest checker size, it would be wise to include even smaller sizes in future studies.

Not even Subject 2 reached the threshold in which half of the channels showed activation over the occipital region. All others were below one-third of the overall total number of channels. This suggests that the optode layout could be even further condensed than it was during the fifth incarnation. This seemingly small area makes sense because only a fraction of the visual cortex is found on the exterior portion of the cerebrum (Fig. 2.10). Much of it is actually housed within the longitudinal fissure, which increases the difficulty to obtain reliable fNIRS data.

The presence of most active channels in the superior region of the layout suggests that sources and detectors could also be included above those in the current configuration. This fact, combined with the low number of channels containing observable responses, may indicate that better statistics can be achieved by shifting the optode arrangement by 5-10% (1-2 rows) toward the crown of the head.

With p-values of <0.0001 and 0.0144, respectively, hair color and hair thickness each appeared to have an effect upon the overall HbO response. The response for black hair was significantly different than brown or blond hair; the response for coarse hair was different than fine hair. On the other hand, only hair color appeared to have a significant effect for Hb responses. The results for brown hair were found to be significantly different from those for

Table 7.2: Summary of quantitative visual cortex data organized by hair type. Within each section and column–like the JMP connecting letters report–if factor levels are not connected by the same letter, then they are considered significantly different ($p < 0.05$). Hemoglobin changes are given in nmol/L.

Hair Color	Subject(s)	ΔHbO	ΔHb
Blond/Light	2, 7, 10	39 ± 9^{b}	-18 ± 3^{b}
Brown	1, 4, 5, 8, 9	57 ± 6^{b}	-7.2 ± 1.8^{a}
Black	3, 6	185 ± 13^{a}	-28 ± 4^{b}
Hair Thickness	**Subject(s)**	**ΔHbO**	**ΔHb**
Fine	2, 4, 7, 10	116 ± 8^{a}	-18 ± 2^{a}
Medium	1, 8, 9	103 ± 9^{ab}	-21 ± 3^{a}
Coarse	3, 5, 6	62 ± 12^{b}	-13 ± 3^{a}

blond and black hair. As mentioned previously, there could potentially be an underlying interaction between the effects of hair color and thickness which could be investigated in future studies. Differences in results based upon hair type were expected, however, particularly since it is known that melanin absorbs NIR light and previous manuscripts have reported the use of participants with light-colored hair.

7.1.3 Overall Subject Comparison

A wide range of hair types were included in order to analyze feasibility across a potential patient population. As expected, there were some variations in the measured responses according to hair color or type. Seen in Tables 7.1 and 7.2, the largest measured magnitude changes in HbO and Hb occurred for participants with very dark hair. This particular result was not expected since the higher quantity of melanin in dark hair would absorb the NIR light more than for light-colored hair. However, the data from those with dark colored hair was generally lower in quality and, therefore, is not necessarily as reliable as data from those with lighter-colored hair. Therefore, further studies are needed to investigate this phenomenon.

Coarser hair appeared to make a greater impact for studying the motor cortex than it

did the visual, perhaps because hair that was long enough was specifically moved aside for visual cortex optode application before the participant donned the cap. For the motor cortex, there was no difference in responses for very sparse (Subject 1) and light-colored hair, which could indicate that the quantity of melanin present in light-colored hair and hair follicles is not enough to have an adverse effect on NIR signals, but there is not enough evidence to confirm this.

7.2 Overall Sensitivity

No significant differences were found in hemodynamic response levels between the two motor tasks for any study participant, which seems to indicate that using either task would be sufficient to study dysfunction in motor pathways. Choice of task could then be the decision of the study administrator with consideration given to each patient/subject; the sequential finger opposition task is more complex, but the grasping task tends to create more bodily motion. The two motor tasks, however, were not the primary focus of this study.

For the visual cortex, it was hoped to measure at least some difference in the level of responses prompted by various stimuli. This was accomplished for only one of the ten participants, the results of which can be seen in Figure 6.7. Achieving an acceptable level of sensitivity in healthy individuals shows the feasibility of using fNIRS to study activation in the visual cortex. This achievement for healthy participants should allow extension to study dysfunction of the visual using fNIRS by providing a basis for comparison. The greatest differences in hemodynamic response were measured between the extra-small (1°) and medium (5°) through extra-large (18°) checker sizes, which indicates at least two potentially reliable stimulus levels to use for studying visual dysfunction. No statistically significant differences were found between the responses of any stimuli for any other subject, which suggests low reliability. However, there appeared to be a decreasing trend in

response magnitude as checker size increased for a few participants, although no differences reached significance. This could indicate that sufficient reliability can be achieved with further optimization.

7.2.1 Overall Repeatability

Lack of repeatability could be caused by at least one of several possible factors. First, the experimental setup may need to be refined. To minimize variation in the procedure used, the same person set up, aligned the cap, and applied the optodes for all three data collection sessions on each participant. However, the participant was asked to fasten the cap so that it was comfortably snug and may not have been as conscientious to consistency as the experimenter. Also, sometimes it took a couple of sessions for the applier to get accustomed to the process for each participant due to variations in head shape and hair. In practice, every person's hair acts differently when attempting to clear a small patch of skin for optode contact. This is true even from one region to another on the same person, which sometimes serves to make optode application particularly challenging and, unfortunately, reduces the ease of performing a completely consistent experimental setup each time. In addition, the times available for data collection were limited. As such, sessions for each participant were not restricted to the exact same time of day or week. The use of caffeine was not prohibited and the level of nearby noise, unfortunately, could not be completely regulated. All of these factors, along with potential boredom from repetition, could contribute to changes in a participant's level of alertness and attentiveness between data collection sessions or even within the same session. A more detailed discussion follows.

7.2.2 Regulation and Quality Control

Procedures and the reasoning behind them were given both verbally as well as briefly within the written consent form which each participant read and signed. Efforts were made by the

experimenter, particularly during the first session, to provide all necessary explanations and prompt the participant to ask questions. However, some information may have been lost in translation or simply forgotten due to the sheer quantity received. Participants did remain quiet and, for the most part, still during data collection. A couple instances were noted when a participant shifted in the chair, although these instances were during rest periods of trials and the participant's head did remain fixed on the chin rest.

The level of attention given to the stimuli, however, is much more difficult to interpret and record. The importance of attention levels, especially for the visual cortex, is an example of a piece of information that could have been lost in translation. Also, despite efforts to perform data collection in a quiet environment, the fNIRS Laboratory is, unfortunately, not soundproof. Sessions occurred during times in which there were no classes scheduled to be held in the adjacent room, but distracting levels of noise were reported in five of these thirty total sessions. Outside noise originated either from the adjacent classroom, offices, hallway, or a combination thereof. In addition, several participants commented that they had difficulty remaining awake and alert, particularly after the third trial. The level of attentiveness during stimulation could have played a role in the observed hemodynamic responses, or lack thereof, in this study (Section 4.5). Slumber or lack of attention could also possibly explain the longer-period signal oscillations noted for a few participants. For future studies, it may be prudent to include an audio cue at the beginning of or just prior to the beginning of a stimulus. Doing so would remind the participants that they need to pay attention to the stimulus. In addition, the number of trials could be limited–even if it would reduce the amount of data available for statistics.

Beyond these factors, it is known that nicotine increases CBF; none of the participants were active smokers. Caffeine has other effects–such as increasing heart rate, metabolism, and vasoconstriction–which actually decrease CBF. In an academic environment, particularly while classes are in session, caffeine use tends to be prevalent. Several participants were known coffee or soda drinkers, although their specific ingestion habits were not of-

ficially recorded. For those on whom fNIRS is already difficult, caffeine ingestion could possibly increase the difficulty of obtaining reliable signals.

That being said, regulation of such commonly-used stimulants may be difficult from a researcher's or clinician's perspective. It is the practice of some fNIRS researchers to request that participants refrain from alcohol or caffeine use for at least 24 hours prior to data collection [120]. However, if fNIRS is extended to the clinical realm, a patient or doctor may not know in advance that such an exam will need to be performed. Hence, intake should at the very least be recorded–not necessarily prohibited. Using fNIRS as a prescreening or diagnosis tool would not merely be focused on the overall CBF, though. It would be focused on abnormalities in the level of hemoglobin changes.

7.3 Data Variability

7.3.1 Oscillations

It has been demonstrated that mean blood pressure (BP) is significantly greater in sitting and standing positions than it is while a person is lying down (supine). Although no significant change was seen in the mean baseline values of HbO, the magnitude of 0.1 Hz oscillations have been proven to be posture-dependent. These oscillations are greatest when standing and least when lying down, as a person would be during an MRI [121]. For this study, subjects are in a seated position. This is a compromise between the magnitudes of spontaneous, regulatory BP oscillations–or Mayer waves. As such, care must be taken during analysis and when comparing results between studies and modalities that utilize another posture.

In a clinical environment, a seated position is the most practical. Standing may allow greater alertness (i.e. focus on the stimulus), but is not necessarily comfortable for the patient during an exam. Standing also introduces a greater risk of motion artifacts. A

supine position, which is used in MRI, would require more space and equipment in the clinic to ensure patient comfort. The increased comfort and motion artifact reduction that may result from a supine position could lead to significantly decreased alertness–especially in a quiet, darkened examination room. Some participants have a difficult enough time remaining alert when seated for the trials. Lying down would only make matters worse from this standpoint. Sitting in a chair allows a compromise between these factors (as well as the spontaneous, Mayer wave oscillations previously mentioned) and facilitates optode placement.

As it has been noted in previous studies, low-frequency oscillations are common in NIRS data, especially with lower magnitude responses like in the visual cortex. Not only do these oscillations appear in the overall time series, but they can survive averaging over many stimulus events [78]. Thus, care must be taken when filtering and processing fNIRS signals, especially for the visual cortex. Unfortunately, not everyone reports details on data processing steps.

7.3.2 Motion Artifacts and Noise

It is rare to see a signal reported from a single stimulus response in scholarly articles. Instead, reported responses are generally averaged over a number of stimuli events, sessions, or even across subjects. While doing so reduces SNR, it does not allow one to see the true variability in the data. Individual responses are generally much noisier than data presented in scholarly articles. Looking at individual stimulus events, then, presents a challenge when trying to comment upon the repeatability of fNIRS measurements. This challenge can be compounded if a person moves during data collection. Motor cortex stimulation, for example, requires some form of movement on the part of the subject (finger tapping, swallowing, etc.) which could introduce motion artifacts or other noise into the data. This was seen in the whole-hand grasping motion versus the sequential finger opposition tasks for this project's validation method (Section 6.2). An advantage of imaging the visual cortex

is that stimulation of this cortical region requires no movement on the part of the subject.

A disadvantage to imaging the visual cortex in adults is the location of this region of the brain. The skull here is generally a bit thicker, not uniformly shaped, and the depth of the cortex varies from person to person. Further, the weight of the optode leads tend to tug the optodes themselves down over time, which could, for instance, lead to detector saturation as a result of optodes losing contact with the skin. For this reason, it is important to have a snug-fitting cap–or other optode retaining device–for each subject and a specific method of loading the optodes into the cap. One solution to help resolve the latter is to load the optodes into the cap while that region is horizontal (i.e., with the subject's head resting face-down on a flat surface) before carefully returning the subject to an upright position without any movement of the optodes and ensuring the leads are secured (not hanging loosely) [122]. In this project, however, there was not enough space to do this comfortably.

Additionally, despite possession of various sizes of commercially-available optode retaining caps, there were still difficulties in achieving a good fit. Even with a variety of cap sizes, there are bound to be adults who have a large quantity of hair or whose head shape does not correctly fit the caps. These subjects may require special modifications in order to obtain a snug fit. First, hair may be particularly difficult to move aside in the occipital region. Women with long hair were asked to part it down the center of their back as if they were going to create pigtails. This helped to keep the hair aside for optode setup, but did not necessarily help the fit of the cap. At times, the sheer quantity of hair significantly increased the amount of space between the cap and scalp. Further, there was one participant in this project whose head was rather flat in both the central and occipital regions. For this participant, extra RIP belts were secured around the cap once the optodes were in place. Otherwise, many optodes would not have achieved contact with the scalp.

Alternative to such modifications, a new optode holder could be designed that only covers the visual cortex/occipital region, but is adjustable to different head shapes and circumferences. Such a new design could also allow denser optode configurations. The

design and production of such equipment could take a good deal of time to perfect–both in terms of creation and determining an ideal optode configuration. For this project, we chose the option of multiple cap sizes due to time constraints. Investigation of a new design, however, is currently underway.

7.4 Resolution

Since fNIRS is limited by its low spatial resolution, groups have begun investigating methods by which to improve upon it. Specifically, diffuse optical tomography (DOT) instruments are being designed with a high-density array of sources and detectors. This provides higher SNR with greater repeatability and spatial resolution over traditional fNIRS. Greater spatial resolution allows two-dimensional reconstruction using signals from each source-detector combination, which results in better localization. DOT operates by converting traditional time-series signals into time-series images.

Zeff et al. [123] describes the development of such a DOT system. Theirs is a CW system (Section 3.1.2) and has a total of 24 sources and 28 detectors with a sampling frequency of 12 Hz. The quantity of optodes arranged in a relatively dense configuration not only allows for lateral image reconstruction, but, due to an increased number of source-detector separation distances, allows for depth reconstruction as well. The reported high-repeatability would mean that fewer stimulus cycles would need to be presented for diagnosis. This means even further reduced time to diagnosis and increased patient comfort. Such systems could be the future of NIRS.

Conclusions

This study has confirmed that fNIRS is, in fact, feasible for studying brain activation in the visual cortex. The results from one participant showed that an appropriate level of sensitivity is achievable. However, the lack of apparent sensitivity shown with the other nine subjects proves that the modality still lacks a sufficient level of reliability for use as a standalone prescreening and diagnostic tool within the clinical realm. Significant differences in the measured activation levels across sessions for several participants also indicates that there is room for improvement in terms of repeatability as well.

In order for fNIRS to be implemented in the clinic, further optimization is needed before acceptable levels of reliability and repeatability can be reached. Since data processing methods have been well explored, this optimization would primarily include improvements in the hardware and experimental setup. One possible improvement in the hardware is reduction of the noise floor. Experimental setup could possibly be improved by implementing a new optode holder design.

Future Work

Using previously-obtained MRI scans of two participants in the NIRS study, theoretical modeling will be performed to better determine the path that detected NIR light actually traveled through each adult's head. The simulation will take into account the specific geometry of the optode arrangements as well as the results reported within the pages of this thesis. Comparisons between the two projects may give a better indication of why hemodynamic responses to the same stimuli appear so different between healthy adults. Along the same lines, further comparisons can and will be examined by completing analysis of the physiological data that was simultaneously collected during this NIRS feasibility study.

Additionally, as remarked upon within the discussion portion of this thesis, current commercially-available optode retaining caps which are based upon the 10-20 system for EEG do not work well for every head. Each head is unique in shape and size and the caps, though made with a material that stretches, do not provide a uniform fit for any given cortical region. This is especially noticeable in the occipital region. For many participants, there was a gap or a loose fit in that area unless a much smaller cap was used and sometimes even that wasn't enough. This resulted in increased pressure on other regions of the head. A new design for an optode holder is currently being developed and tested to facilitate imaging on neonates. This new design project will then be extended to adults in order to promote uniformity and fit a wide variety of head shapes and sizes, particularly for visual cortex studies.

With development of the new optode holder, denser source-detector arrangements will

also be possible. This will allow further clinical feasibility investigations that will be more representative of DOT studies. Future studies will also seek to employ smaller checker sizes as well as a visual hemifield in order to assess the sensitivity and repeatability of fNIRS for hemispherical differences. The addition of monocular testing could help assess the same for the function of each eye.

Bibliography

[1] F. F. Jobsis. Noninvasive, infrared monitoring of cerebral and myocardial oxygen sufficiency and circulatory parameters. *Science (New York, N.Y.)*, 198(4323):1264–1267, Dec 23 1977.

[2] Marco Ferrari and Valentina Quaresima. A brief review on the history of human functional near-infrared spectroscopy (fnirs) development and fields of application. *NeuroImage*, 63(2):921–935, 11/1 2012.

[3] H. Obrig. Nirs in clinical neurology - a 'promising' tool? *NeuroImage*, Apr 2 2013.

[4] E. Hori, K. Takamoto, S. Urakawa, T. Ono, and H. Nishijo. Effects of acupuncture on the brain hemodynamics. *Autonomic Neuroscience*, 157(1-2):74–80, 2010.

[5] C. Hock, K. Villringer, M, F. ller Spahn, M. Hofmann, S. Schuh-Hofer, H. Heekeren, R. Wenzel, U. Dirnagl, and A. Villringer. Near infrared spectroscopy in the diagnosis of alzheimer's disease. *Annals of the New York Academy of Sciences*, 777:22–29, 1996.

[6] JB Zeller, MJ Herrmann, AC Ehlis, T. Polak, and AJ Fallgatter. Altered parietal brain oxygenation in alzheimer's disease as assessed with near-infrared spectroscopy. *American Journal of Geriatric Psychiatry*, 18(5):433–441, 2010.

[7] M. Kameyama, M. Fukuda, Y. Yamagishi, T. Sato, T. Uehara, M. Ito, T. Suto, and M. Mikuni. Frontal lobe function in bipolar disorder: a multichannel near-infrared spectroscopy study. *NeuroImage*, 29(1):172–184, 2006.

[8] M. W. Hemelt, J. T. Barnett, D. F. Bruley, and K. A. Kang. Application of near-ir time-resolved spectroscopy and frequency response analysis for deep vein thrombosis detection. *Biotechnology progress*, 13(5):640–648, Sep-Oct 1997.

[9] F. Okada, N. Takahashi, and Y. Tokumitsu. Dominance of the 'nondominant' hemisphere in depression. *Journal of affective disorders*, 37(1):13–21, 1996.

[10] S. Pu, T. Yamada, K. Yokoyama, H. Matsumura, H. Kobayashi, N. Sasaki, H. Mitani, A. Adachi, K. Kaneko, and K. Nakagome. A multi-channel near-infrared spectroscopy study of prefrontal cortex activation during working memory task in major depressive disorder. *Neuroscience research*, 70(1):91–97, 2011.

[11] M. Sawa, H. Yamashita, K. Fujimaki, G. Okada, T. Takahashi, and S. Yamawaki. Negative correlation between affective symptoms and prefrontal activation during a verbal fluency task: a near-infrared spectroscopy study. *Neuropsychobiology*, 67(2): 103–110, 2013.

[12] H. Bortfeld, E. Fava, and D. A. Boas. Identifying cortical lateralization of speech processing in infants using near-infrared spectroscopy. *Developmental neuropsychology*, 34(1):52–65, 2009.

[13] A. J. Fallgatter, T. J. Muller, and W. K. Strik. Prefrontal hypooxygenation during language processing assessed with near-infrared spectroscopy. *Neuropsychobiology*, 37(4):215–218, 1998.

[14] K. Sakatani, W. Lichty, Y. Xie, S. Li, and H. Zuo. Effects of aging on language-activated cerebral blood oxygenation changes of the left prefrontal cortex: Near in-

frared spectroscopy study. *Journal of stroke and cerebrovascular diseases : the official journal of National Stroke Association*, 8(6):398–403, Nov-Dec 1999.

[15] Ata Akin, Uzay E. Emir, Didem Bilensoy, Gulin Erdogan, Selcuk Candansyar, and Hayrunnisa Bolay. fnirs measurements in migraine. In *Biomedical Optics 2005*, pages 417–423. International Society for Optics and Photonics, 2005.

[16] A. Kleinschmidt, H. Obrig, M. Requardt, K. D. Merboldt, U. Dirnagl, A. Villringer, and J. Frahm. Simultaneous recording of cerebral blood oxygenation changes during human brain activation by magnetic resonance imaging and near-infrared spectroscopy. *Journal of cerebral blood flow and metabolism : official journal of the International Society of Cerebral Blood Flow and Metabolism*, 16(5):817–826, Sep 1996.

[17] N. B. Hampson and C. A. Piantadosi. Near infrared monitoring of human skeletal muscle oxygenation during forearm ischemia. *Journal of applied physiology (Bethesda, Md.: 1985)*, 64(6):2449–2457, Jun 1988.

[18] M. A. Underwood, J. M. Milstein, and M. P. Sherman. Near-infrared spectroscopy as a screening tool for patent ductus arteriosus in extremely low birth weight infants. *Neonatology*, 91(2):134–139, 2007.

[19] K. K. McCully, L. Landsberg, M. Suarez, M. Hofmann, and J. D. Posner. Identification of peripheral vascular disease in elderly subjects using optical spectroscopy. *The journals of gerontology.Series A, Biological sciences and medical sciences*, 52 (3):B159–65, May 1997.

[20] A. Watanabe and T. Kato. Cerebrovascular response to cognitive tasks in patients with schizophrenia measured by near-infrared spectroscopy. *Schizophrenia bulletin*, 30(2):435–444, 2004.

[21] M. Igawa, Y. Atsumi, K. Takahashi, S. Shiotsuka, H. Hirasawa, R. Yamamoto, A. Maki, Y. Yamashita, and H. Koizumi. Activation of visual cortex in rem sleep measured by 24-channel nirs imaging. *Psychiatry and clinical neurosciences*, 55(3): 187–188, Jun 2001.

[22] Christopher O. Olopade, Edward Mensah, Rajarsi Gupta, Dezheng Huo, Daniel L. Picchietti, Enrico Gratton, and Antonios Michalos. Noninvasive determination of brain tissue oxygenation during sleep in obstructive sleep apnea: a near-infrared spectroscopic approach. *Sleep*, 30(12):1747, 2007.

[23] H. Kato, M. Izumiyama, H. Koizumi, A. Takahashi, and Y. Itoyama. Near-infrared spectroscopic topography as a tool to monitor motor reorganization after hemiparetic stroke: a comparison with functional mri. *Stroke; a journal of cerebral circulation*, 33(8):2032–2036, Aug 2002.

[24] S. Nakamura, K. Sakatani, T. Kano, T. Hoshino, N. Fujiwara, Y. Murata, and Y. Katayama. Effects of revascularisation on evoked cerebral blood oxygenation responses in stroke patients. *Advances in Experimental Medicine and Biology*, 662: 525–530, 2010.

[25] D. T. Delpy, M. Cope, P. van der Zee, S. Arridge, S. Wray, and J. Wyatt. Estimation of optical pathlength through tissue from direct time of flight measurement. *Physics in Medicine and Biology*, 33(12):1433–1442, Dec 1988.

[26] Wai-Fung Cheong, Scott A. Prahl, and Ashley J. Welch. A review of the optical properties of biological tissues. *IEEE Journal of Quantum Electronics*, 26(12):2166–2185, 1990.

[27] T. J. Huppert, S. G. Diamond, M. A. Franceschini, and D. A. Boas. Homer: a review of time-series analysis methods for near-infrared spectroscopy of the brain. *Applied Optics*, 48(10):D280–98, Apr 1 2009.

[28] A. Pellicer and M.C. Bravo. Near-infrared spectroscopy: a methodology-focused review. *Seminars in fetal & neonatal medicine*, 16(1):42–49, Feb 2011.

[29] David A. Boas, Maria Angela Franceschini, Andy K. Dunn, and Gary Strangman. Noninvasive imaging of cerebral activation with diffuse optical tomography. *In vivo optical imaging of brain function*, pages 193–221, 2002.

[30] World Hair Research. Hair follicle scalp images, 2010. URL http://www.worldhairresearch.com/?tag=scalp-cross-section.

[31] Keith L. Moore and Arthur F. Dalley. *Clinically oriented anatomy*. Lippincott, Williams & Wilkins, 5th edition, 2006.

[32] M. Hiraoka, M. Firbank, M. Essenpreis, M. Cope, S. R. Arridge, P. van der Zee, and D. T. Delpy. A monte carlo investigation of optical pathlength in inhomogeneous tissue and its application to near-infrared spectroscopy. *Physics in Medicine and Biology*, 38(12):1859–1876, Dec 1993.

[33] E. Okada and D. T. Delpy. Near-infrared light propagation in an adult head model. ii. effect of superficial tissue thickness on the sensitivity of the near-infrared spectroscopy signal. *Applied Optics*, 42(16):2915–2922, Jun 1 2003.

[34] E. Okada and D. T. Delpy. Near-infrared light propagation in an adult head model. i. modeling of low-level scattering in the cerebrospinal fluid layer. *Applied Optics*, 42(16):2906–2914, Jun 1 2003.

[35] C. R. Simpson, M. Kohl, M. Essenpreis, and M. Cope. Near-infrared optical properties of ex vivo human skin and subcutaneous tissues measured using the monte carlo inversion technique. *Physics in Medicine and Biology*, 43(9):2465–2478, Sep 1998.

[36] C. Elwell. *A Practical Users Guide to Near Infrared Spectroscopy*. Hamamatsu Photonics KK, London, UK, 1995.

[37] M. Firbank, M. Hiraoka, M. Essenpreis, and D. T. Delpy. Measurement of the optical properties of the skull in the wavelength range 650-950 nm. *Physics in Medicine and Biology*, 38(4):503–510, Apr 1993.

[38] M. Firbank, E. Okada, and D. T. Delpy. A theoretical study of the signal contribution of regions of the adult head to near-infrared spectroscopy studies of visual evoked responses. *NeuroImage*, 8(1):69–78, Jul 1998.

[39] Gabriele Gratton and Monica Fabiani. Fast optical signals: Principles, methods, and experimental results. *In Vivo Optical imaging of Brain Function*, pages 223–248, 2002.

[40] Pieter van der Zee, Matthias Essenpreis, and David T. Delpy. Optical properties of brain tissue. pages 454–465, 1993. doi: 10.1117/12.154665.

[41] P. Rolfe. In vivo near-infrared spectroscopy. *Annual Review of Biomedical Engineering*, 2:715–754, 2000.

[42] Pieter van der Zee. Measurement and modelling of the optical properties of human tissue in the near infrared, 1992. Ph.D. Thesis.

[43] H. Dehghani, B. R. White, B. W. Zeff, A. Tizzard, and J. P. Culver. Depth sensitivity and image reconstruction analysis of dense imaging arrays for mapping brain function with diffuse optical tomography. *Applied Optics*, 48(10):D137–43, Apr 1 2009.

[44] Frederic Martini and Judi L Nath. *Anatomy & physiology*. Benjamin Cummings, San Francisco, 2 edition, 2010. ISBN 9780321597137; 0321597133; 9780321597205; 0321597206.

[45] Joseph Siry. Visual abilities of the brain, 2013. URL http://myweb.rollins.edu/jsiry/Visual_Cortex.html.

[46] Nida Gleveckas-Martens. Somatosensory system anatomy, 2013.

[47] Y. Hoshi. Functional near-infrared spectroscopy: current status and future prospects. *Journal of Biomedical Optics*, 12(6):062106, Nov-Dec 2007.

[48] W. N. Colier, V. Quaresima, R. Wenzel, M. C. van der Sluijs, B. Oeseburg, M. Ferrari, and A. Villringer. Simultaneous near-infrared spectroscopy monitoring of left and right occipital areas reveals contra-lateral hemodynamic changes upon hemifield paradigm. *Vision research*, 41(1):97–102, Jan 2001.

[49] M. A. McIntosh, U. Shahani, R. G. Boulton, and D. L. McCulloch. Absolute quantification of oxygenated hemoglobin within the visual cortex with functional near infrared spectroscopy (fnirs). *Investigative ophthalmology & visual science*, 51(9): 4856–4860, 2010.

[50] S. Wijeakumar, U. Shahani, D. L. McCulloch, and W. A. Simpson. Neural and vascular responses to fused binocular stimuli: a vep and fnirs study. *Investigative ophthalmology & visual science*, 53(9):5881–5889, Aug 27 2012.

[51] S. Wijeakumar, U. Shahani, W. A. Simpson, and D. L. McCulloch. Localization of hemodynamic responses to simple visual stimulation: an fnirs study. *Investigative ophthalmology & visual science*, 53(4):2266–2273, Apr 2012.

[52] Rdiger Wenzel, Petra Wobst, Hauke H. Heekeren, Kenneth K. Kwong, Stephan A. Brandt, Matthias Kohl, Hellmuth Obrig, Ulrich Dirnagl, and Arno Villringer. Saccadic suppression induces focal hypooxygenation in the occipital cortex. *Journal of Cerebral Blood Flow & Metabolism*, 20(7):1103–1110, 2000.

[53] C. Hock, F. Muller-Spahn, S. Schuh-Hofer, M. Hofmann, U. Dirnagl, and A. Villringer. Age dependency of changes in cerebral hemoglobin oxygenation during brain activation: a near-infrared spectroscopy study. *Journal of cerebral blood flow and*

metabolism : official journal of the International Society of Cerebral Blood Flow and Metabolism, 15(6):1103–1108, Nov 1995.

[54] M. L. Schroeter, S. Zysset, F. Kruggel, and D. Y. von Cramon. Age dependency of the hemodynamic response as measured by functional near-infrared spectroscopy. *NeuroImage*, 19(3):555–564, Jul 2003.

[55] J. R. Stroop. Studies of interference in serial verbal reactions. *Journal of experimental psychology*, 18(6):643, 1935.

[56] J. Steinbrink, A. Villringer, F. Kempf, D. Haux, S. Boden, and H. Obrig. Illuminating the bold signal: combined fmri-fnirs studies. *Magnetic resonance imaging*, 24(4): 495–505, May 2006.

[57] G. Jasdzewski, G. Strangman, J. Wagner, K. K. Kwong, R. A. Poldrack, and D. A. Boas. Differences in the hemodynamic response to event-related motor and visual paradigms as measured by near-infrared spectroscopy. *NeuroImage*, 20(1):479–488, Sep 2003.

[58] M. Wolf, K. von Siebenthal, M. Keel, V. Dietz, O. Baenziger, and H. U. Bucher. Comparison of three methods to measure absolute cerebral hemoglobin concentration in neonates by near-infrared spectrophotometry. *Journal of Biomedical Optics*, 7(2):221–227, Apr 2002.

[59] Lin Tang, Malcolm J. Avison, and John C. Gore. Nonlinear blood oxygen level-dependent responses for transient activations and deactivations in v1 insights into the hemodynamic response function with the balloon model. *Magnetic resonance imaging*, 27(4):449–459, 2009.

[60] Martin Wolf, Ursula Wolf, Jee H. Choi, Vladislav Toronov, L. Adelina Paunescu, Antonios Michalos, and Enrico Gratton. Fast cerebral functional signal in the 100-

ms range detected in the visual cortex by frequency-domain near-infrared spectrophotometry. *Psychophysiology*, 40(4):521–528, 07 2003.

[61] Herbert H. Jasper. The ten twenty electrode system of the international federation. *Electroencephalography and clinical neurophysiology*, 10:371–375, 1958.

[62] J. V. Odom, Michael Bach, Mitchell Brigell, Graham E. Holder, Daphne L. McCulloch, Alma Patrizia Tormene, and Vaegan. Iscev standard for clinical visual evoked potentials (2009 update). *Documenta Ophthalmologica*, 120(1):111–119, 2010.

[63] Jaakko Malmivuo and Robert Plonsey. *Electroencephalography*, pages 257–264. Bioelectromagnetism: principles and applications of bioelectric and biomagnetic fields. Oxford University Press, New York, 1995. ISBN 0195058232. URL http://www.bem.fi/book/13/13.htm.

[64] F. Almoqbel, S. J. Leat, and E. Irving. The technique, validity and clinical use of the sweep vep. *Ophthalmic & physiological optics : the journal of the British College of Ophthalmic Opticians (Optometrists)*, 28(5):393–403, Sep 2008.

[65] M. Heine and T. Meigen. The dependency of simultaneously recorded retinal and cortical potentials on temporal frequency. *Documenta ophthalmologica.Advances in ophthalmology*, 108(1):1–8, Jan 2004.

[66] A. Moskowitz and S. Sokol. Spatial and temporal interaction of pattern-evoked cortical potentials in human infants. *Vision research*, 20(8):699–707, 1980.

[67] Y. Hoshi and M. Tamura. Detection of dynamic changes in cerebral oxygenation coupled to neuronal function during mental work in man. *Neuroscience letters*, 150 (1):5–8, Feb 5 1993.

[68] Y. Hoshi and M. Tamura. Dynamic multichannel near-infrared optical imaging of

human brain activity. *Journal of applied physiology (Bethesda, Md.: 1985)*, 75(4): 1842–1846, Oct 1993.

[69] T. Karen, G. Morren, D. Haensse, A. S. Bauschatz, H. U. Bucher, and M. Wolf. Hemodynamic response to visual stimulation in newborn infants using functional near-infrared spectroscopy. *Human brain mapping*, 29(4):453–460, Apr 2008.

[70] T. Kato, A. Kamei, S. Takashima, and T. Ozaki. Human visual cortical function during photic stimulation monitoring by means of near-infrared spectroscopy. *Journal of cerebral blood flow and metabolism : official journal of the International Society of Cerebral Blood Flow and Metabolism*, 13(3):516–520, May 1993.

[71] H. Obrig, M. Neufang, R. Wenzel, M. Kohl, J. Steinbrink, K. Einhaupl, and A. Villringer. Spontaneous low frequency oscillations of cerebral hemodynamics and metabolism in human adults. *NeuroImage*, 12(6):623–639, Dec 2000.

[72] L. Rovati, G. Salvatori, L. Bulf, and S. Fonda. Optical and electrical recording of neural activity evoked by graded contrast visual stimulus. *Biomedical engineering online*, 6:28, Jul 4 2007.

[73] A. Sassaroli, Y. Tong, BB Frederick, PF Renshaw, BL Ehrenberg, and S. Fantini. Studying brain function with concurrent near-infrared spectroscopy (nirs) and functional magnetic resonance imaging (fmri). In *Biomedical Optics 2005*, pages 161–165. International Society for Optics and Photonics, 2005.

[74] S. Shimada. Brain activity during eye contact measured by functional near-infrared spectroscopy and eye tracking. In *Complex Medical Engineering (CME), 2012 ICME International Conference on*, pages 584–587, 2012.

[75] Gentaro Taga, Fumitaka Homae, and Hama Watanabe. Effects of source-detector distance of near infrared spectroscopy on the measurement of the cortical hemodynamic response in infants. *NeuroImage*, 38(3):452–460, 2007.

[76] Vladislav Y. Toronov, Xiaofeng Zhang, and Andrew G. Webb. A spatial and temporal comparison of hemodynamic signals measured using optical and functional magnetic resonance imaging during activation in the human primary visual cortex. *NeuroImage*, 34(3):1136–1148, 2007.

[77] A. Villringer, J. Planck, C. Hock, L. Schleinkofer, and U. Dirnagl. Near infrared spectroscopy (nirs): a new tool to study hemodynamic changes during activation of brain function in human adults. *Neuroscience letters*, 154(1-2):101–104, May 14 1993.

[78] P. Wobst, R. Wenzel, M. Kohl, H. Obrig, and A. Villringer. Linear aspects of changes in deoxygenated hemoglobin concentration and cytochrome oxidase oxidation during brain activation. *NeuroImage*, 13(3):520–530, Mar 2001.

[79] A. W. Subudhi, B. R. Miramon, M. E. Granger, and R. C. Roach. Frontal and motor cortex oxygenation during maximal exercise in normoxia and hypoxia. *Journal of applied physiology (Bethesda, Md.: 1985)*, 106(4):1153–1158, Apr 2009.

[80] T. Ikegami and G. Taga. Decrease in cortical activation during learning of a multi-joint discrete motor task. *Experimental brain research*, 191(2):221–236, Nov 2008.

[81] M. Hatakenaka, I. Miyai, M. Mihara, S. Sakoda, and K. Kubota. Frontal regions involved in learning of motor skill–a functional nirs study. *NeuroImage*, 34(1):109–116, Jan 1 2007.

[82] Masamichi Morihiro, Tadashi Tsubone, and Yasuhiro Wada. Relation between nirs signal and motor capability. In *Engineering in Medicine and Biology Society, 2009. EMBC 2009. Annual International Conference of the IEEE*, pages 3991–3994. IEEE, 2009.

[83] T. Akiyama, T. Ohira, T. Kawase, and T. Kato. Tms orientation for nirs-functional motor mapping. *Brain topography*, 19(1-2):1–9, Winter 2006.

[84] T. J. Huppert, R. D. Hoge, S. G. Diamond, M. A. Franceschini, and D. A. Boas. A temporal comparison of bold, asl, and nirs hemodynamic responses to motor stimuli in adult humans. *NeuroImage*, 29(2):368–382, Jan 15 2006.

[85] L. Gagnon, R. J. Cooper, M. A. Yucel, K. L. Perdue, D. N. Greve, and D. A. Boas. Short separation channel location impacts the performance of short channel regression in nirs. *NeuroImage*, 59(3):2518–2528, Feb 1 2012.

[86] C. Dormer, T. Ward, and S. McLoone. Towards enhanced biofeedback mechanisms for upper limb rehabilitation in stroke. 2008.

[87] I. Miyai, H. Yagura, M. Hatakenaka, I. Oda, I. Konishi, and K. Kubota. Longitudinal optical imaging study for locomotor recovery after stroke. *Stroke; a journal of cerebral circulation*, 34(12):2866–2870, Dec 2003.

[88] Judith D. Schaechter. Motor rehabilitation and brain plasticity after hemiparetic stroke. *Progress in neurobiology*, 73(1):61–72, 2004.

[89] Pei-Yi Lin, Sang-I Lin, Trevor Penney, and Jia-Jin Jason Chen. Review: applications of near infrared spectroscopy and imaging for motor rehabilitation in stroke patients. *J Med Biol Eng*, 29:210–211, 2009.

[90] M. Mihara, N. Hattori, M. Hatakenaka, H. Yagura, T. Kawano, T. Hino, and I. Miyai. Near-infrared spectroscopy-mediated neurofeedback enhances efficacy of motor imagery-based training in poststroke victims: a pilot study. *Stroke; a journal of cerebral circulation*, 44(4):1091–1098, Apr 2013.

[91] S. Coyle, T. Ward, and C. Markham. Cerebral blood flow changes related to motor imagery, using near-infrared spectroscopy (nirs). 2003.

[92] K. Sagara, K. Kido, and K. Ozawa. Portable single-channel nirs-based bmi system for motor disabilities' communication tools. *Conference proceedings : ...Annual*

International Conference of the IEEE Engineering in Medicine and Biology Society.IEEE Engineering in Medicine and Biology Society.Conference, 2009:602–605, 2009.

[93] Munetaka Haida, Yukito Shinohara, Yoshitoshi Ito, Tsuyoshi Yamamoto, Fumio Kawaguchi, and Hideaki Koizumi. Brain function of an als patient in complete locked-in state by using optical topography. *The Frontier of Mind-Brain Science and Its Practical Applications II*, pages 95–97, 2000.

[94] ISS. OxiplexTS: Near-infrared, non-invasive tissue oximeter, 2013. URL http://www.iss.com/biomedical/instruments/oxiplexTS.html.

[95] A. Torricelli, A. Pifferi, L. Spinelli, R. Cubeddu, F. Martelli, S. Del Bianco, and G. Zaccanti. Time-resolved reflectance at null source-detector separation: improving contrast and resolution in diffuse optical imaging. *Physical Review Letters*, 95(7): 078101, Aug 12 2005.

[96] A. P. Gibson, J. C. Hebden, and S. R. Arridge. Recent advances in diffuse optical imaging. *Physics in Medicine and Biology*, 50(4):R1–43, Feb 21 2005.

[97] NIRx Medical Technologies. Products - fnirs systems. URL http://www.nirx.net/imagers/nirscout.

[98] John McNulty, Michael Born, and Robert S. Pozos. *Near-Infrared Spectroscopy (NIRS)*, pages 423–438. Springer Handbook of Medical Technology. Springer, 2012.

[99] Great Lakes NeuroTechnologies. The bioradio device: Wireless physiological monitoring, 2013.

[100] Harry Graber. Personal correspondence, 2013.

[101] Photon Migration Imaging Laboratory at Massachusetts General Hospital. Homer2,

2013. URL http://www.nmr.mgh.harvard.edu/PMI/resources/homer2/home.htm.

[102] N. Kuboyama, T. Nabetani, K. Shibuya, K. Machida, and T. Ogaki. Relationship between cerebral activity and movement frequency of maximal finger tapping. *Journal of physiological anthropology and applied human science*, 24(3):201–208, May 2005.

[103] David A. Boas. Training session 1: March 4, 2013 (video), 2013. URL http://homer-fnirs.org/documentation/#tutorials.

[104] S. M. Liao, S. L. Ferradal, B. R. White, N. Gregg, T. E. Inder, and J. P. Culver. High-density diffuse optical tomography of term infant visual cortex in the nursery. *Journal of Biomedical Optics*, 17(8):081414, Aug 2012.

[105] Y. Hoshi, S. Kosaka, Y. Xie, S. Kohri, and M. Tamura. Relationship between fluctuations in the cerebral hemoglobin oxygenation state and neuronal activity under resting conditions in man. *Neuroscience letters*, 245(3):147–150, Apr 10 1998.

[106] V. Toronov, M. A. Franceschini, M. Filiaci, S. Fantini, M. Wolf, A. Michalos, and E. Gratton. Near-infrared study of fluctuations in cerebral hemodynamics during rest and motor stimulation: temporal analysis and spatial mapping. *Medical physics*, 27(4):801–815, Apr 2000.

[107] J. Steinbrink, M. Kohl, H. Obrig, G. Curio, F. Syre, F. Thomas, H. Wabnitz, H. Rinneberg, and A. Villringer. Somatosensory evoked fast optical intensity changes detected non-invasively in the adult human head. *Neuroscience letters*, 291(2):105–108, 2000.

[108] D. A. Boas, A. M. Dale, and M. A. Franceschini. Diffuse optical imaging of brain activation: approaches to optimizing image sensitivity, resolution, and accuracy. *NeuroImage*, 23 Suppl 1:S275–88, 2004.

[109] B. Molavi and G. A. Dumont. Wavelet-based motion artifact removal for functional near-infrared spectroscopy. *Physiological Measurement*, 33(2):259–270, Feb 2012.

[110] S. Brigadoi, L. Ceccherini, S. Cutini, F. Scarpa, P. Scatturin, J. Selb, L. Gagnon, D. A. Boas, and R. J. Cooper. Motion artifacts in functional near-infrared spectroscopy: A comparison of motion correction techniques applied to real cognitive data. *NeuroImage*, Apr 29 2013.

[111] R. J. Cooper, J. Selb, L. Gagnon, D. Phillip, H. W. Schytz, H. K. Iversen, M. Ashina, and D. A. Boas. A systematic comparison of motion artifact correction techniques for functional near-infrared spectroscopy. *Frontiers in neuroscience*, 6:147, 2012.

[112] A. Duncan, J. H. Meek, M. Clemence, C. E. Elwell, L. Tyszczuk, M. Cope, and D. T. Delpy. Optical pathlength measurements on adult head, calf and forearm and the head of the newborn infant using phase resolved optical spectroscopy. *Physics in Medicine and Biology*, 40(2):295–304, Feb 1995.

[113] M. Essenpreis, M. Cope, C. E. Elwell, S. R. Arridge, P. van der Zee, and D. T. Delpy. Wavelength dependence of the differential pathlength factor and the log slope in time-resolved tissue spectroscopy. *Advances in Experimental Medicine and Biology*, 333:9–20, 1993. LR: 20061115; JID: 0121103; 0 (Cytochromes); 0 (Hemoglobins); ppublish.

[114] E. Okada, M. Firbank, M. Schweiger, S. R. Arridge, M. Cope, and D. T. Delpy. Theoretical and experimental investigation of near-infrared light propagation in a model of the adult head. *Applied Optics*, 36(1):21–31, Jan 1 1997. GR: Wellcome Trust/United Kingdom; JID: 0247660; ppublish.

[115] Huijuan Zhao, Yukari Tanikawa, Feng Gao, Yoichi Onodera, Angelo Sassaroli, Kenji Tanaka, and Yukio Yamada. Maps of optical differential pathlength factor of human

adult forehead, somatosensory motor and occipital regions at multi-wavelengths in nir. *Physics in Medicine and Biology*, 47(12):2075, 2002.

[116] M. A. Franceschini, V. Toronov, M. Filiaci, E. Gratton, and S. Fantini. On-line optical imaging of the human brain with 160-ms temporal resolution. *Optics express*, 6(3):49–57, Jan 31 2000. JID: 101137103; ppublish.

[117] W. N. Colier, V. Quaresima, B. Oeseburg, and M. Ferrari. Human motor-cortex oxygenation changes induced by cyclic coupled movements of hand and foot. *Experimental brain research.Experimentelle Hirnforschung.Experimentation cerebrale*, 129(3):457–461, Dec 1999.

[118] C. Hirth, K. Villringer, A. Thiel, J. Bernarding, W. Muhlnickl, H. Obrig, U. Dirnagl, and A. Villringer. Towards brain mapping combining near-infrared spectroscopy and high resolution 3d mri. *Advances in Experimental Medicine and Biology*, 413: 139–147, 1997.

[119] H. Obrig and A. Villringer. Near-infrared spectroscopy in functional activation studies. can nirs demonstrate cortical activation? *Advances in Experimental Medicine and Biology*, 413:113–127, 1997.

[120] F. Orihuela-Espina, DR Leff, DRC James, AW Darzi, and GZ Yang. Quality control and assurance in functional near infrared spectroscopy (fnirs) experimentation. *Physics in Medicine and Biology*, 55(13):3701, 2010.

[121] I. Tachtsidis, C. E. Elwell, T. S. Leung, C. W. Lee, M. Smith, and D. T. Delpy. Investigation of cerebral haemodynamics by near-infrared spectroscopy in young healthy volunteers reveals posture-dependent spontaneous oscillations. *Physiological Measurement*, 25(2):437–445, Apr 2004.

[122] Christoph Schmitz. Personal correspondence, 2012.

[123] Benjamin W. Zeff, Brian R. White, Hamid Dehghani, Bradley L. Schlaggar, and Joseph P. Culver. Retinotopic mapping of adult human visual cortex with high-density diffuse optical tomography. *Proceedings of the National Academy of Sciences*, 104(29):12169–12174, 2007.

Appendix A

Supplementary Figures

Distances between the optodes represented in the following layouts are based upon a 128-channel application of the 10-20 system shown in Figure 2.13. Since the 10-20 system is defined by percentages, the exact distances will vary slightly from person to person. Hence, distances given in the figures of this appendix are approximate and rounded to the nearest integer value.

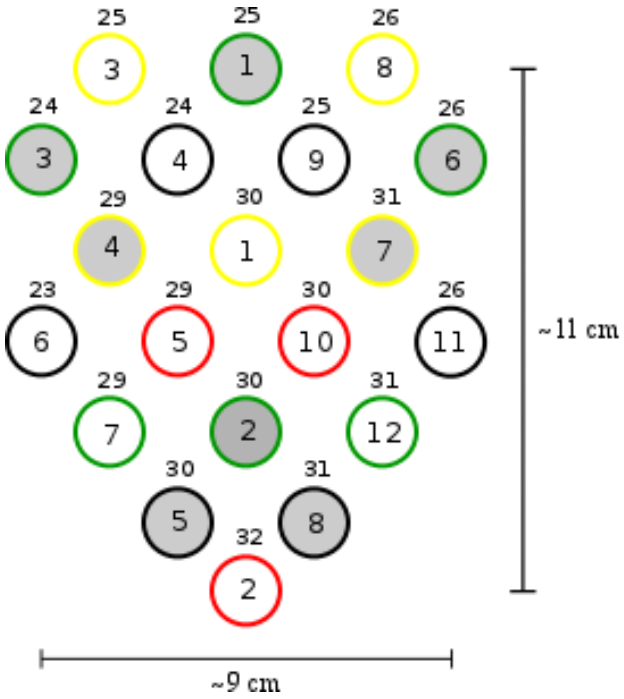

Figure A.1: Original optode layout for studying the visual cortex (posterior view). This was used through the fourth incarnation of the experimental methods. Shaded circles indicate the position of NIR sources and open circles indicate the position of detectors. Both the eight sources and the twelve detectors are numbered. For reference, detector two is placed at the inion and the sources and detector directly above it lie along the midline. The colored rings and the numbers above them give the specific optode holder location on the retaining cap.

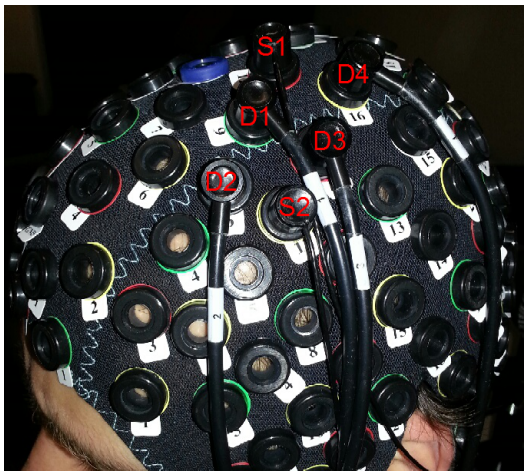

Figure A.2: Original optode layout for studying the motor cortex, as used in the single trial of the third experimental incarnation. This layout utilized two sources (*S*) and four detectors (*D*). Each optode was approximately 2.5-3 cm from the next.

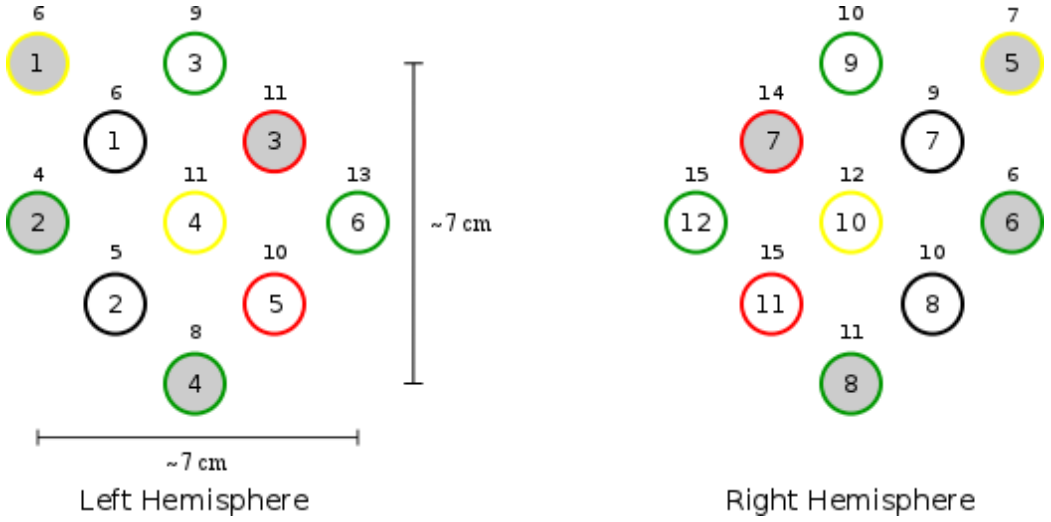

Figure A.3: Optode layout for studying the motor cortex during the concurrent validation study (posterior view). This was used during the fourth incarnation and for the final data collection trials of this project. As in the previous diagram for the visual optode layout, shaded circles refer to source locations, open circles refer to detector locations, and the colored rings and their numbers refer to specific optode holders in the cap. Refer to Figure 4.5 to view how this layout corresponds to positioning on the head.

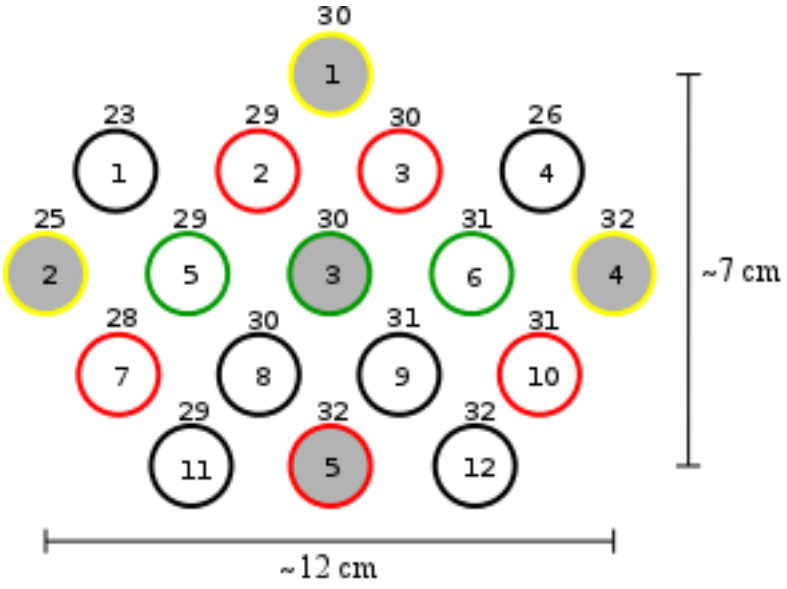

Figure A.4: This optode layout for the visual cortex was the first layout tested during optimization in the fifth experimental incarnation. It is also the one that was chosen for the remainder of the project (Fig. 4.3). This configuration used a total of five sources and twelve detectors to give a sampling rate of 8.929 Hz and a total of 60 possible channels. For reference, source 5 is positioned at the inion. Numbering and color-coding are the same as for the previous figure.

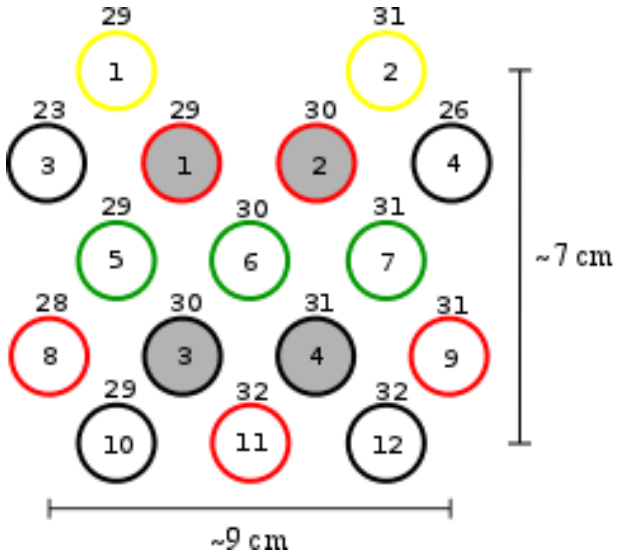

Figure A.5: This optode layout for the visual cortex was the second layout tested during optimization in the fifth experimental incarnation. This configuration used a total of four sources and twelve detectors to give a sampling rate of 10.42 Hz and a total of 48 possible channels. For reference, detector 11 is positioned at the inion. Numbering and color-coding are the same as for the previous figures in this appendix.

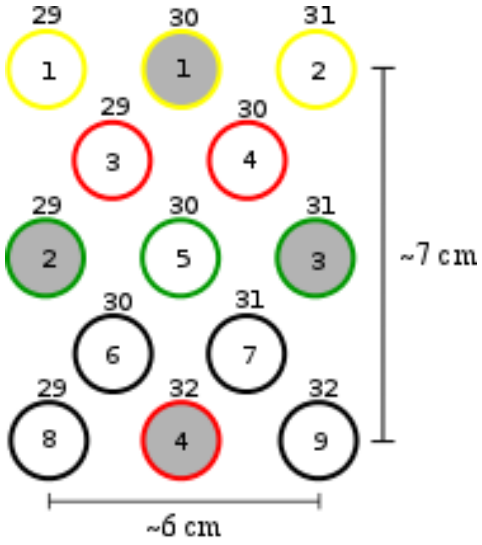

Figure A.6: This optode layout for the visual cortex was the third layout tested during optimization in the fifth experimental incarnation. This configuration used a total of four sources and nine detectors to give a sampling rate of 10.42 Hz and a total of 36 possible channels. For reference, source 4 is positioned at the inion. Numbering and color-coding are the same as for the previous figures in this appendix.

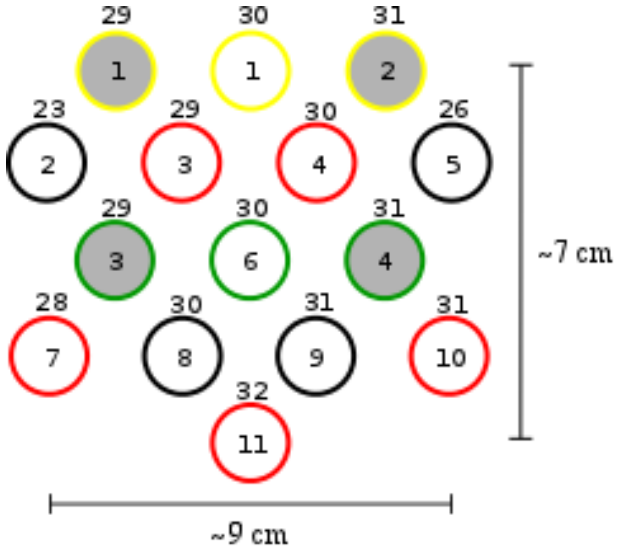

Figure A.7: This optode layout for the visual cortex was the fourth layout tested during optimization in the fifth experimental incarnation. This configuration used a total of four sources and eleven detectors to give a sampling rate of 10.42 Hz and a total of 44 possible channels. For reference, detector 11 is positioned at the inion. Numbering and color-coding are the same as for the previous figures in this appendix.

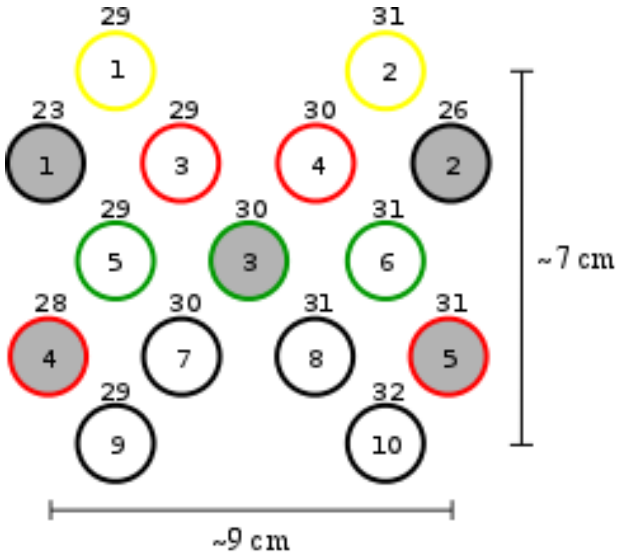

Figure A.8: This optode layout for the visual cortex was the final layout tested during optimization in the fifth experimental incarnation. This configuration used a total of five sources and ten detectors to give a sampling rate of 8.929 Hz and a total of 50 possible channels. For reference, detectors 9 and ten are positioned on either side of the inion. Numbering and color-coding are the same as for the previous figures in this appendix.

Appendix B

Supplementary Results

The following figures and tables provide additional results that are not contained within the body of this thesis.

B.1 The Motor Cortex

Included here are HbO and Hb signals obtained from subjects two through ten. These signals were from a representative channel for each participant and include all eight stimulus events from the bilateral sequential finger opposition task. An additional example is shown for the second participant to offer a visual comparison of the responses for the grasping and finger opposition tasks. An example of the hemodynamic responses for the first subject was given previously in Figure 6.1. Following these appended figures is a summary table containing the mean responses–of events that showed activation–for all subjects by data collection session and stimulus task.

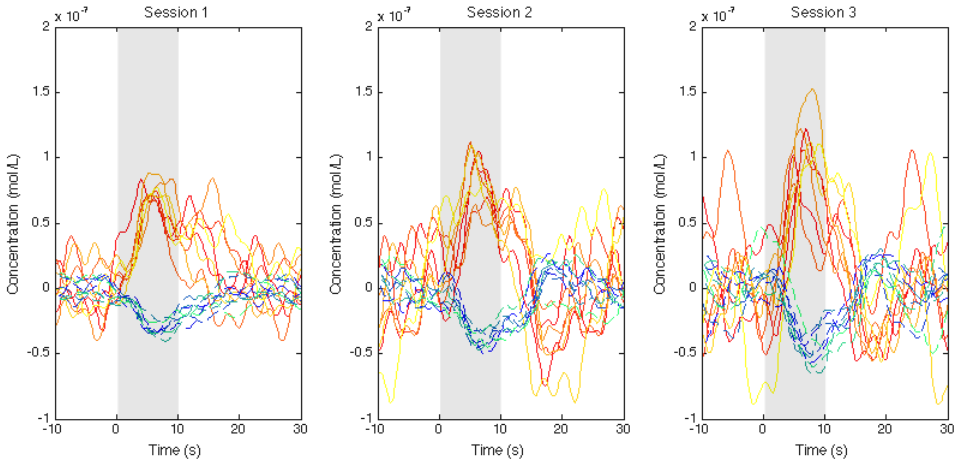

Figure B.1: Hemodynamic responses for three trials of the finger opposition task–one from each data collection session–for Subject 2. All eight stimulus events from each trial are overlaid on a single graph for a representative channel. HbO curves range from red (first event) to yellow (eighth event) and Hb curves range from blue to green. The shaded region indicates the duration of the stimulus.

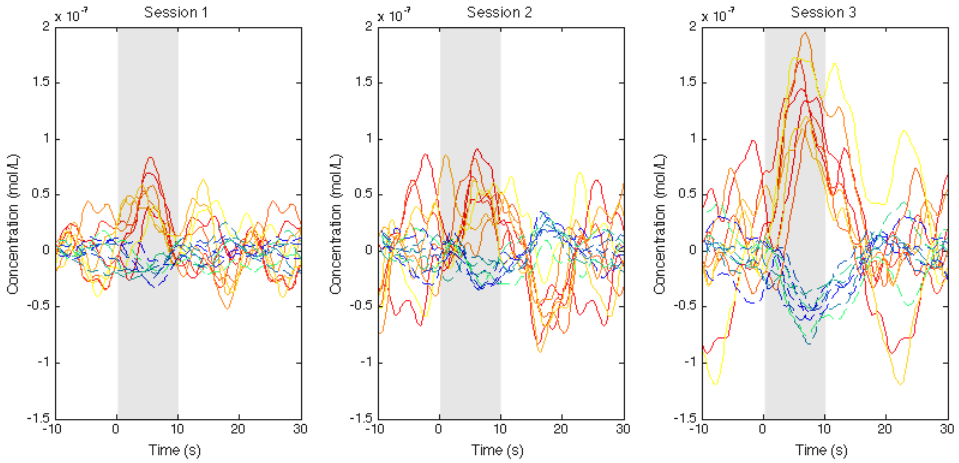

Figure B.2: Hemodynamic responses for three trials of the hand grasping task–one from each data collection session–for Subject 2. All eight stimulus events from each trial are overlaid on a single graph for a representative channel. HbO curves range from red (first event) to yellow (eighth event) and Hb curves range from blue to green. The shaded region indicates the duration of the stimulus. Note that the curves are much noisier for this whole-hand grasping task than for the sequential finger opposition task, which is shown–for the same participant–in the previous figure.

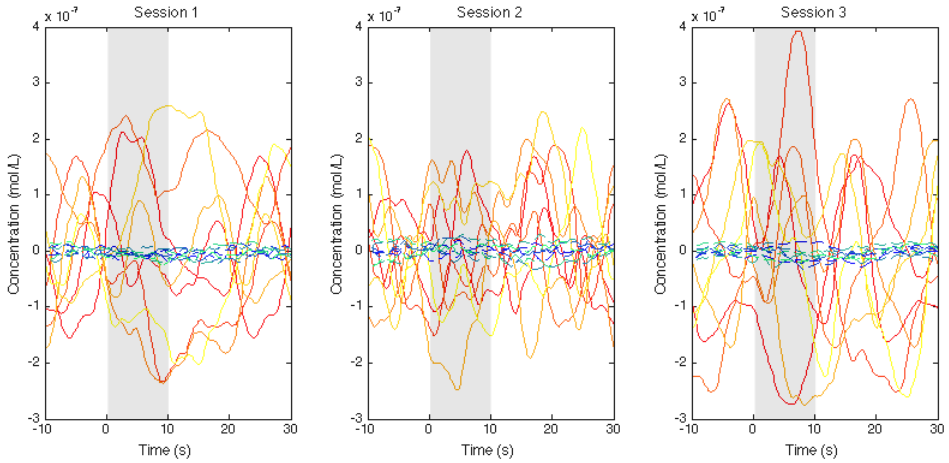

Figure B.3: Hemodynamic responses for three trials of the finger opposition task–one from each data collection session–for Subject 3. All eight stimulus events from each trial are overlaid on a single graph for a representative channel. HbO curves range from red (first event) to yellow (eighth event) and Hb curves range from blue to green. The shaded region indicates the duration of the stimulus.

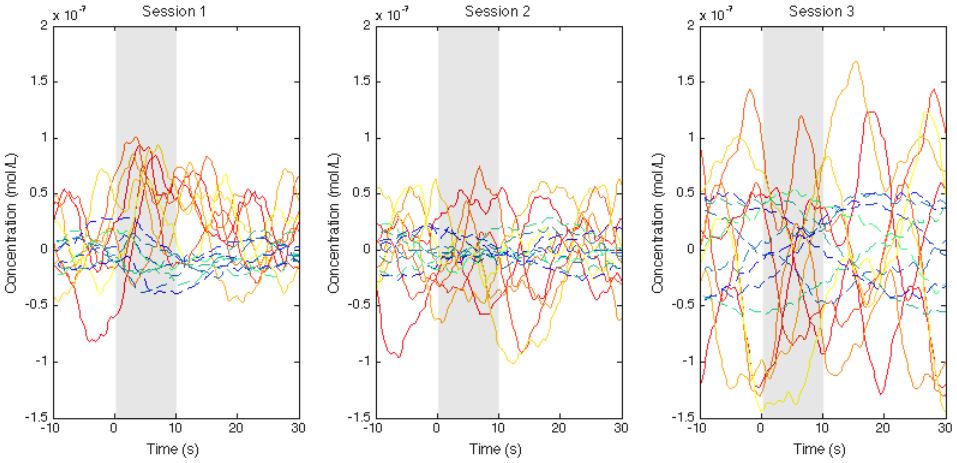

Figure B.4: Hemodynamic responses for three trials of the finger opposition task–one from each data collection session–for Subject 4. All eight stimulus events from each trial are overlaid on a single graph for a representative channel. HbO curves range from red (first event) to yellow (eighth event) and Hb curves range from blue to green. The shaded region indicates the duration of the stimulus.

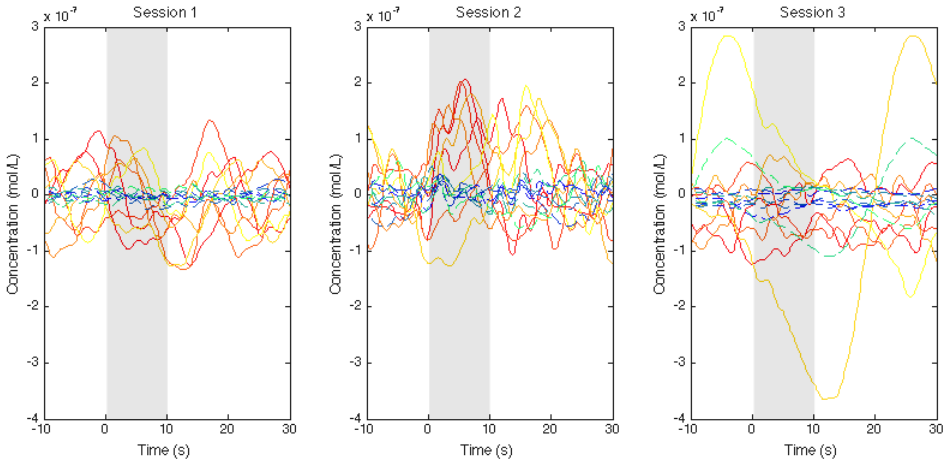

Figure B.5: Hemodynamic responses for three trials of the finger opposition task–one from each data collection session–for Subject 5. All eight stimulus events from each trial are overlaid on a single graph for a representative channel. HbO curves range from red (first event) to yellow (eighth event) and Hb curves range from blue to green. The shaded region indicates the duration of the stimulus.

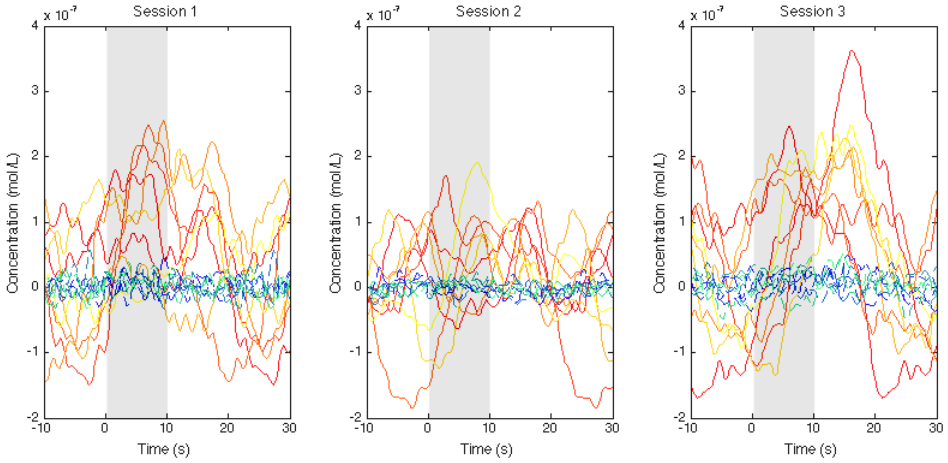

Figure B.6: Hemodynamic responses for three trials of the finger opposition task–one from each data collection session–for Subject 6. All eight stimulus events from each trial are overlaid on a single graph for a representative channel. HbO curves range from red (first event) to yellow (eighth event) and Hb curves range from blue to green. The shaded region indicates the duration of the stimulus.

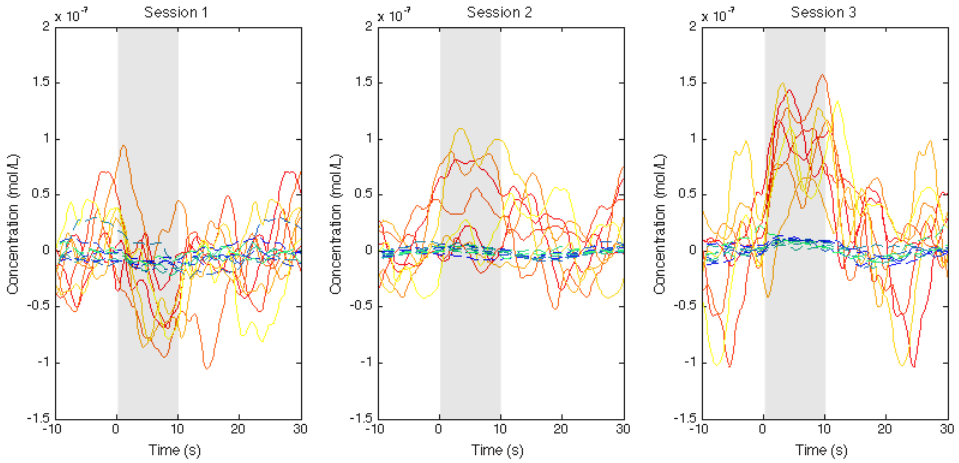

Figure B.7: Hemodynamic responses for three trials of the finger opposition task–one from each data collection session–for Subject 7. All eight stimulus events from each trial are overlaid on a single graph for a representative channel. HbO curves range from red (first event) to yellow (eighth event) and Hb curves range from blue to green. The shaded region indicates the duration of the stimulus.

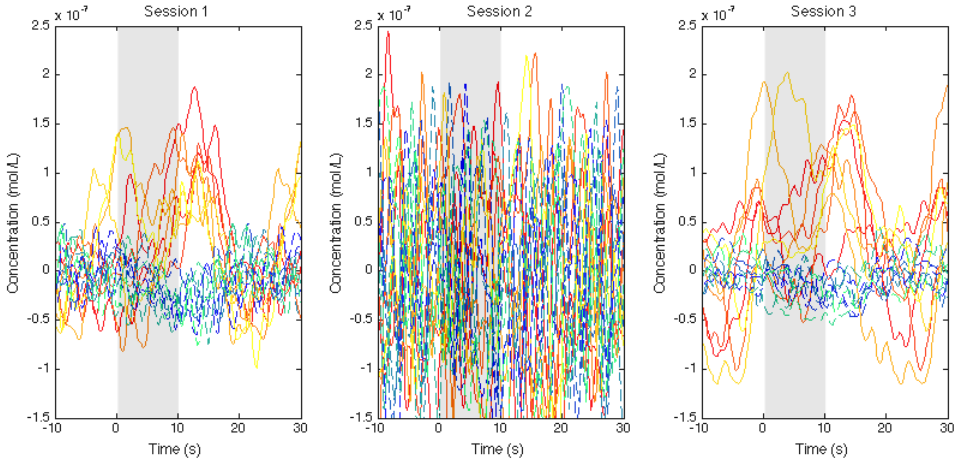

Figure B.8: Hemodynamic responses for three trials of the finger opposition task–one from each data collection session–for Subject 8. All eight stimulus events from each trial are overlaid on a single graph for a representative channel. HbO curves range from red (first event) to yellow (eighth event) and Hb curves range from blue to green. The shaded region indicates the duration of the stimulus.

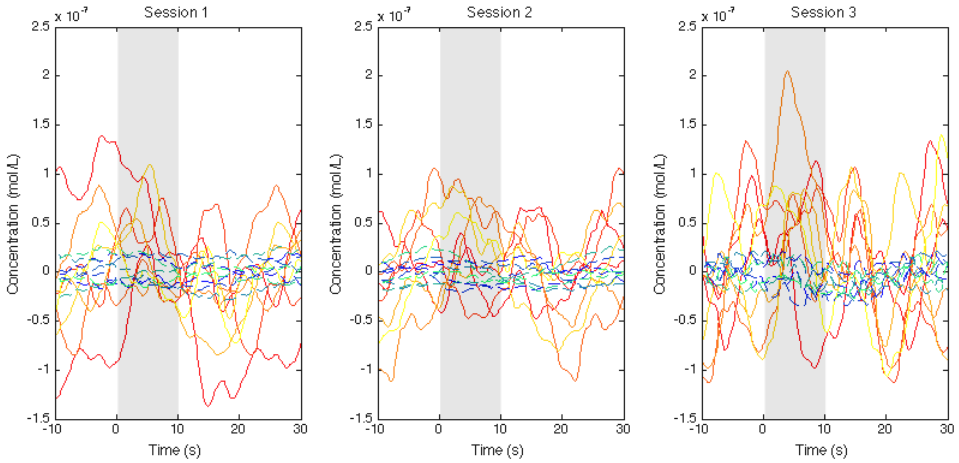

Figure B.9: Hemodynamic responses for three trials of the finger opposition task–one from each data collection session–for Subject 9. All eight stimulus events from each trial are overlaid on a single graph for a representative channel. HbO curves range from red (first event) to yellow (eighth event) and Hb curves range from blue to green. The shaded region indicates the duration of the stimulus.

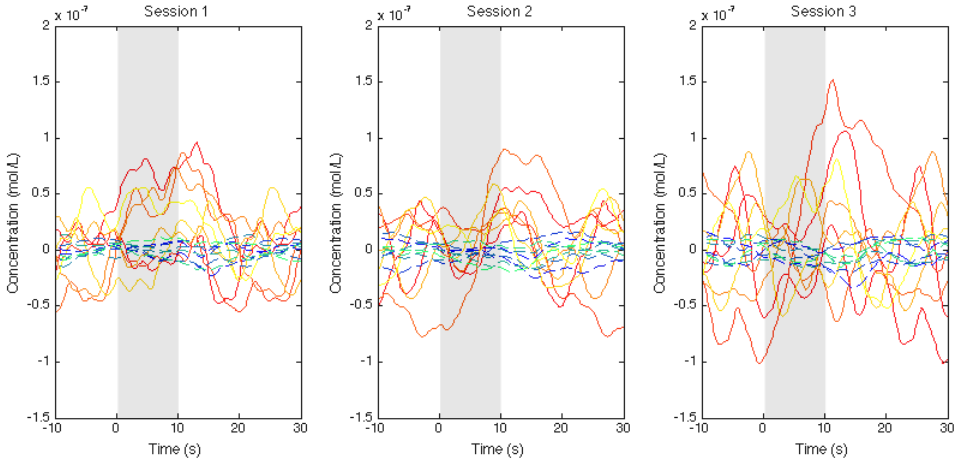

Figure B.10: Hemodynamic responses for three trials of the finger opposition task–one from each data collection session–for Subject 10. All eight stimulus events from each trial are overlaid on a single graph for a representative channel. HbO curves range from red (first event) to yellow (eighth event) and Hb curves range from blue to green. The shaded region indicates the duration of the stimulus.

Table B.1: Quantitative statistics for the motor cortex, as illustrated in Figures 6.3 and 6.4, for the most consistent data channel across each of ten participants. Concentration changes are given in units of nmol/L and uncertainty is reported as standard error. Note: The use of a * indicates a significant difference from all the other sessions for a participant. A † indicates a significant difference only between those marked with the same. In other words, the p-values for these particular statistics are less than 0.05.

		Sample Size	ΔHbO	ΔHb
Subject 1	Session 1	16	94 ± 7	-27.6 ± 1.7
	Session 2	16	$76 \pm 5^{\dagger}$	-31.8 ± 1.8
	Session 3	16	$106 \pm 6^{\dagger}$	$-40.3 \pm 1.2^{*}$
	Grasping	24	86 ± 6	-30.4 ± 1.8
	Tapping	24	98 ± 5	-36.0 ± 1.4
Subject 2	Session 1	16	66 ± 5	-27 ± 2
	Session 2	16	78 ± 8	-35 ± 3
	Session 3	16	$129 \pm 11^{*}$	$-56 \pm 5^{*}$
	Grasping	24	89 ± 11	-35 ± 5
	Tapping	24	94 ± 6	-43 ± 2
Subject 3	Session 1	7	230 ± 40	-15 ± 2
	Session 2	11	180 ± 20	-26 ± 3
	Session 3	7	230 ± 40	-24 ± 4
	Grasping	16	$2.0\text{E}2 \pm 20$	-22 ± 3
	Tapping	9	230 ± 30	-23 ± 3
Subject 4	Session 1	8	88 ± 8	-27 ± 7
	Session 2	4	74 ± 17	-13 ± 8
	Session 3	5	120 ± 40	-52 ± 7
	Grasping	6	$85 \pm 10.$	-34 ± 11
	Tapping	11	98 ± 18	-29 ± 6
Subject 5	Session 1	4	140 ± 20	-24 ± 11
	Session 2	9	$180. \pm 17$	-16 ± 11
	Session 3	0	–	–
	Grasping	5	180 ± 30	-14 ± 12
	Tapping	8	158 ± 15	-22 ± 12
Subject 6	Session 1	13	157 ± 15	-31 ± 4
	Session 2	11	170 ± 20	-38 ± 8
	Session 3	6	$280 \pm 50^{*}$	-52 ± 9
	Grasping	10	$200. \pm 19$	-37 ± 7
	Tapping	20	180 ± 20	-39 ± 5
Subject 7	Session 1	8	73 ± 14	-24 ± 4
	Session 2	11	$84 \pm 10.$	-22 ± 2
	Session 3	12	77 ± 7	-15 ± 2
	Grasping	13	81 ± 7	-21 ± 3
	Tapping	18	77 ± 8	$-20. \pm 2$
Subject 8	Session 1	10	123 ± 13	-69 ± 9
	Session 2	0	–	–
	Session 3	10	146 ± 16	$-50. \pm 6$
	Grasping	6	133 ± 13	-73 ± 16
	Tapping	14	142 ± 13	-54 ± 4
Subject 9	Session 1	9	149 ± 17	-26 ± 6
	Session 2	11	220 ± 30	-11 ± 5
	Session 3	7	129 ± 15	-31 ± 6
	Grasping	6	190 ± 20	-22 ± 4
	Tapping	14	140 ± 20	-19 ± 6
Subject 10	Session 1	10	82 ± 9	-12 ± 3
	Session 2	9	58 ± 12	$-20. \pm 2$
	Session 3	5	$1.0\text{E}2 \pm 5$	-21 ± 6
	Grasping	12	66 ± 7	-15.0 ± 1.6
	Tapping	12	88 ± 16	-19 ± 4

Table B.2: Results of additional analysis for overall motor cortex data. The Fit Model option was used in JMP to perform effect tests on subject (blocking factor), data collection session, and task type. Within each section and column–like the JMP connecting letters report–if factor levels are not connected by the same letter, then they are considered significantly different ($p < 0.05$). All units are nmol/L. This analysis will be extended after thesis submission and included in a future publication.

Subject	ΔHbO	ΔHb
1	92 ± 8^{cd}	-33 ± 2^{bc}
2	91 ± 8^{cd}	-39 ± 2^{c}
3	212 ± 12^{a}	-23 ± 3^{ab}
4	95 ± 14^{cd}	-31 ± 4^{abc}
5	176 ± 16^{ab}	-22 ± 5^{ab}
6	188 ± 11^{ab}	-39 ± 3^{c}
7	$77 \pm 10.^{d}$	-19 ± 3^{a}
8	136 ± 13^{bc}	-58 ± 4^{d}
9	176 ± 11^{ab}	-22 ± 3^{ab}
10	$80. \pm 12^{cd}$	-18 ± 3^{a}

Session	ΔHbO	ΔHb
1	121 ± 6^{b}	-27.0 ± 1.7^{a}
2	126 ± 6^{b}	-27.9 ± 1.8^{a}
3	$150. \pm 7^{a}$	-36.7 ± 1.9^{b}

Task	ΔHbO	ΔHb
Tapping	133 ± 5^{a}	-31.2 ± 1.5^{a}
Grasping	132 ± 5^{a}	-29.9 ± 1.5^{a}

Table B.3: Quantitative statistics for the motor cortex for the most consistent data channel over the right hemisphere across each of ten participants during a unilateral tapping task. Concentration changes are given in units of nmol/L and uncertainty is reported as standard error. The use of a * indicates a significant difference ($p < 0.05$) from all the other sessions for a participant. A † indicates a significant difference only between those marked with the same.

		Sample Size	ΔHbO	ΔHb
Subject 1	Session 1	11	51 ± 9	-24 ± 3
	Session 2	10	49 ± 7	-18 ± 2
	Session 3	12	52 ± 3	$-20. \pm 3$
Subject 2	Session 1	8	69 ± 5	-28.4 ± 1.7
	Session 2	8	64 ± 8	-28.3 ± 1.8
	Session 3	7	$122 \pm 14^{*}$	$-53 \pm 4^{*}$
Subject 3	Session 1	3	270 ± 40	-19 ± 8
	Session 2	5	370 ± 40	-9 ± 8
	Session 3	3	190 ± 60	-18 ± 3
Subject 4	Session 1	2	97 ± 14	$-64 \pm 3^{\dagger}$
	Session 2	3	62 ± 17	$-10. \pm 8^{\dagger}$
	Session 3	1	$138 \pm -$	$-58 \pm -$
Subject 5	Session 1	8	56 ± 3	-11.5 ± 1.6
	Session 2	6	55 ± 14	-8 ± 5
	Session 3	5	$70 \pm 20^{*}$	3 ± 17
Subject 6	Session 1	10	160 ± 20	-18 ± 3
	Session 2	5	80 ± 30	-13 ± 2
	Session 3	5	90 ± 30	-14 ± 2
Subject 7	Session 1	4	78 ± 4	-21 ± 4
	Session 2	6	$63 \pm 10.$	-17 ± 3
	Session 3	4	79 ± 9	-14 ± 5
Subject 8	Session 1	4	$190 \pm 60^{*}$	-29 ± 5
	Session 2	1	$70 \pm -$	$5 \pm -$
	Session 3	4	110 ± 30	-17 ± 8
Subject 9	Session 1	5	155 ± 19	-3 ± 5
	Session 2	7	128 ± 19	-11 ± 4
	Session 3	3	$250 \pm 40^{*}$	-2 ± 2
Subject 10	Session 1	7	53 ± 16	-11 ± 3
	Session 2	9	65 ± 12	$-7 \pm 3^{\dagger}$
	Session 3	9	99 ± 12	$-18 \pm 3^{\dagger}$

Table B.4: Quantitative statistics for the motor cortex for the most consistent data channel over the left hemisphere across each of ten participants during a unilateral tapping task. Concentration changes are given in units of nmol/L and uncertainty is reported as standard error. The use of a * indicates a significant difference ($p < 0.05$) from all the other sessions for a participant. A † indicates a significant difference only between those marked with the same. This analysis will be extended after thesis submission and included in a future publication.

		Sample Size	ΔHbO	ΔHb
Subject 1	Session 1	16	78 ± 8	-23 ± 2†
	Session 2	12	69 ± 11	-27 ± 4
	Session 3	11	94 ± 9	-36 ± 4†
Subject 2	Session 1	8	74 ± 5	-31 ± 3
	Session 2	8	89 ± 6	-43 ± 3
	Session 3	8	137 ± 12*	-67 ± 6*
Subject 3	Session 1	3	280 ± 60	-20. ± 5
	Session 2	5	310 ± 20	-15 ± 4
	Session 3	2	240 ± 1.0E2	-22.9 ± 0.8
Subject 4	Session 1	4	96 ± 15	-20 ± 20
	Session 2	0	–	–
	Session 3	1	144 ± –	-20 ± –
Subject 5	Session 1	9	92 ± 13	-16 ± 3
	Session 2	5	90 ± 40	-17 ± 8
	Session 3	4	210 ± 30*	-15 ± 15
Subject 6	Session 1	6	170 ± 40	-21 ± 6
	Session 2	5	2.0E2 ± 40	-47 ± 8
	Session 3	1	3.0E2 ± –	-22 ± –
Subject 7	Session 1	7	97 ± 18	-9 ± 3
	Session 2	4	154 ± 9	-9 ± 4
	Session 3	3	140 ± 30	-12 ± 4
Subject 8	Session 1	5	125 ± 19	-76 ± 9*
	Session 2	1	195 ± –	-197 ± –*
	Session 3	6	140 ± 20	-35 ± 8*
Subject 9	Session 1	2	130 ± 40	-23.7 ± 0.3
	Session 2	3	110 ± 20	-2.0 ± 1.5
	Session 3	3	140 ± 20	-22 ± 9
Subject 10	Session 1	7	53 ± 7	-15 ± 4
	Session 2	8	43 ± 12	-21 ± 5
	Session 3	4	62 ± 14	-28 ± 8

B.2 The Visual Cortex

This section contains Hbo and Hb signals obtained from Subjects 1 and 3-10. These signals were taken from a representative channel for each participant and include all eight stimulus events using the smallest checker size (1°). An example of the hemodynamic responses for Subject 2 was previously given in Figure 6.5. Following these appended figures is a table containing the mean responses–of events that showed activation–for all subjects by data collection session and checker size.

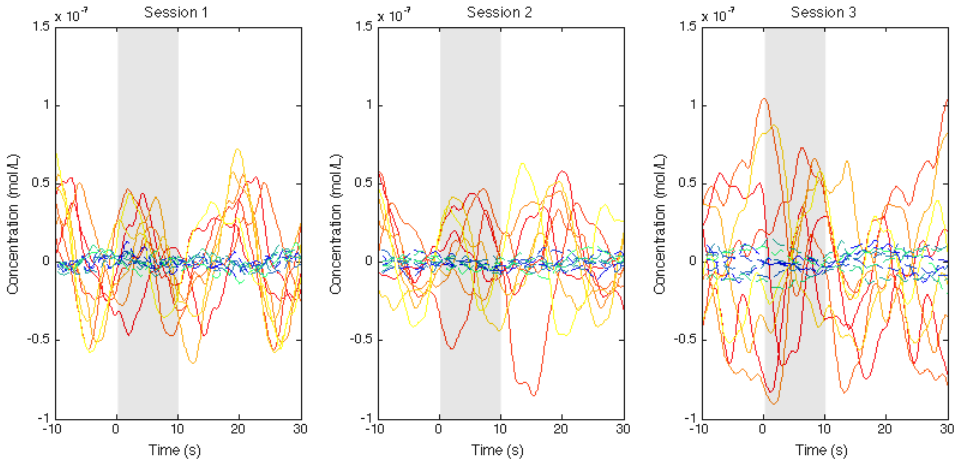

Figure B.11: Hemodynamic responses for three trials using the extra-small checker size–one trial from each data collection session–for Subject 1. All eight stimulus events from each trial are overlaid on a single graph for a representative channel. HbO curves range from red (first event) to yellow (eighth event) and Hb curves range from blue to green. The shaded region indicates the duration of the stimulus.

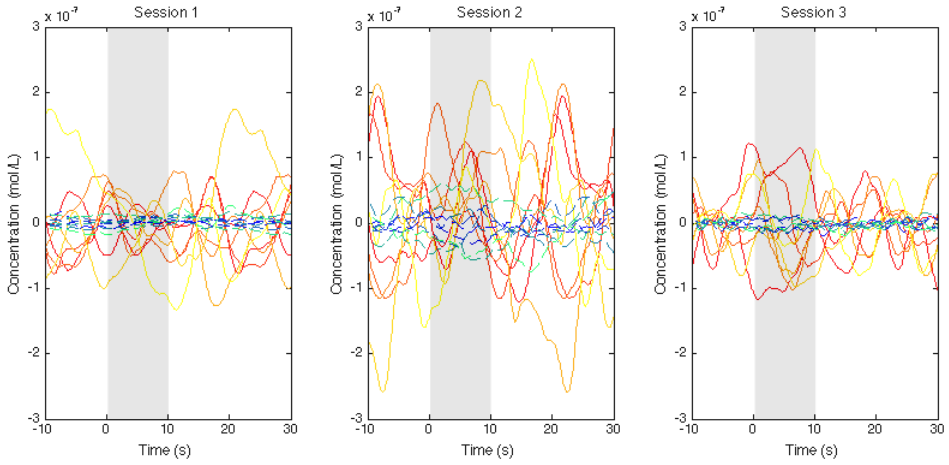

Figure B.12: Hemodynamic responses for three trials using the extra-small checker size–one trial from each data collection session–for Subject 3. All eight stimulus events from each trial are overlaid on a single graph for a representative channel. HbO curves range from red (first event) to yellow (eighth event) and Hb curves range from blue to green. The shaded region indicates the duration of the stimulus.

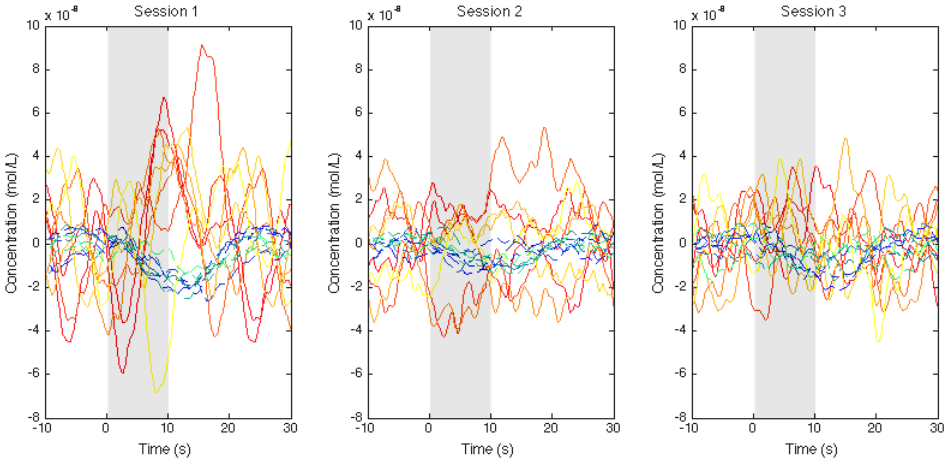

Figure B.13: Hemodynamic responses for three trials using the extra-small checker size–one trial from each data collection session–for Subject 4. All eight stimulus events from each trial are overlaid on a single graph for a representative channel. HbO curves range from red (first event) to yellow (eighth event) and Hb curves range from blue to green. The shaded region indicates the duration of the stimulus.

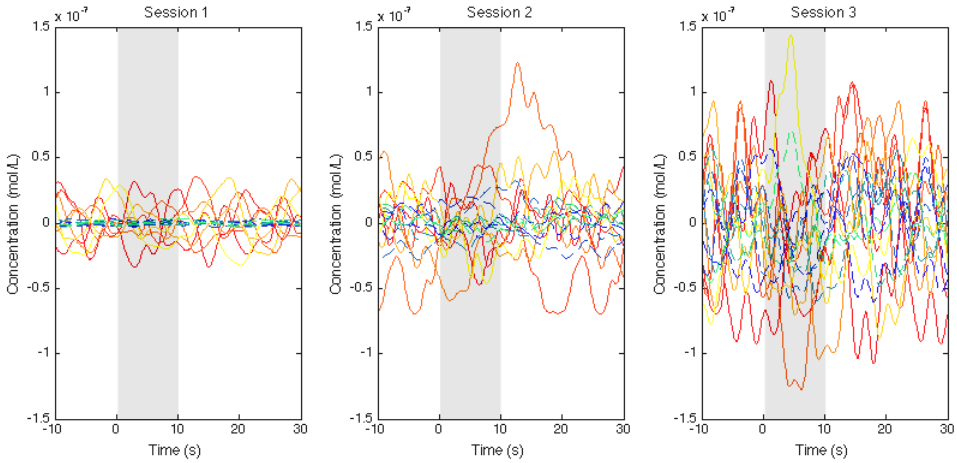

Figure B.14: Hemodynamic responses for three trials using the extra-small checker size–one trial from each data collection session–for Subject 5. All eight stimulus events from each trial are overlaid on a single graph for a representative channel. HbO curves range from red (first event) to yellow (eighth event) and Hb curves range from blue to green. The shaded region indicates the duration of the stimulus.

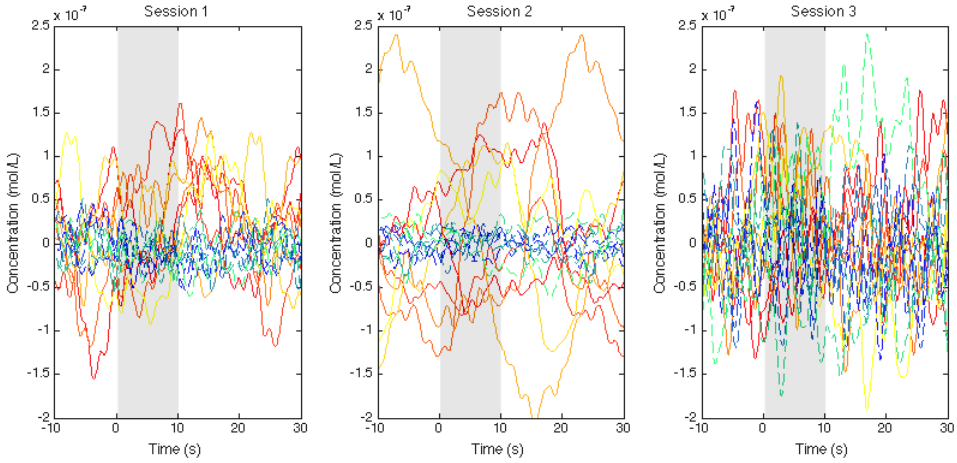

Figure B.15: Hemodynamic responses for three trials using the extra-small checker size–one trial from each data collection session–for Subject 6. All eight stimulus events from each trial are overlaid on a single graph for a representative channel. HbO curves range from red (first event) to yellow (eighth event) and Hb curves range from blue to green. The shaded region indicates the duration of the stimulus.

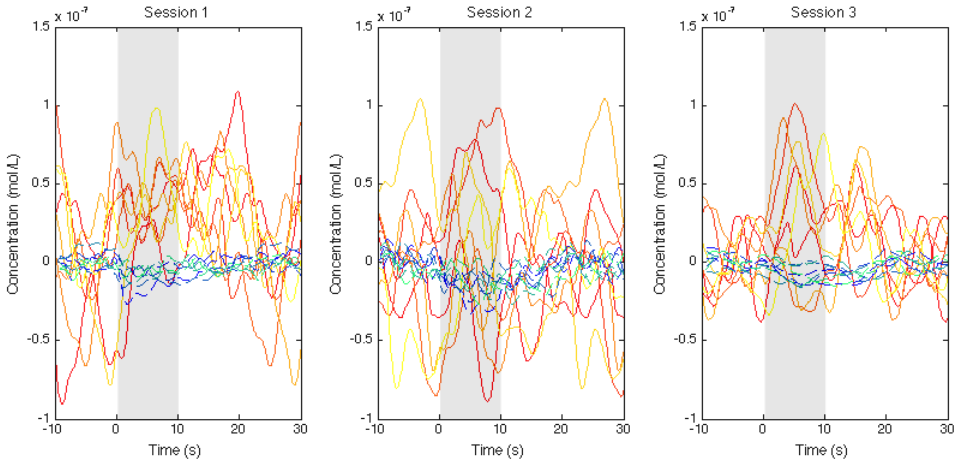

Figure B.16: Hemodynamic responses for three trials using the extra-small checker size–one trial from each data collection session–for Subject 7. All eight stimulus events from each trial are overlaid on a single graph for a representative channel. HbO curves range from red (first event) to yellow (eighth event) and Hb curves range from blue to green. The shaded region indicates the duration of the stimulus.

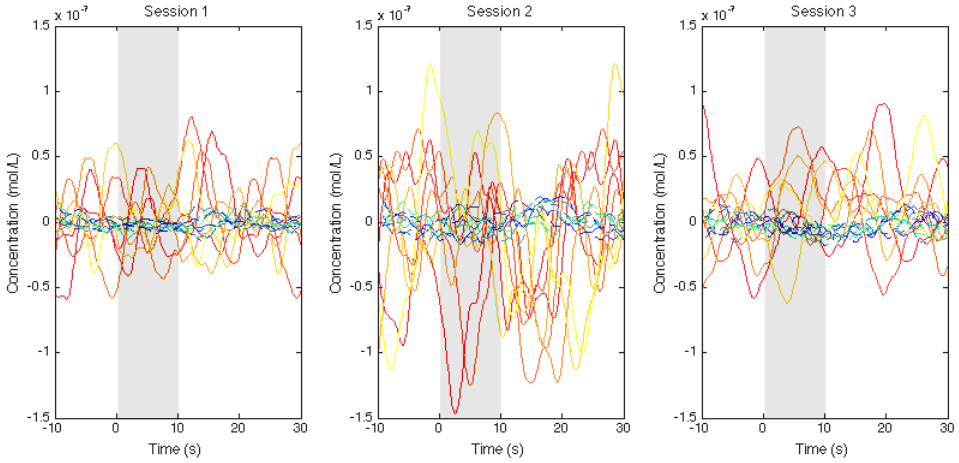

Figure B.17: Hemodynamic responses for three trials using the extra-small checker size–one trial from each data collection session–for Subject 8. All eight stimulus events from each trial are overlaid on a single graph for a representative channel. HbO curves range from red (first event) to yellow (eighth event) and Hb curves range from blue to green. The shaded region indicates the duration of the stimulus.

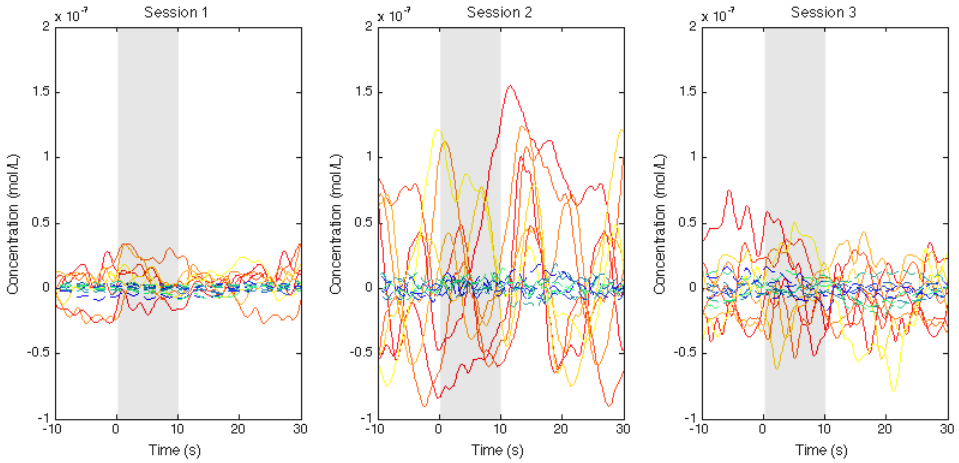

Figure B.18: Hemodynamic responses for three trials using the extra-small checker size–one trial from each data collection session–for Subject 9. All eight stimulus events from each trial are overlaid on a single graph for a representative channel. HbO curves range from red (first event) to yellow (eighth event) and Hb curves range from blue to green. The shaded region indicates the duration of the stimulus.

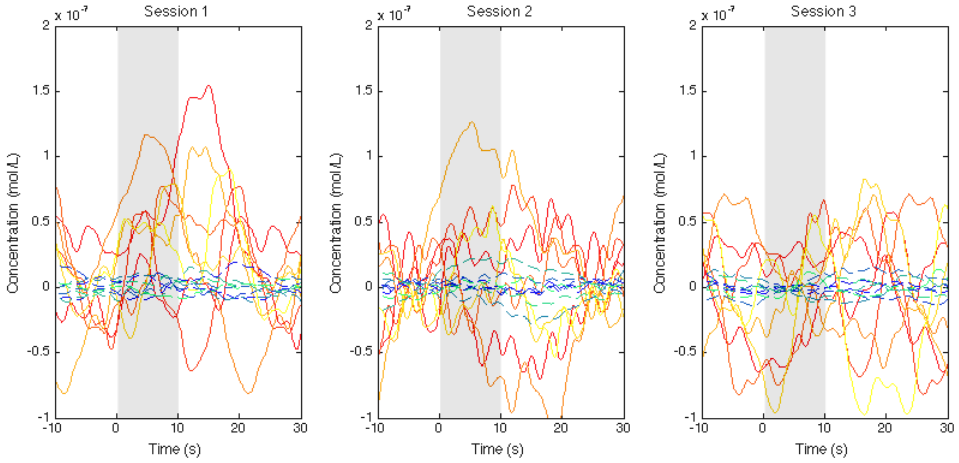

Figure B.19: Hemodynamic responses for three trials using the extra-small checker size–one trial from each data collection session–for Subject 10. All eight stimulus events from each trial are overlaid on a single graph for a representative channel. HbO curves range from red (first event) to yellow (eighth event) and Hb curves range from blue to green. The shaded region indicates the duration of the stimulus.

Table B.5: Quantitative statistics for the visual cortex, as illustrated in Figures 6.7 and 6.8, for the most consistent data channel across each of ten participants. Concentration changes are given in units of nmol/L and uncertainty is reported as standard error. Note: The use of a * indicates a significant difference from all the other sessions or checker sizes for a participant. A † or § indicates a significant difference only between those marked with the same. In other words, the p-values for these particular statistics are less than 0.05.

		Sample Size	ΔHbO	ΔHb
Subject 1	Session 1	6	$23.4 \pm 4.4^\dagger$	-9 ± 3
	Session 2	11	$60. \pm 12$	-5 ± 2
	Session 3	8	$80. \pm 14^\dagger$	-8 ± 3
	XS	5	62 ± 17	-11 ± 3
	S	8	37 ± 9	-5.8 ± 1.9
	M	4	80 ± 30	-5 ± 5
	L	6	60 ± 20	-7 ± 4
	XL	2	64 ± 7	-6 ± 2
Subject 2	Session 1	38	53 ± 3	$-17.6 \pm 0.9^*$
	Session 2	39	64 ± 4	$-23.6 \pm 1.4^*$
	Session 3	40	$92 \pm 5^*$	$-36.4 \pm 1.9^*$
	XS	24	$102 \pm 6^*$	$-38 \pm 3^\dagger$
	S	24	$82 \pm 6^\dagger$	$-30.3 \pm 1.9^\S$
	M	23	62 ± 5	$-24 \pm 2^\dagger$
	L	22	$57 \pm 4^\dagger$	$-20.6 \pm 1.8^{\dagger,\S}$
	XL	24	$45 \pm 3^\dagger$	$-16.7 \pm 0.5^{\dagger,\S}$
Subject 3	Session 1	14	$114 \pm 16^\dagger$	-8.5 ± 1.6
	Session 2	11	$240 \pm 60^\dagger$	-14 ± 9
	Session 3	8	$120. \pm 16$	-8 ± 3
	XS	3	180 ± 70	-22 ± 16
	S	8	150 ± 40	-12 ± 3
	M	4	110 ± 20	-4 ± 3
	L	9	110 ± 20	-6.4 ± 1.8
	XL	9	220 ± 70	$-11 \pm 10.$
Subject 4	Session 1	21	65 ± 15	$-3.2 \pm 1.6^\dagger$
	Session 2	15	120 ± 30	$-15 \pm 3^\dagger$
	Session 3	13	54 ± 17	-7 ± 3
	XS	15	60 ± 20	-9 ± 3
	S	6	130 ± 60	-13 ± 4
	M	11	90 ± 30	$-10. \pm 4$
	L	12	80 ± 20	-4 ± 2
	XL	15	60 ± 20	-3 ± 3
Subject 5	Session 1	9	24 ± 3	-1.7 ± 0.7
	Session 2	2	28 ± 8	-5.1 ± 0.8
	Session 3	0	–	–
	XS	2	21 ± 9	-0.4 ± 0.5
	S	5	31 ± 3	-2.3 ± 1.2
	M	0	–	–
	L	1	$18 \pm$ N/A	$-2.2 \pm$ N/A
	XL	5	24 ± 6	-4.3 ± 1.1
Subject 6	Session 1	19	141 ± 11	$-40. \pm 5^*$
	Session 2	17	148 ± 16	$-17 \pm 4^*$
	Session 3	3	211 ± 5	$-110 \pm 20^*$
	XS	8	150 ± 20	$-32 \pm 10.$
	S	9	136 ± 14	-35 ± 8
	M	10	170 ± 20	-43 ± 15
	L	8	130 ± 20	$-33 \pm 10.$
	XL	4	177 ± 9	-27 ± 14
Subject 7	Session 1	15	$40. \pm 7$	-5.9 ± 1.5
	Session 2	8	45 ± 9	-9 ± 2
	Session 3	12	$58 \pm 10.$	-4.7 ± 1.7
	XS	8	43 ± 11	-7.4 ± 1.8
	S	7	52 ± 13	-8 ± 3
	M	9	48 ± 11	-5.6 ± 1.9
	L	4	50 ± 20	-5.2 ± 1.9
	XL	7	$50. \pm 9$	-5 ± 2
Subject 8	Session 1	13	58 ± 6	$-7 \pm 0.8^\dagger$
	Session 2	7	$81 \pm 16^\dagger$	-10.8 ± 3
	Session 3	18	$51 \pm 4^\dagger$	$-15.5 \pm 1.7^\dagger$
	XS	8	$55 \pm 10.$	-15 ± 2
	S	8	61 ± 7	-10.4 ± 1.6
	M	5	59 ± 7	-12 ± 4
	L	10	62 ± 12	-13 ± 3
	XL	7	55 ± 8	-9 ± 3
Subject 9	Session 1	10	53 ± 7	-9.1 ± 1.9
	Session 2	11	89 ± 8	-16 ± 2
	Session 3	15	89 ± 17	-13 ± 3
	XS	8	$90. \pm 12$	-15 ± 5
	S	7	$80. \pm 14$	-5 ± 3
	M	8	60 ± 10	-11 ± 3
	L	8	100 ± 30	-15 ± 3
	XL	5	59 ± 4	-19 ± 2
Subject 10	Session 1	16	49 ± 7	-9 ± 3
	Session 2	7	$40. \pm 4$	-6 ± 2
	Session 3	16	49 ± 5	-3.7 ± 1.7
	XS	8	44 ± 5	-4 ± 3
	S	4	35 ± 11	-1 ± 8
	M	10	37 ± 6	-5.9 ± 1.3
	L	9	59 ± 7	-9 ± 3
	XL	8	$57 \pm 10.$	-5 ± 2

Table B.6: Results of additional analysis for overall visual cortex data. The Fit Model option was used in JMP to perform effect tests on subject (blocking factor), data collection session, and checker size. Within each section and column–like the JMP connecting letters report–if factor levels are not connected by the same letter, then they are considered significantly different ($p < 0.05$). All units are nmol/L.

Subject	ΔHbO	ΔHb
1	56 ± 12^{b}	-7 ± 3^{a}
2	69 ± 5^{b}	-25.9 ± 1.3^{b}
3	$160. \pm 10.^{a}$	-12 ± 2^{a}
4	$80. \pm 8^{b}$	-7.8 ± 2.0^{a}
5	29 ± 16^{b}	-6 ± 4^{a}
6	152 ± 9^{a}	-37 ± 2^{c}
7	50 ± 10^{b}	-6 ± 2^{a}
8	$60. \pm 9^{b}$	-11 ± 2^{a}
9	80 ± 10^{b}	-12 ± 2^{a}
10	$50. \pm 9^{b}$	-6 ± 2^{a}

Session	ΔHbO	ΔHb
1	67 ± 5^{b}	-9.9 ± 1.1^{a}
2	86 ± 5^{a}	-10.6 ± 1.3^{a}
3	82 ± 6^{ab}	-18.4 ± 1.3^{b}

Checker Size	ΔHbO	ΔHb
XS	84 ± 6^{a}	-17.4 ± 1.5^{b}
S	81 ± 6^{a}	-14.3 ± 1.5^{ab}
M	77 ± 7^{a}	-13.3 ± 1.6^{ab}
L	72 ± 6^{a}	-10.8 ± 1.5^{a}
XL	79 ± 7^{a}	-9.0 ± 1.6^{a}